

Climate Change Impacts on Thermal Performance of Residential Buildings

Soroush Samareh Abolhassani

A Thesis

in

the Department

of

Building, Civil and Environmental Engineering

Presented in Partial Fulfilment of the Requirements

for the Degree of Master of Applied Science (Building Engineering)

at Concordia University

Montreal, Quebec, Canada

July 2018

© Soroush Samareh Abolhassani, 2018

CONCORDIA UNIVERSITY  
School of Graduate studies

This is to certify that the thesis prepared

By: Soroush Samareh Abolhassani

Entitled Climate Change Impacts on Thermal Performance of Residential Buildings

And submitted in partial fulfillment of the requirements for the degree of

**Master of Applied Science (Building Engineering)**

Complies with the regulations of the University and meets the accepted standards with respect to originality and quality.

Signed by the final Examining Committee:

\_\_\_\_\_ Chair

Dr. C. Mulligan

\_\_\_\_\_ Examiner

Dr. L. Wang

\_\_\_\_\_ Examiner

Dr. C. Mulligan

\_\_\_\_\_ Examiner

Dr. C. El Ayoubi

\_\_\_\_\_ Supervisor

Dr. F. Haghghat

\_\_\_\_\_ Supervisor

Dr. A. Nazemi

Approved by

\_\_\_\_\_

Chair of Department or Graduate Program Director

July 2018

\_\_\_\_\_

Dean of Faculty

## **Abstract**

### Climate Change Impacts on Thermal Performance of Residential Buildings

Soroush Samareh Abolhassani

Climate change has altered regular temperature patterns and various climate variables on a global scale, causing growing concerns about future food, water and energy security. Immediate action should be taken to understand the extent of climate change while also proposing adaptation strategies to cope with the projected future climate conditions. From the energy security perspective, particularly in consideration of the ever-increasing human population, an important aspect to understand is the impact of climate change on the energy consumption of residential buildings. Understanding the impact of climate change on building energy consumption is not only beneficial for advising efficient energy-saving measures, but also for understanding future energy requirements. Various studies have already shown that climate change effects heating and cooling loads of buildings in various climates around the world. However, there is a lack of comprehension of the effects of climate change on energy consumption in Quebec. In addition, some of the methodologies employed to address the impact of climate change in buildings may be not be accurate or accessible to practitioners. The present study tries to fill this gap by advising a simple procedure that can be implemented in day-to-day engineering practice for a detailed understanding of the effects of climate change on building energy consumption. The methodology is applied to a residential building in Montreal, Quebec (Canada), using the state-of-the-art climate model projections for the periods of 2011-2040 (short-term future), 2041-2070 (midterm future), and 2071-2100 (long-term future) and under low and high greenhouse gas concentration scenarios. In brief, the available projections of five global climate models was studied for two particular weather parameters, namely dry-bulb temperature and shortwave radiation. The projections were downscaled at the point location and at an hourly resolution using a cascade model based on a quantile mapping bias correction method and a modified quantile-based k-nearest neighbor method. The downscaled projections were used as inputs to TRNSYS, an energy simulation software, in order to quantify the heating and cooling loads as well as judge the overall performance of the residential building in Montreal. This methodology can provide a basis for

detailed understanding of the impacts of climate change on building energy consumption. Considering the applied case study, it is understood that climate change will not only change the intensity of the heating and cooling loads but can also change the empirical distribution of hourly energy consumption, particularly during peak loads.

## **Acknowledgments**

I would like to express my deepest gratitude and respect to my supervisors, Professors Fariborz Haghghat and Ali Nazemi, who supported me throughout my research and study at Concordia University. They have devoted their time to assisting me throughout the duration of this project and they were always welcoming, even meeting with me out of the normal office hours. I am, and always will be, sincerely grateful for the opportunity they have given me in realizing this project, for their guidance, and their constant support. The freedom that they gave me and their trust in my abilities was truly rewarding for me

I also want to deeply thank my colleagues (Behrang, Emilie, Helene, Dave, Mahmood, Maryam, Jenny, Ying, Li, Karthik, and Mojtaba) for their kindness, their humour, their help and their patience with my English. This experience would have been completely different without the fun and relaxed atmosphere in our office.

Last, but not least, my sincere and heartfelt thanks go out to my mother, Azadeh Sohrabian, my father, Said Samareh Abolhassani, my grandfather, Mr. Mashallah Samareh Abolhassani, and my sister, Aysa Samareh Abolhassani.

# Table of Contents

Abstract.....	iii
Acknowledgments.....	v
Table of Contents.....	vi
List of Figures.....	viii
List of Tables.....	x
Notation.....	xii
Symbols and Abbreviation.....	xiii
1. Introduction.....	1
1.1. Research objectives.....	3
1.2. Thesis outline.....	3
2. Literature review.....	4
2.1. Climate change impact assessment paradigm.....	4
2.1.1. Global circulation model.....	4
2.1.2. Future projections under climate change conditions.....	5
2.1.2.1. Special report on emissions.....	5
2.1.2.2. Representative concentration pathways.....	8
2.1.3. Spatial and temporal downscaling of climate model projections.....	10
2.1.3.1. Dynamical downscaling method.....	11
2.1.3.2. Statistical downscaling method.....	11
2.1.3.2.1. Morphing Method (Delta Method).....	14
2.1.3.2.2. Bias correction.....	14
2.1.3.3. Hybrid downscaling methods.....	16
2.1.3.3.1. Statistical downscaling model (SDSM).....	16
2.1.3.3.2. Bias-corrected spatial disaggregation (BCSD).....	17
2.2. Impact of climate change on building energy consumption.....	17
2.2.1. Zone 0: Extremely hot.....	22
2.2.2. Zone 1: Very hot.....	22
2.2.3. Zone 2: Hot.....	24
2.2.4. Zone 3: Warm.....	26
2.2.5. Zone 4: Mixed.....	27
2.2.6. Zone 5: Cool.....	28
2.2.7. Zone 6: Cold.....	29
2.2.8. Zone 7: Very cold.....	29
2.2.9. Zone 8: Subarctic/arctic.....	29
2.3. Shortcoming of the existing literature.....	30
3. Methodology.....	32
3.1. Case study.....	32
3.2. Building simulation tool (TRNSYS).....	34
3.3. Projecting future climate.....	36
3.3.1. Global circulation models and future scenarios selection.....	37
3.3.2. Downscaling.....	39
3.3.2.1. Multiplicative quantile mapping.....	39
3.3.2.2. Additive quantile mapping.....	40
3.3.3. Disaggregation.....	42
3.4. Using generated future weather data as an input of building energy simulation software.....	44
4. Results and discussion.....	47
4.1. Weather data.....	47
4.1.1. RCP4.5.....	47

4.1.1.1.	Ensemble analysis results.....	47
4.1.2.	RCP8.5 .....	49
4.1.2.1.	Ensemble analysis results.....	49
4.1.3.	Comparison (RCP4.5 and RCP8.5).....	51
4.2.	Load calculation.....	51
4.2.1.	Heating load RCP4.5.....	56
4.2.1.1.	Ensemble analysis results.....	56
4.2.1.2.	Uncertainty assessment .....	61
4.2.2.	Heating load RCP8.5.....	63
4.2.2.1.	Ensemble analysis results.....	63
4.2.2.2.	Uncertainty assessment .....	68
4.2.3.	Comparison (RCP4.5 and 8.5).....	70
4.2.4.	Cooling load RCP4.5 .....	71
4.2.4.1.	Ensemble analysis results.....	71
4.2.4.2.	Uncertainty assessment .....	76
4.2.5.	Cooling load RCP8.5 .....	79
4.2.5.1.	Ensemble analysis results.....	79
4.2.5.2.	Uncertainty assessment .....	84
4.2.6.	Comparison (RCP4.5 and 8.5).....	86
5.	Conclusion, limitation, and future work .....	87
5.1.	Concluding remarks on the present work.....	87
5.2.	Future work .....	90
References	.....	92

## List of Figures

Figure 1: Representative concentration pathways based on radiative forcing [2] .....	8
Figure 2. Different downscaling methods .....	10
Figure 3: The procedure of bias correction quantile mapping downscaling method [31] .....	15
Figure 4: Summary of results for Hong Kong, China .....	24
Figure 5: Photo of the experimental house [85].....	33
Figure 6: Weekly occupancy schedule on the ground floor.....	34
Figure 7: Framework for generating local future weather data.....	36
Figure 8: Framework for generating local future diffuse horizontal, and direct normal radiation .....	36
Figure 9: Methodology showing the bias correction (quantile mapping) downscaling process .....	41
Figure 10: Cumulative distribution function of GCM bias corrected, observation, and GCM historical data compared for three weather parameters; a) Daily dry bulb temperature, and b) Daily radiation .....	41
Figure 11: The procedure of disaggregation method for temporal downscaling .....	42
Figure 12: Methodology showing the temporal downscaling (disaggregation) process.....	44
Figure 13: Connection between the TMY file and type 16 mode 2 in TRNSYS model.....	46
Figure 14: Cumulating distribution function of hourly temperature based on RCP4.5 in four periods of historical, 2011-2040, 2041-2070, and 2071-2100 and ensemble GCM model .....	48
Figure 15: Cumulating distribution function of hourly temperature based on RCP8.5 in four periods of 1961-1990, 2011-2040, 2041-2070, and 2071-2100 and ensemble GCM model.....	50
Figure 16: Cumulating distribution function of the hourly heating load based on RCP4.5 in four periods of 1961-1990, 2011-2040, 2041-2070, and 2071-2100 and ensemble GCM model.....	56
Figure 17: Hourly relative frequency of heating load based on RCP4.5 on January in four periods of 1961-1990, 2011-2040, 2041-2070, and 2071-2100 and ensemble GCM model. ....	57
Figure 18: Percentage of climate change effect on different parts of the hourly heating load based on RCP4.5 in January in four different periods of 1961-1990, 2011-2040, 2041-2070, and 2071-2100.....	60
Figure 19: Cumulating distribution function of the hourly heating load based on RCP8.5 in four periods of 1961-1990, 2011-2040, 2041-2070, and 2071-2100 and ensemble GCM model.....	63
Figure 20: Hourly relative frequency of heating load based on RCP8.5 in January in four periods of 1961-1990, 2011-2040, 2041-2070, and 2071-2100 and ensemble GCM model. ....	64
Figure 21: Percentage of climate change effect on different parts of the hourly heating load based on RCP8.5 in January in four different periods of 1961-1990, 2011-2040, 2041-2070, and 2071-2100.....	67
Figure 22: Cumulating distribution function of the hourly cooling load based on RCP4.5 in four periods of 1961-1990, 2011-2040, 2041-2070, and 2071-2100 and ensemble GCM models. ....	72

Figure 23: Hourly relative frequency of cooling load based on RCP4.5 in July in four periods of 1961-1990, 2011-2040, 2041-2070, and 2071-2100 and ensemble GCM model ..... 73

Figure 24: Percentage of climate change effect on different parts of the hourly cooling load based on RCP4.5 in July in four different periods of 1961-1990, 2011-2040, 2041-2070, and 2071-2100. .... 76

Figure 25: Cumulating distribution function of the hourly cooling load based on RCP8.5 in four periods of 1961-1990, 2011-2040, 2041-2070, and 2071-2100 and ensemble GCM model. .... 79

Figure 26: Hourly relative frequency of cooling load based on RCP8.5 in July in four periods of 1961-1990, 2011-2040, 2041-2070, and 2071-2100 and ensemble GCM model ..... 80

Figure 27: Percentage of climate change effect on different parts of the hourly cooling load based on RCP8.5 in July in four different periods of 1961-1990, 2011-2040, 2041-2070, and 2071-2100. .... 83

## List of Tables

Table 1. Description of SRES future scenarios [14,15,17].....	7
Table 2: Description of RCP future scenarios [2,18].....	9
Table 3. Advantages and disadvantages of downscaling methods [10,22–26].....	12
Table 4: Description of climate zones based on ASHRAE 169-2013[61].....	17
Table 5. The GCM models, future scenarios, downscaling methods, energy tool, and the region of a case study that have been used in previous studies.....	18
Table 6: Summary of cooling results for Zone 0A .....	22
Table 7: Summary of heating and cooling load results for Zone 1A* .....	23
Table 8: Summary of heating and cooling load results for Zone 2 .....	25
Table 9: Summary of heating and cooling load results for Zone 2 .....	25
Table 10: Selected global circulation models with their latitude and longitude grid points .....	37
Table 11: Selected global circulation models with their latitude and longitude grid points .....	38
Table 12: Statistical values of ensemble model of hourly temperature and radiation based on RCP4.5 in four periods of 1961-1990, 2011-2040, 2041-2070, 2071-2100.....	49
Table 13: Statistical values of ensemble model of hourly temperature and radiation based on RCP8.5 in four periods of 1961-1990, 2011-2040, 2041-2070, 2071-2100.....	50
Table 14: Statistical values of ensemble model of hourly heating and cooling load based on RCP4.5 in four periods of 1961-1990, 2011-2040, 2041-2070, and 2071-2100.....	52
Table 15: Statistical values of ensemble model of hourly heating and cooling load based on RCP8.5 in four periods of 1961-1990, 2011-2040, 2041-2070, 2071-2100. ....	54
Table 16: Total heating and cooling load, and total load per year based on RCP4.5 in four different periods of 1961-1990, and 2011-2040, 2041-2070, and 2071-2100.....	55
Table 17: Total heating and cooling load, and total load per year based on RCP8.5 in four different periods of 1961-1990, and 2011-2040, 2041-2070, and 2071-2100.....	56
Table 18: Relative frequency of different parts of the hourly heating load on December, January, and February based on RCP4.5 in four different periods of 1961-1990, 2011-2040, 2041-2070, and 2071-2100 .....	58
Table 19: Statistical values of different GCM models of the hourly heating load based on RCP4.5 in four periods of 1961-1990, 2011-2040, 2041-2070, 2071-2100. ....	62
Table 20: Relative frequency of different parts of the hourly heating load in December, January, and February based on RCP8.5 in four different periods of 1961-1990, 2011-2040, 2041-2070, and 2071-2100. ....	65

Table 21: Statistical values of different GCM models of the hourly heating load based on RCP8.5 in four periods of 1961-1990, 2011-2040, 2041-2070, 2071-2100. ....	69
Table 22: Relative frequency of different parts of the hourly cooling load in Jun, July, and August based on RCP4.5 in four different periods of 1961-1990, 2011-2040, 2041-2070, and 2071-2100.....	75
Table 23: Statistical values of different GCM models of the hourly cooling load based on RCP4.5 in four periods of 1961-1990, 2011-2040, 2041-2070, and 2071-2100.....	78
Table 24: Relative frequency of different parts of the hourly cooling load in Jun, July, and August based on RCP8.5 in four different periods of 1961-1990, 2011-2040, 2041-2070, and 2071-2100.....	82
Table 25: Statistical values of different GCM models of the hourly cooling load based on RCP8.5 in four periods of 1961-1990, 2011-2040, 2041-2070, 2071-2100. ....	85

## Notation

$\langle x_o \rangle$	Monthly mean of $x_o$ and
$a_m$	Coefficient obtained by the variances of $\Delta x_m$ , $x_o$ , and $\langle x_o \rangle$ .
$H\_GCM_{k,QM}^{fut}$	Downscaled of future weather data by additive quantile mapping
$H\_GCM_{k,QM}^{mul}$	Downscaled of future weather data by multiplicative quantile mapping
$I_b$	Beam radiation on a horizontal surface
$I_d$	Diffuse horizontal radiation
$K_T$	Clearness index
$T_a$	Ambient temperature
$F_{H\_GCM_k}^{basper}$	Cumulative distribution function of the GCM data (historical baseline data);
$F_{H\_GCM_k}^{fut}$	Cumulative distribution function of the GCM future data
$F_{H\_GCM_k}^{fut}$	Cumulative distribution function of GCM future data.
$F_{H\_OBS_k}^{basper-1}$	Inverse cumulative distribution function (quantile function) for the observation in month $k$ .
$a_m$	coefficient obtained from the GCM.
$I$	Global horizontal radiation.
rh	Relative humidity
$x$	future data
$x_o$	present data
$\alpha$	Solar altitude angle
$\Delta x_m$	absolute monthly change

## **Symbols and Abbreviation**

AR4	Fourth assessment report of the IPCC
Avg	Average
BCSD	Bias-corrected spatial disaggregation
CDF	Cumulative distribution functions
CH <sub>4</sub>	Methane
CMIP5	Coupled model inter-comparison project 5
CO <sub>2</sub>	Carbon dioxide
DSY	Design summer year
EPW	EnergyPlus weather data format
GCMs	Global circulation models
GHG	Greenhouse gases
IPCC	Intergovernmental panel on climate change
KNN	k-nearest neighbor
Max	Maximum
NO <sub>2</sub>	Nitrous oxide
PBL	Netherlands environmental assessment agency
PCA	Principal component analysis
QM	Quantile mapping
RCPs	Representative concentration pathways
SDSM	Statistical downscaling model
SRES	Special report on emission scenarios
STD	Standard deviation
SWR	Solar shortwave radiation
TAR	Third assessment report of the IPCC
TMY	Typical meteorological year
TRY	Test reference year

# Chapter 1

## 1. Introduction

Solar radiation has been referred to as the engine driving the energy balance of the Earth's climate system [1]. The Earth's energy balance has been unchanged for a long period of time whereby almost half of the solar shortwave radiation (SWR) is absorbed by the Earth, approximately 30% is reflected by the cloud cover, aerosols, surface albedo or greenhouse gases (GHG) and the remaining 20% is absorbed by the atmosphere [2]. However, the increasing anthropogenic emissions due to greenhouse gases have disturbed the Earth's temperature balance. In addition, it is known that the majority of the Earth's outgoing radiation is found in the infrared range of the electromagnetic spectrum [4, 5]. This type of radiation is also known as long-wave radiation, which is emitted and reflected from the surface of the Earth or may be absorbed by water vapor, clouds, methane (CH<sub>4</sub>), carbon dioxide (CO<sub>2</sub>), nitrous oxide (NO<sub>2</sub>), and other GHG gases. Due to this absorption process, these gases may emit long-wave radiation, which when reflected into the atmosphere, increases the Earth's surface temperature. In short, this is the greenhouse effect.

Changes in the levels of incoming and outgoing radiation can lead to changing the net energy balance of the Earth. The extraterrestrial radiation does not significantly change over time, because of the sunspot of the solar cycle. However, the changes in outgoing long-wave radiation may cause fluctuations in the Earth's surface temperature, its albedo, the emissivity of the atmosphere as well as the greenhouse effect noted above. According to the Intergovernmental Panel on Climate Change (IPCC), the scientific evidence for the warming of the climate system, as a result of greenhouse gas effects and anthropogenic activities, is unquestionable [5]. In 2015, the change in global temperature was 0.75 °C higher than the average temperature between 1961-1990. The highest recorded temperature since 1850 was recorded in 2016 with a 0.87 °C above the average temperature of 1961-1990 [6]. Based on climate model projections, if anthropogenic greenhouse effects persists, the average temperature for the period 2081-2100 is expected to be 4.8 °C higher than the average temperature for the period 1986-2005 [7].

One of the direct consequences of climate change is the changing weather patterns, manifested with hotter and drier summers as well as colder and damper winters in the North America [8]. This directly impacts people's lifestyles, including their energy consumption. This concept can be perceived as a driving force and a critical parameter in understanding energy demand. It will also affect the energy system capacity as well as energy supply and distribution, all of which are key elements of energy security. Previous studies aimed at assessing the impacts of climate change on the thermal performance of buildings concluded that cooling loads will increase, heating loads will decrease, and the total load will decrease in colder regions and will increase in warmer regions. The current findings, however, are limited geographically and in some cases based upon inadequate and/or inaccessible methodologies for practitioners.

Although the previous studies provided an insight to the impact of climate change on future energy requirements of buildings, they embody several limitations and shortcomings. First, the results of climate projections are uncertain and quickly become outdated when new projections become available. As a result, many of the previous impact studies are no longer reliable. Second, a key issue is the mismatch between the spatiotemporal scale of future climate projections and the scale in which the weather data is required for impact assessment. Avoiding this mismatch requires using a systematic approach for downscaling climate projection into finer scales. However, the majority of available and current studies make use of either overly simplistic or extremely complex methods for spatial and temporal downscaling. This hinders the use of these methodologies in real-world applications. Another challenge is the uncertainty in climate projections. According to IPCC guidelines, several models should be considered in order to provide reliable projections. This is known as the ensemble approach, which is widely overlooked in building energy studies. Finally, the majority of previous studies mainly investigate the general behavior of the heating and cooling loads and therefore, there is a lack of studies analyzing the details of these loads, particularly the peak loads which can be highly affected by the climate change.

By examining both climate change science and building engineering concurrently, this research study proposes a set of improvements for analyzing the impact of climate change on building energy consumption. In addition, there is the greater objective of providing a methodology that can be applied by practitioners in real-world contexts. To demonstrate the practicability of the proposed methodology, the suggested procedure is applied to assess the

thermal performance of a building in Montreal, Canada. Considering the case study, a detailed perspective is provided on the changes in the heating and cooling loads as well as the total energy consumption under climate change conditions.

### **1.1. Research objectives**

To address the aforementioned gaps, the main objectives of this thesis are as follows:

- 1- To develop a procedure to generate future weather data for building thermal analysis by employing compatible spatial and temporal downscaling processes.
- 2- To study the impact of future climate change on heating and cooling loads of residential buildings in a colder climate, i.e. Quebec-Canada, by analyzing their intensity and frequency under different climate projections.

### **1.2. Thesis outline**

Chapter 2 contains the fundamentals of climate change weather data generation and critical reviews of previous studies on climate change impact on thermal performance of buildings. Chapter 3 reports the framework of future weather data generation by describing the downscaling and disaggregation methods as well as the process of using this weather data as an input to the energy simulation software, TRNSYS. Chapter 4 discusses the obtained results from future weather data and heating and cooling load (general behavior and detailed behavior) based under low and high greenhouse gas concentration scenarios. Moreover, this chapter analyzes the heating and cooling loads in three states of ensemble (average of different global circulation models), comparison (different representative concentration pathways), and uncertainty assessment (comparison the obtained results of different global circulation models). Chapter 5 summarizes the conclusions of this research and proposed recommendations for future studies.

# Chapter 2

## 2. Literature review

This chapter outlines the main elements of the science of climate change impact assessment and provides a comprehensive review on the previous studies related to building energy consumption in two segments: (i) the general behavior of the heating/cooling loads and peak loads, as well as (ii) the existing limitations in current approaches with a greater goal of justifying the suggested development in this thesis.

### 2.1. Climate change impact assessment paradigm

#### 2.1.1. Global circulation model

Despite certain limitations, Global Circulation Models (GCMs) are the most reliable scientific tools to look at the past and future evolutions in the global climate. In brief, they are three-dimensional mathematical models that show the effects of greenhouse gases, solar heating, and atmospheric water-vapor on the climate using the principal physical processes [9]. They can provide information about the heat storage in soil, radiation, precipitation, cloud cover, surface heat flux, moisture, sea ice, and the mass transfer at the grid scale [10]. The scale is identified as spatial resolution based on the latitude and longitude of a desired location. Current GCMs have coarse spatial resolution, ranging between 100 to 500 km. The modeling process in GCMs involves separating the world's land mass into grids and constructing and solving a series of equations based on horizontal momentum, mass continuity, and hydrostatic equilibrium among other parameters. By solving the equations at a given time step for each grid of land, the output of each solution is used as an initial state for the next time step. The length of each time step may vary between 30 minutes and 3 hours, depending on the model. However, the results are usually provided at a daily scale, and when aggregated, can provide reliable estimations of seasonal and annual changes in climate for the sake of impact assessment.

The most up-to-date GCM results are released by IPCC through Coupled Model Inter-comparison Project 5 (CMIP5). Indeed, different climate models in the group of CMIP5 lead to

different simulation results. However, all climate models are able to respond to radiative forcing because of greenhouse gas emissions and aerosols, which may change radiation patterns. The group of CMIP5 models share some important common features, which provide a legitimate basis for their application of studying climate change. These features can be summarized as the following [11]:

- a) Ability to respond to radiation alteration.
- b) Ability to capture the effect of volcanic eruptions and change the energy balance of the Earth.
- c) Ability to measure the radiation absorbed and reflected through the surface or atmosphere.
- d) Ability to evaluate the ocean and atmosphere dynamics considering that momentum is transferred from one media to another.
- e) Ability to capture the effect of greenhouse gases and aerosol on the Earth climate, sea ice, and polar ice sheets.
- f) Ability to show different feedbacks like the change in the amount of CO<sub>2</sub> absorption or emission from land or ocean and also, the relationship and interaction between clouds and water-vapor as a result of climate change.

### **2.1.2. Future projections under climate change conditions**

Various future climate condition scenarios are modeled by considering various economic, demographic, technologic, and lifestyle trends according to which future climatic conditions are predicted [12]. They provide insights to mitigate the impact of climate change for different possible future scenarios [13].

#### **2.1.2.1. Special report on emissions**

The Special Report on Emission Scenarios (SRES) has been published by the IPCC in 2000. Various scenarios have been described in this report for projecting future climates by taking into consideration different levels of GHG emissions. The SRES future scenarios have been used in the Third and Fourth Assessment Report of the IPCC, also called TAR and AR4 and have been published in 2001 and 2007, respectively. SRES future scenarios are baseline scenarios which do not consider means for limiting GHG emissions [14]. Based on the development plans and future economic situations, six emission scenarios have defined and formulated namely A1F1, A1B,

A1T, A2, B1 and B2, [15]. The main features of the SRES emission scenarios are shown in Table 1. For instance, based on scenarios B1 and A1F1, the planetary temperature is expected to increase 1.1-2.9 °C and 2.4-6.4 °C to the year 2099, respectively [16].

Table 1. Description of SRES future scenarios [14,15,17]

Scenario	A1F1	A1B	A1T	A2	B1	B2
<b>Description</b>	An integrated world which can be categorized based on the type of energy used in the future: Fossil-fuels (Fossil intensive)			A world which is very inharmonious.	A world which is more integrated and friendly from an ecological point of view.	A world which is more divided and friendly from an ecological point of view.
<b>Economy</b>	The economy which is developing rapidly.			A regional economic development.	A growing economy like A1 with a fast-developing service and information sector.	The economy is growing intermediately.
<b>Population</b>	It assumes the population in 2050 to be 9 billion, which will then gradually decrease.			A world with constantly increasing population.	Fast growing world population which is expected to reach 9 billion in 2050, followed by a decrease thereafter	The population is increasing continuously, but at a slower rate than A2 emission scenarios.
<b>Technology</b>	New and more efficient technologies are rapidly emerging.			Slower change in technology compared to A1 scenario.	The availability and implementation of clean technologies and energies are reducing.	The technology is changing faster and is more fragmented in comparison to A1 and B1 emission scenarios.
<b>Lifestyle</b>	The world is becoming more converge and unique in terms of lifestyle and culture between the regions.			A world becoming increasingly independent and nations more reliant.	The economic, social and environmental stability have a global solution.	The economic, social and environmental stability have a local solution.

### 2.1.2.2. Representative concentration pathways

CMIP5 provides new pathways for projecting future climate. These new pathways are called Representative Concentration Pathways (RCPs) and provide four scenarios for various levels of greenhouse gas concentrations. The four pathways also refer to the amount of total radiative forcing that will be experienced until the year 2100. Radiative forcing is the cumulative measure of human emissions and GHGs from all sources expressed in Watts's per square meter. These four different climate scenarios have been labelled RCP2.6, RCP4.5, RCP6, and RCP8.5, and are based on change in the radiative forcing compared to pre-industrial conditions with the rate of +2.6, +4.5, +6.0, and +8.5  $\text{W/m}^2$ , respectively. The RCPs are determined based on socioeconomic information, which relies on various assumptions regarding technology, demography, policy and institutional futures [13]. Figure 1 displays the behavior of all future scenarios of RCPs. The main characteristics of the RCP future scenarios are shown in Table 2 which is based on the radiative forcing (Difference between the sunlight absorbed by the Earth and energy radiated back to space).

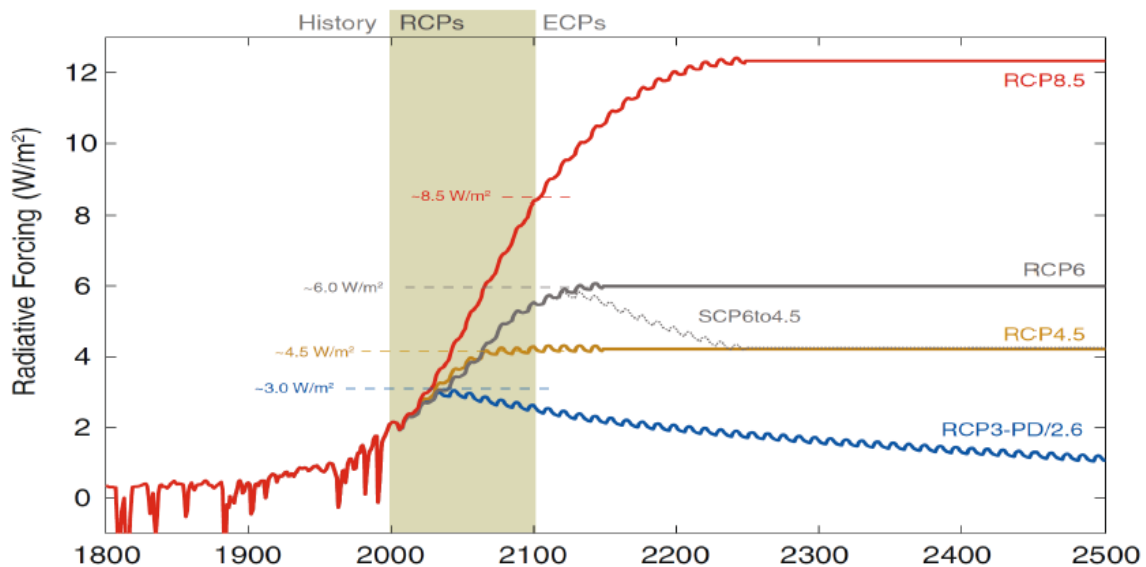


Figure 1: Representative concentration pathways based on radiative forcing [2]

Table 2: Description of RCP future scenarios [2,18]

RCP	RCP2.6	RCP4.5	RCP6	RCP8.5
<b>Developed by</b>	PBL Netherlands environmental assessment agency	Pacific northwest national laboratory in the U.S.	National institute for environmental studies in Japan	International institute for applied system analysis in Austria
<b>Comparable SRES</b>	None	B1	B2	A1F1
<b>Description</b>	A scenario which will reach about 3 W/m <sup>2</sup> (equal to 490 ppm CO <sub>2</sub> equivalent) till the year 2100, after which it will decrease to 2.6 W/m <sup>2</sup>	A scenario that will be stabilized with an overshooting 4.5 W/m <sup>2</sup> up to the year 2100 (~650 ppm CO <sub>2</sub> equivalent)	A scenario which will be stabilized with an overshooting of 6 W/m <sup>2</sup> (~850 ppm CO <sub>2</sub> equivalent) to the year 2100	A scenario where the radiative forcing will increase at the beginning to the end leading to 8.5 W/m <sup>2</sup> (equivalent to 1370 ppm CO <sub>2</sub> equivalent) up to the year 2100 timeline
<b>Assumptions</b>	<ul style="list-style-type: none"> <li>•Declining use of oil</li> <li>•Low energy intensity</li> <li>•A world population of 9 billion by the year 2100</li> <li>•Use of croplands increase due to bio-energy production</li> <li>•More intensive animal husbandry</li> <li>•Methane emissions reduced by 40%</li> <li>•CO<sub>2</sub> emissions stay at today's level until 2020, then decline and become negative in 2100</li> <li>•CO<sub>2</sub> concentrations peak around 2050, followed by a modest decline to around 400 ppm by 2100</li> </ul>	<ul style="list-style-type: none"> <li>•Lower energy intensity</li> <li>•Strong reforestation programs</li> <li>•Decreasing use of croplands and grasslands due to yield increases and dietary changes</li> <li>•Stringent climate policies</li> <li>•Stable methane emissions</li> <li>•CO<sub>2</sub> emissions increase only slightly before decline commences around 2040</li> </ul>	<ul style="list-style-type: none"> <li>•Heavy reliance on fossil fuels</li> <li>•Intermediate energy intensity</li> <li>•Increasing use of croplands and declining use of grasslands</li> <li>•Stable methane emissions</li> <li>•CO<sub>2</sub> emissions peak in 2060 at 75% above today's levels, then decline to 25% above today</li> </ul>	<ul style="list-style-type: none"> <li>•The future without policy changes of reducing the emissions</li> <li>•Three times today's CO<sub>2</sub> emissions by 2100</li> <li>•The rapid increase in methane emissions</li> <li>•Increased use of croplands and grassland which is driven by an increase in population</li> <li>•A world population of 12 billion by 2100</li> <li>•The lower rate of technology development</li> <li>•Heavy reliance on fossil fuels</li> <li>•High energy intensity</li> <li>•No implementation of climate policies</li> </ul>

### 2.1.3. Spatial and temporal downscaling of climate model projections

Although GCMs are able to represent the general behavior of global climate, their grid resolution is too coarse to be used at the local and/or regional scale. A typical spatial horizontal resolution is 300 km by 300 km with a temporal resolution of 24 hours. However, impact assessment needs to be done at a much finer spatiotemporal resolution. The common method for addressing the mismatch between the scales in which GCM outputs are available and the scale in which impact assessment requires, is downscaling [19]. Downscaling is a method which increases the resolution of weather data from the large-scale GCMs to the local scale data (see Figure 2). There are two types of downscaling, spatial and temporal. As its name implies, spatial downscaling refers to distance and has 20 km to the point scale of resolution. Spatial downscaling can be divided into two main approaches namely dynamical and statistical downscaling. Dynamical downscaling refers to using regional climate models (RCM) and uses the GCM models as boundary conditions to increase the resolution. Moreover, the statistical downscaling refers to using the statistical mathematical methods to downscale the GCM or RCM to the point scale.

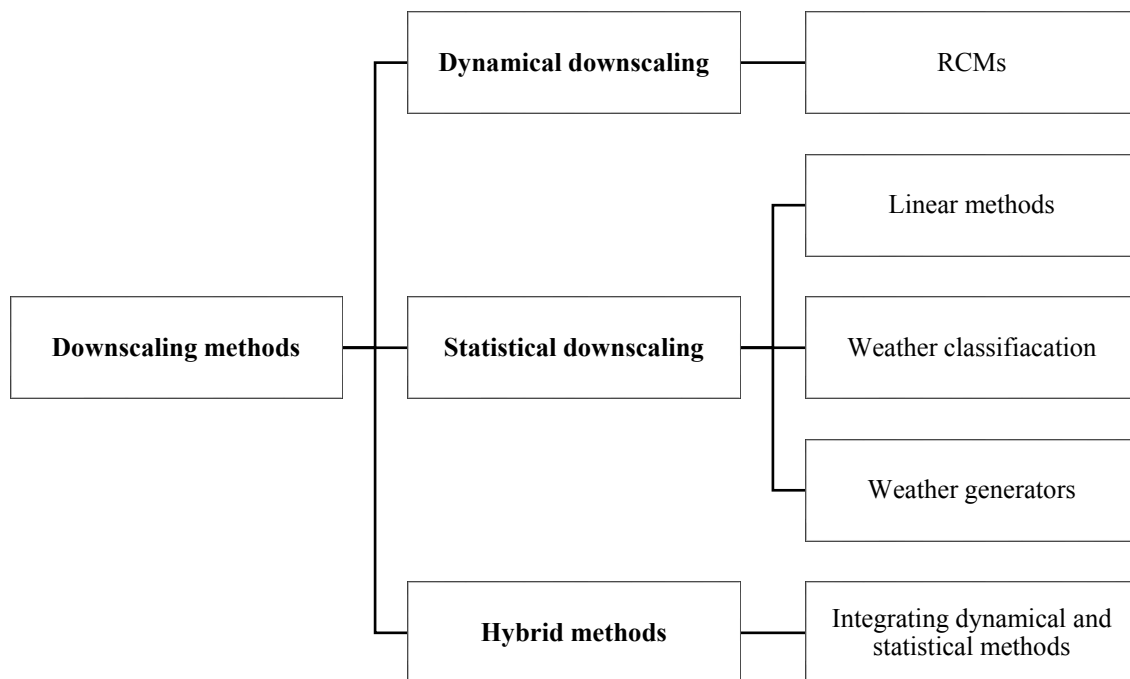


Figure 2. Different downscaling methods

### **2.1.3.1. Dynamical downscaling method**

Dynamical downscaling aims at improving the spatial and temporal resolution of GCMs through Regional Climate Models (RCMs). In this approach, GCM outputs provide the boundary conditions for the RCM. As a result, RCM is a nested modeling approach and therefore, RCM features are similar to GCM features but in a higher resolution, either between one to five km or 20 to 50 km [20]. One of the advantages of the RCMs is their ability to consider atmospheric processes and land cover changes that can affect climate change. One of the main disadvantages of RCMs is that they are computationally demanding and comparable in this demand to GCMs [10].

This method may entail a systematic bias; therefore, it is recommended to solve the equations and apply statistical corrections to have a better relationship between the observed data and the RCMs outputs [21]. Since the scale of RCMs are not in the point scale, they are not suitable for applying weather data in energy simulation software. For developing RCMs, high computational power, as well as sufficient financial resources, are required.

### **2.1.3.2. Statistical downscaling method**

The statistical downscaling method can give a relationship between different time scales as well as a relationship between two spatial resolutions. The advantages and disadvantages of these methods are shown in Table 3. In this section, two common statistical downscaling methods (i.e. morphing and bias correction) are presented in detail.

Table 3. Advantages and disadvantages of downscaling methods [10,22–26].

<b>Methods</b>	<b>Advantages</b>	<b>Disadvantages</b>
<b>2. Statistical downscaling</b>	<ul style="list-style-type: none"> <li>• Can produce the weather data in a very large resolution or in the local stations.</li> <li>• Can downscale several kinds of variables.</li> <li>• Since it is computationally inexpensive, more than one or two scenarios and GCMs can be used.</li> <li>• Suitable when computational equipment is limited.</li> <li>• Higher simulation speed than dynamical downscaling.</li> <li>• Has different methods which make it possible to apply statistical method for different goals, locations and case studies.</li> <li>• The software and methods are easily available, and their analysis is easy.</li> </ul>	<ul style="list-style-type: none"> <li>• Always considers constant relationship between the GCMs or RCMs and the observational data during the climate change periods.</li> <li>• Requires high quality daily observational data which may be unavailable for some areas.</li> <li>• Sensitive to GCMs or their bias where the latter can affect statistical downscaling.</li> <li>• Some methods are unable to produce daily or hourly data which is necessary for impact assessment on energy systems point of view.</li> </ul>
<b>2.1. Linear methods</b>	<ul style="list-style-type: none"> <li>• Easy to apply and interpret.</li> <li>• Can downscale all variables.</li> </ul>	<ul style="list-style-type: none"> <li>• It does not perform well for extreme events.</li> <li>• Only one relationship can be made between the input and output.</li> <li>• Data should be normally distributed.</li> <li>• When extrapolating, the method assumes that the relationship between regional and global climate is unchanged.</li> <li>• The results are highly affected (more than the other methods) by the duration of the measured data.</li> </ul>
<b>2.2. Weather classification</b>	<ul style="list-style-type: none"> <li>• Finds a relationship between large scale and station scale, so it can downscale the data to the surface.</li> <li>• Applicable for both non-normally and normally distributed data.</li> </ul>	<ul style="list-style-type: none"> <li>• Requires an extra step (data classification) compared to other methods.</li> <li>• Requires a large amount of data (30 years to be more reliable), and high computational capacity for calculation.</li> <li>• Cannot produce data without the historical data.</li> <li>• Analog method assumes similar climate conditions have similar socio-economic condition.</li> <li>• Analog method needs data such as population growth and technological advance, etc.</li> <li>• It should always be calibrated since it may fail if there are missing data</li> </ul>

---

### 2.3. Weather generator

- Wet and dry periods can be calculated.
  - Able to predict more than one possible future weather data, so it is possible to have all possible future scenarios.
  - Able to produce several series from the GCMs that are suitable for assessing the uncertainty.
  - Daily (or even hourly) weather data can be produced.
  - Most of the time the variables are stable and consistent.
  - El Nino and La Nina phenomena can be considered.
  - The method is computationally inexpensive.
  - The relationship between the variables can be considered.
  - Was commonly used for producing current data.
  - Requires large amount of data and if it misses the data, it will fail.
  - None of the weather generators can check the coherency between the variables (e.g. some predictions are unreasonable such as high insolation in a rainy day).
  - Several time series should be produced for statistical simulations.
  - Fails if climate change has low frequency.
  - Needs long and high quality observational weather data for validation, etc.
  - When there is no air conditioning system the statistical features should be considered constant.
  - Assumes constant relationship between the large and local scales during the climate change period.
  - All the realizations are affected by the quality of GCMs.
  - The produced data are discrete time instead of transient.
  - Often normally distributed data for the maximum and minimum temperature are used and produced (e.g. LARS-WG).
-

### 2.1.3.2.1. *Morphing Method (Delta Method)*

The Delta method or the Morphing method is a linear method of statistical downscaling which has been used in several impact assessment studies for spatial and temporal downscaling [27–29]. This method can essentially be carried out in three ways:

1- Shifting the present data by adding the predicted data, which is a monthly mean:

$$x = x_0 + \Delta x_m \quad (1)$$

where  $x$  is the future data,  $x_0$  is the present data, and  $\Delta x_m$  is the absolute monthly change.

2- Stretching present hourly data with monthly predicted data:

$$x = a_m x_0 \quad (2)$$

where  $a_m$  is the coefficient obtained from the GCM. The stretching method is also appropriate for downscaling of wind data.

3- Combination of ‘shift’ and ‘stretch’ of present data where the data shift by adding the predicted value (which is monthly) and then is stretched by the coefficient obtained from the GCM [19]:

$$x = x_0 + \Delta x_m + a_m (x_0 - \langle x_0 \rangle) \quad (3)$$

where  $\langle x_0 \rangle$  is the monthly mean of  $x_0$  and  $a_m$  is the coefficient obtained by the variances of  $\Delta x_m$ ,  $x_0$ , and  $\langle x_0 \rangle$ . This combination method uses mostly the morphing of dry bulb temperature from the GCM data to predict the maximum, minimum and the average temperatures of the data in a very high resolution [19]. It can also be used for the morphing of test reference year (TRY) and design summer year (DSY) weather data files [19]. Several morphing equations have been developed [19,27,30]. However, it cannot remove all the existing bias between the GCM historical and observation data.

### 2.1.3.2.2. *Bias correction*

The bias correction downscaling method has received considerable attention [31,32]. The most significant benefit of this mathematical approach is that it is straightforward and fast. This can be desirable especially for large weather datasets (e.g. for 30 years and more). It comprises the following steps. First, the gridded observation parameters are aggregated to the GCM grid scale which has a resolution of nearly 200 km. Then, using the quantile mapping (QM), bias in the GCM

data is removed [33]. The QM method is defined based on the one-by-one mapping between the cumulative distribution functions (CDF) of the historical GCM data and the observed data. Figure 3 shows the procedure for performing the QM method.

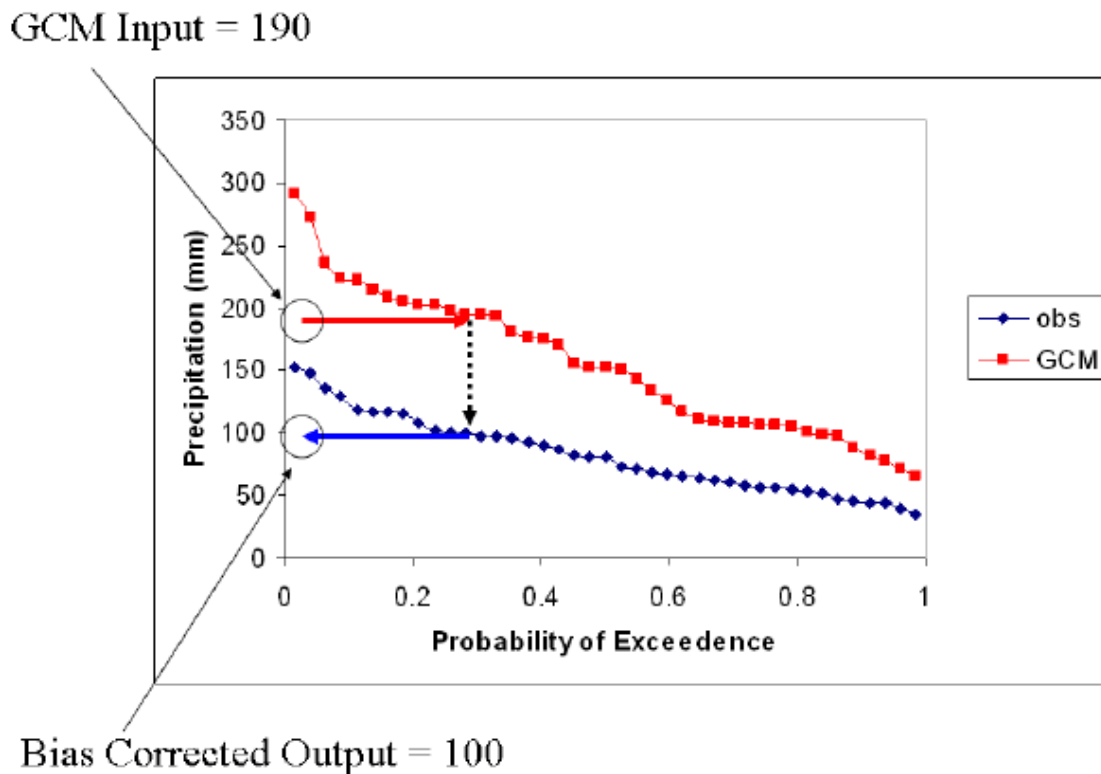


Figure 3: The procedure of bias correction quantile mapping downscaling method [31]

To perform QM, monthly data is separated such that all the data belonging to each month is placed in one matrix and CDF values are calculated for each month matrix. For the CDF of each parameter in a specific month, a CDF with the same probability in the same period is obtained from the observed data. This new value would be the bias-corrected GCM for that specific month. It should be noted that the method assumes the bias to be constant. Besides, all the natural existing features or nature of the extremes in the observation data are transferred to the GCM data to remove all biases.

The QM method is computationally efficient and can consider small changes or higher orders of moments [31,34–36]. Based on the stationary (or time-invariant) assumption, the QM method can be applied to any time period of interest [37–40]. However, given a stationary assumption, this method can result in a change in the trend of the raw model [36]. Several studies

reported that the QM method is one of the most preferable downscaling methods [31,36,37,41]. The standard non-parametric QM method was used in some studies to maintain the trend of the raw model projection [42–45]. Moreover, Burger et al. [46] applied the trended QM method which was found to be appropriate for the monthly data; however, the stationary assumption was considered for the daily data. Besides the above mentioned method, a new downscaling method was developed and named the quantile delta mapping [46,47]. This process is not constrained by the stationary assumption and requires further investigation prior to implementation.

Li et al. [48] developed a mathematical code for the bias correction method to significantly simplify it. Similarly, several bias correction methods have been developed [37,48–50]. Bias correction is reported to work well for hydrological and climate change impact assessments [41,51–54]. Comparing different downscaling methods, it was found that the bias correction method yields superior results compared to the other methods especially for hydrological projects and for datasets involving precipitation [36,55]. Furthermore, the bias correction method can improve the accuracy of the mean, standard deviation and other statistical parameters [35].

Finally, among all bias correction downscaling methods, quantile mapping has proven to be the only method to be able to correct all statistical properties, such as mean, standard deviation, quantile etc., whereas other bias correction methods can only correct the daily mean values [56]. Moreover, this is one of the simplest and the most straightforward methodologies to match the statistical properties.

The aforementioned merits are the main reasons for applying quantile mapping bias correction for spatial downscaling in this project.

### **2.1.3.3. Hybrid downscaling methods**

This method can include more than one downscaling method. For instance, the dynamical downscaling can be applied followed by statistical downscaling to generate the local scale weather data.

#### **2.1.3.3.1. *Statistical downscaling model (SDSM)***

The statistical downscaling mode performs multiple linear regressions to downscale the weather data spatially and temporally and converts them to daily or hourly data [57]. This method

requires locally observed daily data and large-scale data means [58]. This method can generate statistical results such as variance and frequencies among others [58].

**2.1.3.3.2. Bias-corrected spatial disaggregation (BCSD)**

This method is preferable for hydrological projects, and comprises of two steps:

- **Bias correction:** First a comparison is made between the past GCM weather data and observed weather data in the same spatial scale and time period. Thereafter, future weather data are generated using the GCM data.
- **Weather generation:** In different temporal and spatial scales, there is one condition that the variables of predictor and predictand should be the same which BCSD transfers the features of predictor to predictand. BCSD is computationally efficient [59]. Examples of institutions that used BCSD for producing a set of downscaled climate weather data for the entire globe include The World Bank, The Nature Conservancy, Climate Central, and Santa Clara University (available in their climate change knowledge portal) [60].

**2.2. Impact of climate change on building energy consumption**

In this section, the studies that have assessed the impacts of climate change on the general behavior of the energy loads are presented based on their investigated climate. A summary of the studies indicating their investigated climates (based on ASHRAE 169-2013, Table 4) is presented in **Error! Reference source not found.**

Table 4: Description of climate zones based on ASHRAE 169-2013[61]

<b>Zone</b>	<b>Description</b>	<b>Zone</b>	<b>Description</b>
0A1	Extremely hot humid	4A10	Mixed humid
0B2	Extremely hot dry	4B11	Mixed dry
1A3	Very hot humid	4C12	Mixed marine
1B4	Very hot dry	5A13	Cool humid
2A5	Hot humid	5B14	Cool dry
2B6	Hot dry	5C15	Cool marine
3A7	Warm humid	6A16	Cold humid
3B8	Warm dry	6B17	Cold dry
3C9	Warm marine	718	Very cold
		819	Subarctic/arctic

Table 5. The GCM models, future scenarios, downscaling methods, energy tool, and the region of a case study that have been used in previous studies

Year (Ref)	GCM	Future scenario	Downscaling	Periods	Energy tool Parameters	Weather parameters	Region	Climate zone	Building characteristics
[62] 2008	• UKCIP02	• B1 • B2 • A2 • A1FI	• Morphing	• July 2006 • 2050s	TRNSYS	• Ambient temperature • Wind speed • Wind direction • Atmospheric pressure	<b>UK:</b> Manchester	5A	Faraday Tower, University of Southampton (21.6 m × 21.6 m covering 10 stories).
[63] 2010	Average of: • CCCMA • CNRM • CSIRO-MK3.5 • GISS-AOM • GISS-EH • IAP-FGOALS • IPSL-CM4 • MICRO-M • MRI-GCM232	• A1B • A1F1 • B1	• OZClim (weather generator)	• 1990 • 2010 • 2030 • 2050 • 2070 • 2090	AccuRate <sup>6</sup>	• Dry bulb temperature • Relative humidity • Global solar radiation	<b>Australia:</b> Alice Springs Darwin Hobart Melbourne Sydney	2B 0A 4A 3A 3A	A modern detached brick veneer residential house was used to achieve 2-star, 5-star and 7-star energy efficiency in the five cities.
[64] 2011	• MIRCO3-2-MED <sup>1</sup>	• A1B • B1	• Morphing	• 2011-2030 • 2046-2065 • 2080-2099	EnergyPlus	• Dry bulb temperature <sup>7</sup> • Precipitation • Global solar radiation <sup>8</sup> • Specific humidity	<b>China:</b> Hong Kong	1A	An office building, 40 stories high and fully air-conditioned with a plan view of 36 m × 36 m. Also, A typical low-rise residential building model, which is common in the U.S.
[65] 2012	• MAGICC • SCENGEN	• P50 <sup>2</sup>	• MAGICC/SCENGEN v. 5.3 (weather generator)	• 1961-1990 • 2025 • 2050 • 2075	Degree day method	• Temperature	<b>Iran</b> <sup>10</sup>	3B	A typical Iranian residential building.
[66] 2012	• MIROC3.2_H	• A1B • B1	• PCA <sup>3</sup>	• 1971-2000 <sup>4</sup> • 1979-2008 <sup>5</sup> • 2001-2100	Combining Visual DOE 4.1 and regression method	• Dry bulb temperature • Wet bulb temperature • Global solar radiation • Summer set-point temperature <sup>9</sup>	<b>China:</b> Beijing Harbin Hong Kong Kunming Shanghai	4A 7 1A 3C 3A	Fully air-conditioned office buildings.
[16] 2013	• HadCM3	• A2	• CCWorldWeatherGen (weather generator)	• 2020s • 2050s • 2080s	EnergyPlus	• Dry bulb temperature • Dew point temperature • Relative humidity	<b>UK:</b> Manchester	5A	Faraday Tower, University of Southampton (21.6 m × 21.6 m covering 10 stories).

						<ul style="list-style-type: none"> <li>• Global horizontal solar radiation intensity</li> </ul>			
[67] 2016	<ul style="list-style-type: none"> <li>• HadGEM2</li> </ul>	<ul style="list-style-type: none"> <li>• RCP2.6</li> <li>• RCP4.5</li> <li>• RCP6</li> <li>• RCP8.5</li> </ul>	<ul style="list-style-type: none"> <li>• RCM</li> <li>• Morphing</li> </ul>	<ul style="list-style-type: none"> <li>• 2050-2059</li> <li>• 2090-2099</li> </ul>	EnergyPlus	<ul style="list-style-type: none"> <li>• Dry bulb temperature</li> <li>• Relative humidity</li> <li>• Global solar radiation</li> </ul>	<b>Sweden:</b> Växjö	6A	Residential apartment with 1,420 m <sup>2</sup> area and 6 floors.
[68] 2016	<ul style="list-style-type: none"> <li>• HadCM3</li> </ul>	<ul style="list-style-type: none"> <li>• A2</li> </ul>	<ul style="list-style-type: none"> <li>• CCWorldWeatherGen (weather generator)</li> </ul>	<ul style="list-style-type: none"> <li>• 2020</li> <li>• 2050</li> <li>• 2080</li> </ul>	EnergyPlus	<ul style="list-style-type: none"> <li>• Temperature</li> <li>• Wind speed</li> <li>• Relative humidity</li> <li>• Precipitation</li> </ul>	<b>Brazil:</b> Belém Curitiba Florianópolis	0A 3A 2A	A single-family social house with the total area of 38.16 m <sup>2</sup> .
[27] 2017	<ul style="list-style-type: none"> <li>• HadCM3</li> </ul>	<ul style="list-style-type: none"> <li>• A2</li> <li>• A1F1</li> </ul>	<ul style="list-style-type: none"> <li>• Morphing</li> </ul>	<ul style="list-style-type: none"> <li>• 2040-2069</li> </ul>	TAS	<ul style="list-style-type: none"> <li>• Air temperature</li> <li>• Relative humidity</li> </ul>	<b>USA:</b> Chicago Miami Philadelphia Phoenix	5A 1A 4A 2B	A typical low-rise residential building (3-story of 14 m × 8 m with 336 m <sup>2</sup> total area) and a typical 6-story office building (40 m × 20 m).
[69] 2017	<ul style="list-style-type: none"> <li>• CMNR CM5</li> <li>• HadGEM2-AO</li> <li>• HadGEM2-ES</li> <li>• MPI-ESM-LR</li> <li>• IPSL-CM5A-LR</li> </ul>	<ul style="list-style-type: none"> <li>• RCP2.6</li> <li>• RCP8.5</li> </ul>	<ul style="list-style-type: none"> <li>• CCWorldWeatherGen (weather generator)</li> </ul>	<ul style="list-style-type: none"> <li>• 2020s</li> <li>• 2050s</li> <li>• 2080s</li> </ul>	HEED v. 4.0. Solar-5	<ul style="list-style-type: none"> <li>• Dry bulb temperature</li> </ul>	<b>Lithuania:</b> Kaunas	6A	A 3-story residential building with 12 apartments, with 532 m <sup>2</sup> total area.
[28] 2017	<ul style="list-style-type: none"> <li>• HadCM3</li> <li>• CESM1</li> </ul>	<ul style="list-style-type: none"> <li>• A2</li> <li>• RCP2.6</li> <li>• RCP4.5</li> <li>• RCP8.5</li> </ul>	<ul style="list-style-type: none"> <li>• Morphing</li> </ul>	<ul style="list-style-type: none"> <li>• 2020–2089</li> </ul>	EnergyPlus	<ul style="list-style-type: none"> <li>• Dry bulb temperature</li> <li>• Relative humidity</li> <li>• Atmospheric pressure</li> <li>• Extraterrestrial horizontal radiation</li> <li>• Wind speed</li> <li>• Wind direction</li> <li>• Total sky cover</li> </ul>	<b>USA:</b> Akron Los Angeles Miami Phoenix Washington DC	5B 3B 1A 2B 4A	Total building area of 4,982.19 m <sup>2</sup> with 3 stories and 15 thermal zones in a medium-size office reference model.
[70] 2011	<ul style="list-style-type: none"> <li>• UKCP09</li> <li>• UKCIP02</li> </ul>	<ul style="list-style-type: none"> <li>• A1F1</li> <li>• A1B</li> <li>• B1</li> </ul>	<ul style="list-style-type: none"> <li>• Morphing</li> </ul>	<ul style="list-style-type: none"> <li>• 2020s</li> <li>• 2030s</li> <li>• 2050s</li> <li>• 2080s</li> </ul>	EnergyPlus	<ul style="list-style-type: none"> <li>• Maximum dry bulb temperature</li> <li>• Minimum dry bulb temperature</li> <li>• Annual mean dry bulb temperature</li> </ul>	<b>UK:</b> Edinburgh London Manchester	5A 4A 5A	A 2-story building (main occupied area of 3,081.8 m <sup>2</sup> ) comprised of 25 zones including 14 main occupied zones (e.g. meeting rooms, classrooms, offices and a library).
[71] 2016	<ul style="list-style-type: none"> <li>• JMA</li> <li>• Soga</li> </ul>	<ul style="list-style-type: none"> <li>• A2</li> </ul>	<ul style="list-style-type: none"> <li>• RCM20 developed by JMA (RCM)</li> </ul>	<ul style="list-style-type: none"> <li>• 1981-2000</li> <li>• 2031-2050</li> </ul>	TAS	<ul style="list-style-type: none"> <li>• Air temperature</li> <li>• Absolute humidity</li> </ul>	<b>Japan:</b> Naha Sapporo	2A 5A	An 8-story office building with dimensions of 33.6 m × 24.6 m ×

				• 2081-2100		• Solar radiation • Wind direction • Wind velocity	Tokyo	3A	3.6 m (3.8 m high at ground floor).
[72] 2012	• HadCM3	• A2	• Morphing	• 2020 • 2050	TRNSYS	• Dry bulb temperature • Horizontal radiation • Relative humidity • Wind speed	<b>Canada:</b> Montreal <b>USA:</b> Massena	6A 6A	The building is divided vertically in three apartments of 97 m <sup>2</sup> each and one mechanical/storage room located in the basement.
[73] 2013	• ECHAM5 • CCSM3 • CNRM • HadCM3 • IPSL	• A1B • A2 • B1	• RCA3 (RCM)	• 1980-2000 • 2081-2100	BETSI	• Dry bulb temperature • Global horizontal Radiation	<b>Sweden:</b> Stockholm	6A	1400 representative residential buildings, distributed in 30 municipalities with different populations and climate conditions.
[30] 2014	• HadCM3	• A1F1 • A2 • B1	• Morphing	• 2020 • 2050 • 2080	EnergyPlus	• Dry bulb temperature • Global horizontal solar radiation • Relative humidity • Diurnal temperature variation • Wind speed	<b>USA:</b> Atlanta Baltimore Chicago Colorado Springs Houston Las Vegas Madison Miami Minneapolis Nashville New York City Portland (ME) San Diego San Francisco Seattle	3A 4A 5A 5B 2A 3B 5A 1A 6A 3A 4A 6A 3B 3C 4C	Apartment, hospital, hotel, single family house, medium office, small office, restaurant, mall and school with the area between 146 and 16,886 m <sup>2</sup> .
[29] 2016	• MIRCO3.2- MED	• A1B • A2 • B1	• Morphing	• 2000s • 2020s • 2050s • 2080s	EnergyPlus	• Dry bulb temperature • Relative humidity • Global solar radiation	<b>Taiwan:</b> Taipei	2A	Four typical residential units with indoor floor area of around 100 m <sup>2</sup> and a ceiling height of 3.5 m.
[74] 2016	• IAG-USP <sup>11</sup>	• RCP8.5	• RCM	• 1975-2005 • 2015-2044 • 2045-2074 • 2076-2096	TAS	• Dry bulb temperature • Relative humidity	<b>Brazil:</b> Sao Paulo	2A	The living rooms of three dwellings.
[75] 2008	• 23 different GCM models	• A1B	• Morphing	• 1991-2000 • 2045-2054	DOE-2	• Daily maximum surface temperature • Daily minimum surface temperature	<b>Canada:</b> Calgary Vancouver <b>USA:</b>	7 4C	23 typical commercial and 3 residential buildings.

							Billings	6B	
							Boulder	3B	
							Los Angeles	3B	
							Phoenix	2B	
							Portland (OR)	4C	
							Sacramento	3B	
							Salt Lake City	5B	
							San Francisco	3C	
[76] 2016	• HadCM3	• A2	• CCWorldWeatherGen (weather generator)	• 2020 • 2050 • 2080	Energy Plus	• Dry bulb temperature • Global solar radiation	<b>Portugal:</b> Lisbon	3A	District of Alvalade with 810 buildings.
[77] 2011	• ECHAM5/MP I-OM	• A1B	• CCLM (RCM)	• 1960-2060	Degree day method	• Temperature	<b>Germany</b>		Different types of residential building stock.
[78] 2017	• MRI-CGCM3	• RCP4.5	• Regression model	• 1960-2010 • 2015-2039	SIMEDIF	• Dry bulb temperature • Relative humidity	<b>USA:</b> Santa Rosa	3C	10 compact single dwellings.
[79] 2015	• CSIRO	• A1B • B1	• Morphing	• TMY 2070	AccuRate	• Maximum dry bulb temperature • Minimum dry bulb temperature • Global solar radiation	<b>Australia:</b> Adelaide	3B	A conventional residential brick veneer house having one floor with living area of 204.5 m <sup>2</sup> , a garage with area of 35.5 m <sup>2</sup> , 4 bedrooms, 2 bathrooms and 1 kitchen
[80] 2010	• MIROC3.2-H	• A1B • B1	• WCRP (RCM)	• 1979-2008 • 2009-2100	Regression model	• Dry bulb temperature • Global solar radiation	<b>China:</b> Hong Kong	2A	Residential buildings with 20 stories or more
[81] 2015	• GFDL	• A2	• PRIMA (RCM) • Analogs method	• 2004 • 2052 • 2089	BEND	• Daily precipitation • Maximum dry bulb temperature • Minimum dry bulb temperature	<b>USA</b> <sup>12</sup>		26,000 representative buildings with different types, sizes, vintages, and characteristics.

<sup>1</sup> Selected based on comparing the following models: BCCR: BCM2 (Norway), CSIRO: MK3 (Australia), INM: CM3 (Russia), NASA: GISS AOM (USA), MIROC3-2 H (Japan), MIRCO3-2 MED (Japan)

<sup>2</sup> Average of A1, A2, B1, and B2

<sup>3</sup> A statistical method for finding the relationships between different variables

<sup>4</sup> For four cities in mainland China

<sup>5</sup> For Hong Kong

<sup>6</sup> Made by coupling of two different software

<sup>7</sup> Monthly mean, maximum and minimum air temperature change

<sup>8</sup> Monthly mean

<sup>9</sup> A variable Z which was a function of the dry bulb temperature, wet bulb temperature and global solar radiation

<sup>10</sup> 43 zones of Iran with different climate conditions

<sup>11</sup> Combination of the RCM system (RegCM4), supplied by the Geophysical Fluid Dynamics Laboratory (GFDL) global model

<sup>12</sup> EIC (the eastern interconnection)

### 2.2.1. Zone 0: Extremely hot

Few studies have analyzed the effects of climate change on energy loads in buildings located in this zone. Such buildings only require cooling due to the high ambient temperature. As presented in Table 4, zone 0 includes two subzones based on the humidity. Nevertheless, to the best of the authors' knowledge, no study has been conducted for zone 0B. In addition, the available studies have focused solely on residential buildings, confirming the need for future studies in this thermal zone.

Using the same weather generator downscaling method, two cities located in Australia and Brazil have been analyzed based on two different emission scenarios. Therefore, it is not acceptable to compare the results on the same basis. Table 6 shows a summary of the results. Overall, for the year 2100 all the changes are justifiable by description of the emission scenarios, however in the year 2050 results for Belem City in Brazil shows inharmonious results. In other words, the results surpass the expected emissions based on the studied emission scenarios. This will require further investigations in the future in this zone.

Table 6: Summary of cooling results for Zone 0A

Year	Australia [63]			Brazil [68]
	B1	A1B	A1F1	A2
2020	-	-	-	43%
2050	39%	48%	57%	70%
2100	61%	90%	135%	111%

### 2.2.2. Zone 1: Very hot

Similar to zone 0, to the best of the authors' knowledge, there has been no study for zone 1B. Again, this emphasizes lack of studies for very/extremely hot and dry regions. Existing studies for zone 1A (see Table 7) investigated the effect of climate change on the energy loads for a series of buildings in Hong Kong, China (two studies [64,66]) and Miami, USA (three studies [27,28,30]). While the majority of the studies used morphing downscaling, one study used principal component analysis (PCA) [66]. The two studies in China utilized the same emission scenarios (i.e. A1B as well as B1), however, the downscaling methods employed were different.

One study [66] only considered an office building whereas the other [64] studied the impacts on a residential building as well as offices. Analysis of the results (Figure 4) indicates that the cooling load will continuously increase in Hong Kong for both residential and office buildings. Interestingly, the amount of increase for B1 scenario was found to be more than A1B during the 2011-2030 period, whereas for the later periods, A1B resulted in higher cooling loads. This is justifiable by the behavior of the SRES emission scenarios, which for the period of 2011-2030 is higher for B1 compared to A1B1. However, as of 2030, the reversed trend is observed.

Table 7: Summary of heating and cooling load results for Zone 1A\*

<b>Hong Kong, China</b>					
<b>Type</b>	<b>Emission scenario</b>	[66]	[64]		
		<b>2001-2100</b>	<b>2011-2030</b>	<b>2046-2065</b>	<b>2080-2099</b>
Office	A1B	Slightly higher	C: 2.6%	C: 7.8%	C: 14.3%
	B1	C: 14.1% H: -23.6%	C: 2.8%	C: 6.5%	C: 9.9%
Residential	A1B	-	C: 3.7%	C: 13.4%	C: 24.0%
	B1	-	C: 3.9%	C: 10.9%	C: 16.5%
<b>Miami, USA</b>					
			[27]	[28]	
			<b>2040-2069</b>	<b>2080</b>	
Office	A1F1	-	-	C: 16.4% H: -23.7%	-
	A2	-	-	C: 12.4% H: -18.1%	T: 12.8%
	RCP8.5	-	-	-	T: 11.2 %
Residential	A1F1	-	-	C: 36.4%	-
	A2	-	-	C: 26.6%	-

\* C: cooling load, H: heating load, T: total load

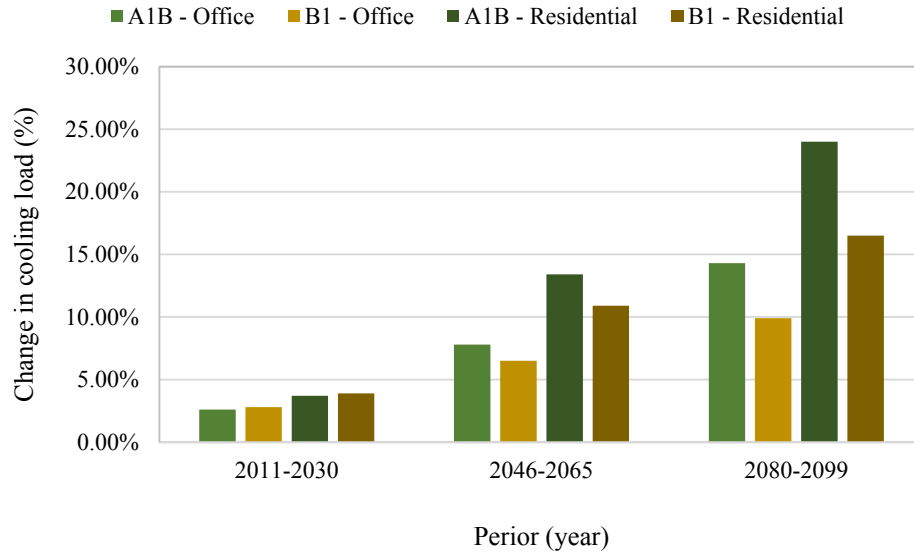


Figure 4: Summary of results for Hong Kong, China

### 2.2.3. Zone 2: Hot

The studies in this zone (Table 8 and Table 9) were spread around the world, investigating both 2A (six studies [29,30,68,71,74,80]) and 2B (four studies [27,28,75]) subzones. Overall, morphing downscaling method and EnergyPlus software were commonly used in these studies. Interestingly, all the studies used SRES emission scenarios, except for one which used RCP8.5 [28], the worst case scenario. This shows that there is a lack of studies in this zone evaluating the performance of buildings using more moderate RCP future scenarios.

Table 8: Summary of heating and cooling load results for Zone 2

Type	Emission scenario	2040-2069	2009-2100	2020	2040	2050	2080	2090	2100
Office	A2				C: 9.2% [71]			C: 16.5% [71]	
Residential	A2			H: -64.0% [68]		H: -82.0% [68]	H: -98.0% [68]		
	Average of A1B, A2, B1			C: 31% [29]		C: 59% [29]	C: 82% [29]		
Office	A1F1	C: 9.2% H: -13.5% [27]					-		
	A2	C: 6.6% H: -9.5% [27]					T: 14.0% [28]		
	RCP8.5	-					T: 15.4% [28]		
Residential	A1F1	C: 24.2% H: -48.9% [27]					-		
	A2	C: 17.4% H: -35.4% [27]							

Table 9: Summary of heating and cooling load results for Zone 2

Type	Emission scenario	2040-2069 [27]	2080 [28]
Office	A1F1	C: 9.2% H: -13.5%	-
	A2	C: 6.6% H: -9.5%	T: 14.0%
	RCP8.5	-	T: 15.4%
Residential	A1F1	C: 24.2% H: -48.9%	-
	A2	C: 17.4% H: -35.4%	

Four studies in the cities of Florianopolis (Sweden), Taipei (Taiwan), and Phoenix (USA) on cooling, heating and total load have been done based on the A2 emission scenario and considering a residential building as a case study. The results show that the cooling load in 2020, 2050, and 2080 in the city of Florianopolis (Sweden) will increase by 70%, 120%, and 197% respectively, while in the city of Phoenix (USA) will rise by 17.4% in 2040-2069. By observation, it becomes evident that there is a substantially large difference between the obtained in the

aforementioned studies. This difference can be justified by the base year against which these changes have been compared to, which in [68] is the year 2016 while [27] used a typical meteorological year (TMY). While the difference in the base year can be a cause of the discrepancy, the different methods for downscaling, disaggregation, and the energy simulation software are also likely to have influenced the results. Moreover, the total energy in 2080 by the same emission scenario and type of building in Phoenix (USA) will grow by 14%.

In addition, in the cities of Alice Springs (Australia), and Phoenix (USA), the heating and cooling load based on the A1F1 emission scenario in a residential building has been analyzed as a case study. The heating and cooling loads in the city of Alice Springs (Australia) [63] in 2050 will change by -65% and +84% and in the year 2100 will change by -94%, and +283%, respectively. Moreover, in Phoenix (USA) [27] in 2040-2069 with the same emission scenario and building type, the heating and cooling load will change by +24.2%, and -48.9%, respectively. By simple observation, there is a substantial difference between the obtained results, especially regarding the cooling loads.

#### **2.2.4. Zone 3: Warm**

All subsections of zone 3 have been studied in 12 cities around the world including Melbourne and Sydney (Australia), Shanghai and Kunming (China), Curitiba (Brazil), Tokyo (Japan), Lisbon (Portugal), Los Angeles, Boulder, Sacramento, San Francisco, and Santa Rosa (USA). This zone has received the highest number of investigations and has employed the largest variety of methods. Overall, the weather generator downscaling method and the Energy Plus software was frequently used in these studies. Interestingly, all the studies used SRES emission scenario, except [28] which used RCP2.6, RCP4.5, RCP8.5, and [82] which only used RCP4.5.

According to the obtained results, [63] shows an increase of 90% and 208% in cooling load and a decrease of 36% and 60% in heating load for 2050 and 2100, respectively in the residential buildings. Evidently, the rise in the cooling load is more considerable than the decrease in the heating load. Surprisingly, [66] shows an increase of 11.4% in cooling load and a decline of 55.7% in heating load during the period of 2001-2100 in office buildings. This indicates that the decrease in the heating load is more than the rise in the cooling load, which is in contradiction to [63]. Furthermore, the only study that has analyzed the heating and cooling load based on A2 emission

scenario in residential building is [68], and its obtained results show that the heating load in 2020, 2050, and 2080 will decrease by 63%, 79%, and 94%, respectively. The cooling load will also increase by 113%, 210%, and 400%, respectively. Moreover, [71] has only evaluated the cooling load in office buildings in 2040 and 2090, and the results show that the cooling load will increase by 16.6% and 24.7%, respectively. This shows that the increase in the cooling load in office buildings is much less than in residential buildings. Moreover, in both residential and office buildings the rise in the cooling load in the third period is much more than those during the other periods. Based on RCP8.5 [28], the total energy load in office buildings will increase by 14.4% and based on RCP4.5 [82], and the cooling load will rise by 14.6% in 2015-2039 in residential buildings.

#### **2.2.5. Zone 4: Mixed**

Similar to zones 0 and 2, to the best of the authors' knowledge, there has been no study on zone 4B. This emphasizes the lack of studies in mixed dry regions. Zone 4 has been studied in 6 different cities such as Hobart (Australia), Beijing (China), Philadelphia (USA), Washington (USA), Vancouver (Canada), Portland (OR,USA). The majority of the studies in this zone have applied the morphing method in order to downscale and DOE energy simulation software for simulation. Furthermore, most of the studies used SRES emission scenario, except for one which used RCP2.6, RCP4.5, and RCP8.5 [28].

According to the obtained results from [63], in 2050 and 2100 the cooling load will go up by 104%, and 275% respectively, and the heating load will fall by 25%, and 42% respectively in residential buildings. This proves that the increase in the cooling load is much more than decrease in the heating load for this zone. Conversely, [66] has shown that in the period of 2001-2100 the cooling load will increase by 20.4% and the heating load will decrease by 26.6%, which shows that the decrease of the heating load is larger than the increase of the cooling load, which contradicts [63]. Moreover, [21] has compared the results achieved by the residential and office buildings. The results indicate that in the period of 2040-2069, the cooling load will increase by 27% and 6.7% respectively for the residential and office buildings. This demonstrates that the increase in the cooling load for residential buildings is noticeably larger compared to the cooling loads of office buildings, which is similar to the obtained results from [68] and [71] in zone 3. In addition, based on [66] in 2050 and 2100 the cooling load will increase by 133% and 572%

respectively, while the heating load will decrease by 28% and 58%, respectively. However, the results from [27] in the period of 2040-2069 show less changes in cooling and heating loads compared to [63], which analyzed the heating and cooling loads in both residential and office buildings. The results from [27] indicate that the cooling load will increase by 35.2% and 9% in residential and office buildings, respectively and the heating load will decrease by 27.4% and 14.8%, respectively. Likewise, the rise in the cooling load and the decrease in the heating load in office buildings are smaller than the changes experienced in residential buildings. Moreover, in [27] an increase in the cooling load in residential buildings is more than the decrease in the heating loads, which directly contrasts the findings for office buildings. Overall, the aforementioned studies depict the significance of impact assessment studies on thermal performance of residential buildings.

#### **2.2.6. Zone 5: Cool**

Four studies have been done in zone 5 in the cities of Chicago (USA), Salt Lake City (USA), and Sapporo (Japan). Most of these studies have employed the morphing method for downscaling but two of them used TAS as the energy simulation software. Based on A1F1 emission scenario the [27] has concluded that for residential and office buildings during the 2040-2069 period the cooling load will increase by 24.8%, and 7%, respectively. In addition, [71] indicates that during 2040 and 2090 the cooling load will rise by 22.9%, and 31.8% for the office buildings, which is larger than the results suggested in the [27] offices. Interestingly, the cooling load in [30] will increase by 60% in 2080. This significant contradiction in the cooling loads results can be justified by the fact that using different downscaling and disaggregation methods yields different results, especially considering that both applied the same energy simulation software TAS. Furthermore, similar to previous studies, according to the A1F1 emission scenario during the 2040-2069, the heating and cooling loads of residential buildings is more heavily affected by climate change compared to office buildings. Moreover, the effect of climate change in residential buildings more strongly affects the cooling load than the heating load, which can be found to be the reverse for office buildings. The aforementioned results which are the same for all thermal zones can be obtained from [71] for zone 5.

### **2.2.7. Zone 6: Cold**

Zone 6 has been studied in 6 different cities of Vaxjo and Stockholm (Sweden), Kaunas (Lithuania), Montreal (Canada), Minneapolis and Billings (USA). The studies in this zone are spread around the world investigating both the 6A (five studies [30,67,69,72,73]) and 6B (one study [75]) subzones. In this zone there are few studies that used representative concentration pathways of [67] and [69] as a future scenario.

Based on RCP8.5, in 2050, [67] indicates the heating load will decrease by 20-26% and the cooling load will increase by 45-73%. Meanwhile, the total load has been investigated in [69], and in 2020, it will increase by 13.3-13.5% and in 2080 it will decline by 26.7-29.6%. This outcome was predictable based on the results of [67].

Based on the observed lack of study regarding the heating and cooling loads, it is important to be analyzing the loads in greater detail. Therefore, a more in-depth study into heating and cooling loads can be beneficial for specialists as well as engineers for more accurate mitigation.

### **2.2.8. Zone 7: Very cold**

Zone 7 has been investigated in two cities of Harbin (China), and Calgary (Canada) and the common morphing method was used for downscaling. Moreover, there are a few studies that used TRNSYS such as [66], which indicates that during 2001-2100 the cooling load will increase by 18.5% and the heating load will drop by 22.3%, whereas [75] reports that the total load will increase by 2-10% for commercial buildings and 5-12% for residential buildings. This is in direct contradiction with [66].

### **2.2.9. Zone 8: Subarctic/arctic**

In recent years, the northernmost and southernmost arctic regions have suffered from severe temperature surges, extensive ice loss and lower snowfalls [83]. Nevertheless, there has been no study regarding the effect of climate change on the buildings in this zone, requiring further investigation.

### **2.3. Shortcoming of the existing literature**

A number of relevant studies into the impact of climate change on the thermal performance of buildings have been reviewed. The previous studies employed different methods for downscaling and disaggregation, including morphing method (delta method), regional climate models, weather generators, and regression models. These methods are either notably simplistic or extremely complex for spatial and temporal downscaling purposes, making them undesirable for real applications.

The main limitations of previous spatiotemporal downscaling are as follows:

- 1- Some of these methods are overly simplistic such as the delta method, which is unable to remove the bias of all existing statistical properties such as mean, standard deviation, quantile, etc. Moreover, the delta method can work with the normally distributed data and therefore it does not perform well when the data slightly deviates normal distribution, for example, when considering radiation in an unclear sky.
- 2- Some of the downscaling methods require high computational capacity, especially for large weather datasets like weather generators.
- 3- The literature review shows the lack of studies in the disaggregation portion of impact assessment on the thermal performance of buildings. There are a few studies that use weather classification. However, the applied method is based on the KNN (k-nearest neighbor) method which uses the Euclidean distance for data matching. When integrated with the quantile mapping bias correction, this method has a significant disadvantage of perturbing the quantile relationships made by quantile mapping. This disadvantage can reduce the compatibility between the downscaling of spatial and temporal resolutions.
- 4- Most of spatial and temporal downscaling methods suffer from lack of consistency and compatibility between spatial and temporal downscaling, which reduces their practicality in real day-to-day projects.

One of the downsides of previous impact assessment studies regarding the thermal performance of buildings is the lack of study on climate change approaches. The lack of available studies in this field and the downscaling and disaggregation methods prevent these kinds of

projects from being applicable for real case studies. The purpose of this study is to decrease the drawbacks of previous downscaling and disaggregation methods by attempting to provide a consistent method to generate future climate data.

# Chapter 3

## 3. Methodology

This chapter investigates a systematic methodology for doing impact assessment of climate change on the thermal performance of a typical residential building in Canada. The term “performance” is assessed based on the heating and cooling loads. When considering energy use, energy consumption simulations are carried out using an entire house as the case study. The first part of this chapter explains the selected case study, and the other following sections will provide an explanation regarding how to produce the future weather data and how to use it for the heating and cooling load analysis. Therefore, this methodology chapter is divided into three main parts: presenting the case study, explaining the projection process for the future climate, and using the generated future weather data as an input of the building energy simulation software.

### 3.1. Case study

The building to be modeled is a bungalow type residence with two heated floors: the ground floor and the basement [84]. It contains a bedroom with an en-suite bathroom, two additional bedrooms and a completed basement. The building was constructed in the 1960s but has recently undergone significant renovations. Figure 5 below presents the façade of the case study residential house.



Figure 5: Photo of the experimental house [85].

The house is located in a residential area and its front façade is oriented  $N46.5^\circ$ . The dimensions of the house are of approximately  $12.802\text{ m} * 8.128\text{ m}$  ( $42\text{ ft.} * 26\frac{2}{3}\text{ ft.}$ ) with a living area of  $104\text{ m}^2$  ( $1119\text{ sq. ft.}$ ). The roof of the residence has a slope of  $4/10$  and its surfaces are at  $20^\circ$  horizontal. The exterior wall is made of brick veneer with an overall thermal resistance of  $3.61\text{ m}^2\text{K/W}$ .

The home lighting system and occupant behavior was counted as additional gains rather than being set by default in TRNBuild. The three occupants of the building make up a simple family with a father, a mother and a child. Only areas with occupations of more than 30 minutes were considered. Figure 6 below shows the occupation times of each zone per floor (the building comprises of 8 different zones). In addition to lighting and occupancy, some household appliances such as cooker, TV, computer and monitor, and water heater allow to bring gains inside the residence which has been recorded by sensors every 5 minutes and validated.

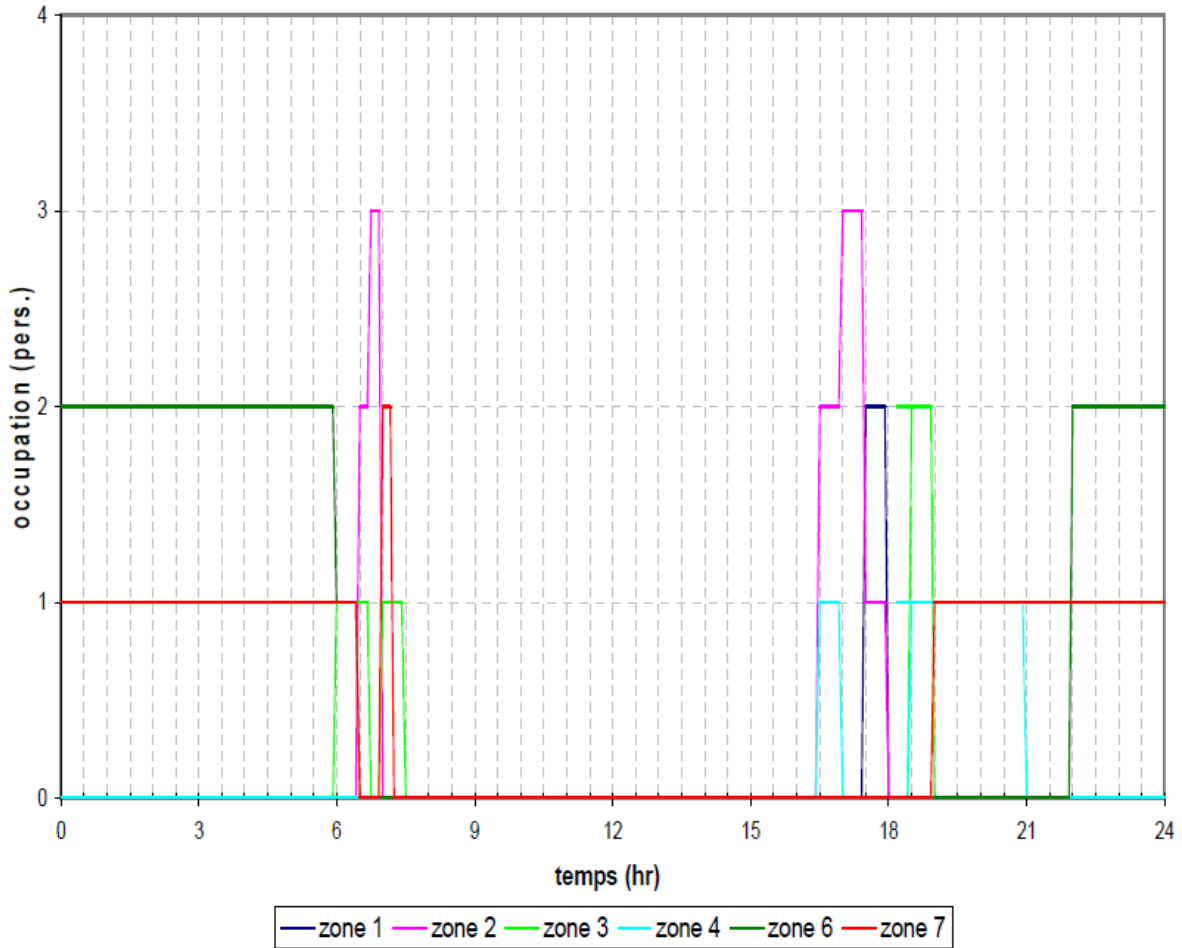


Figure 6: Weekly occupancy schedule on the ground floor

### **3.2. Building simulation tool (TRNSYS)**

The energy simulation software used in this project is TRNSYS. The model has been validated and is ready for application. Similar to other modeling exercises, it was important to verify all inputs and active parameters such as dry bulb temperature, dew point temperature, relative humidity, wind velocity, atmospheric pressure, total horizontal radiation, horizontal beam radiation, total diffuse radiation on the horizontal, and beam radiation. It is also important to select the proper CMIP5 parameters to be used as inputs into the TRNSYS software after operating spatiotemporal downscaling. In the current project, Type 109 was used, which allows the program to separate the beam and diffuse radiation as well as generate an output beam radiation for each surface [164, 165].

TMY2 includes 29 parameters namely dry bulb temperature, dew point temperature, relative humidity, atmospheric station pressure, extraterrestrial horizontal radiation, extraterrestrial normal radiation, horizontal infrared radiation intensity, global horizontal radiation, direct normal radiation, diffuse horizontal radiation, global horizontal illuminance, direct normal illuminance, diffuse horizontal illuminance, zenith luminance, wind direction, wind speed, total sky cover, opaque sky cover, visibility, ceiling height, present weather observation, present weather codes, precipitable water, aerosol optical depth, snow depth, days since last snowfall, albedo, liquid precipitation depth, and liquid precipitation quantity. Based on the extent of the influence these parameters exert on the thermal performance of buildings, the following parameters have been chosen for downscaling in the present study.

- Dry Bulb Temperature
- Radiation

The longest known lifetime of carbon dioxide in the atmosphere is 100 years, moreover, every cycle of carbon dioxide can last approximately 30 years in the atmosphere. Therefore, one cycle can last up to 2040 before the simulation may process another carbon cycle [19]. This is why the assessment of the thermal performance of buildings in Canada has been done for three periods: short-term (2011–2040), mid-term (2041–2070), and long-term (2071–2100).

In the present study, a building located in Montreal has originally been modeled and validated by TRNSYS without considering a cooling system. However, in order to better understand the impact of climate change on energy consumption, it is necessary to implement a simple cooling system. For the current project, a cooling system added to the model based on ASHRAE standards and the set point of 26 °C was applied.

According to the ASHRAE Standard 55–2013 (Thermal Environmental Conditions for Human Occupancy) [88], the thermal comfort threshold is approximately between 19.4 to 27.7 °C. Specifically, this range depends on the humidity, warm cloth, season and the amount of activity. In the present study, the temperature of 26 °C is considered as an overheating and dangerous condition and a cooling system should prevent the temperature from exceeding this threshold. Given this information, the heating and cooling loads could be calculated accordingly.

### 3.3. Projecting future climate

The process of generating future local weather data by means of spatial and temporal downscaling as well as separating diffuse and direct radiation is shown in Figure 7. For the current project, it was required to have hourly data for the station scale in order to downscale the historical and future GCM data. The GCM data is provided as daily data with low resolution; thus, it is necessary to increase the resolution and disaggregate it from daily to hourly historical and future local weather data.

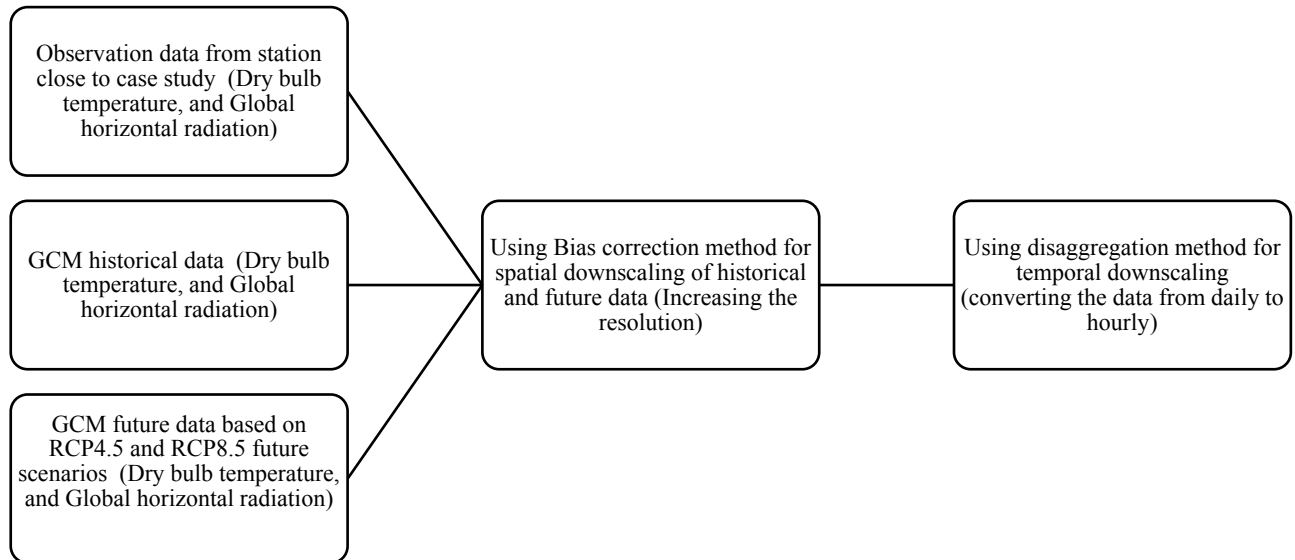


Figure 7: Framework for generating local future weather data

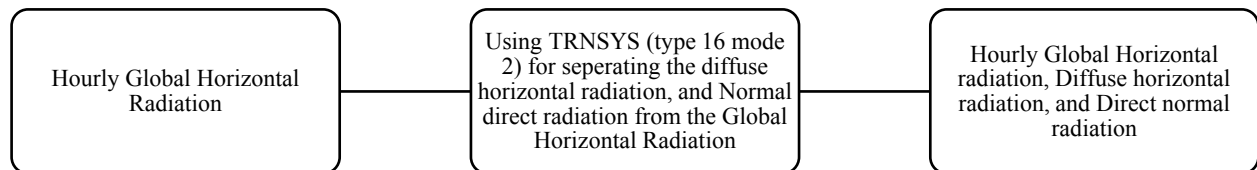


Figure 8: Framework for generating local future diffuse horizontal, and direct normal radiation

It is important to analyze the diffuse horizontal and direct normal radiation based on Figure 8. The detailed procedure for obtaining them from global horizontal radiation is explained in section 3.4.

### 3.3.1. Global circulation models and future scenarios selection

CMIP5 models have been thoroughly studied using all possible models, integrating parameters of dry bulb temperature, and solar radiation at the same time; they also have generated complete historical datasets and two RCPs (RCP4.5 and RCP8.5). Five global circulation models have been chosen for comparison in this project and are presented in Table 10. The global circulation models

Table 11 have been selected such that the whole boundary of the alteration between available global circulation models for using in this project [89].

Following the selection of the appropriate GCM models, it is important to determine the nearest observational weather station, which is an important step for conducting downscaling procedures. For downscaling with bias correction method, the GCM and local weather data (observational data) should be prepared. A Matlab code was then designed to extract all the information from the GCM models such as the latitudes and longitudes of all the grid points. It is necessary to provide the number of cells for the matlab code in order to extract these data; therefore, the grid points number for each GCM model close to our station coordinate were extracted (Table 10). The grid points numbers were used to generate historical data and two RCP4.5 and RCP8.5 data.

Table 10: Selected global circulation models with their latitude and longitude grid points.

<i>Models name</i>	<i>Latitude grid point</i>	<i>Longitude grid point</i>
<i>CanESM2</i>	49	103
<i>MIROC_ESM</i>	49	103
<i>CNRM_CM5</i>	97	205
<i>MIROC5</i>	97	205
<i>IPSL_CM5A_LR</i>	72	77

Table 11: Selected global circulation models with their latitude and longitude grid points

<i>Models name</i>	<i>Institution</i>	<i>Resolution</i>	
		Latitude	Longitude
<i>CanESM2</i>	Canadian Centre for Climate Modelling and Analysis	2.7906	2.8125
<i>MIROC_ESM</i>	Japan Agency for Marine-Earth Science and Technology, Atmosphere and Ocean Research Institute (The University of Tokyo), and National Institute for Environmental Studies	2.7906	2.8125
<i>CNRM_CM5</i>	Centre National de Recherches Meteorologiques / Centre Europeen de Recherche et Formation Avancees en Calcul Scientifique (CNRM/CERFAC)	1.4008	1.40625
<i>MIROC5</i>	Atmosphere and Ocean Research Institute (The University of Tokyo), National Institute for Environmental Studies, and Japan Agency for Marine Earth Science and Technology	1.4008	1.40625
<i>IPSL_CM5A_LR</i>	Institut Pierre Simon Laplace	1.8947	3.75

There are three sets of climate data namely historical GCM, historical observation, and future GCM data. The historical and future GCM data can be obtained from the CMIP5 website (World Climate Research Program; Coupled Model Inter-comparison Project 5 [CMIP5]) [90]. From this, the desired data for air temperature, and downwelling shortwave radiation from 1850 to 2005 and from 2005 to 2100 can be downloaded. On the other hand, observational data can be obtained from a weather station such as the one located in Dorval, Montreal (Montreal/Pierre Elliott Trudeau INTLA Quebec) which is located at Latitude of 45°28'00.000" N and Longitude 73°45'00.000" W. Again, the desired data may be saved from the [91] website for further analysis.

### 3.3.2. Downscaling

Through the QM (Quantile mapping) method, the GCM model data can be mapped by cumulative distribution function (CDF) on the observation data. For bias correction of the historical baseline data, the following function can be computed.

$$H_{GCM_{k,QM}^{basper}} = F_{H_{OBS_k^{basper}}}^{-1} \left[ F_{H_{GCM_k^{basper}}} \left( H_{GCM_k^{basper}} \right) \right] \quad k = 1, \dots, 12 \quad (1)$$

where  $F_{H_{GCM_k^{basper}}}$  is the cumulative distribution function of the GCM data (historical baseline data);  $F_{H_{OBS_k^{basper}}}^{-1}$  is the inverse cumulative distribution function (quantile function) for the observation in month  $k$ .

Based on Bennett et al., (2014) [92], it is more appropriate to correct the variables of precipitation, solar radiation, and humidity by multiplicative quantile mapping, and the variables of mean, maximum, and minimum temperature by additive quantile mapping.

#### 3.3.2.1. Multiplicative quantile mapping

To this end, it is necessary to define a ratio by cumulative distribution function using the observation and baseline data to downscale future data by multiplying this ratio by the GCM future data. This ratio can be defined as below:

$$R_k \left[ F_{H_{GCM_k^{fut}}} \left( H_{GCM_k^{fut}} \right) \right] = \frac{F_{H_{OBS_k^{basper}}}^{-1} \left[ F_{H_{GCM_k^{fut}}} \left( H_{GCM_k^{fut}} \right) \right]}{F_{H_{GCM_k^{basper}}}^{-1} \left[ F_{H_{GCM_k^{fut}}} \left( H_{GCM_k^{fut}} \right) \right]} \quad k = 1, \dots, 12 \quad (2)$$

where  $F_{H_{GCM_k^{fut}}}$  is the cumulative distribution function of the GCM future data;  $R_k$  can be found for the baseline period and applied to downscale the future data.

$$H_{GCM_{k,QM}^{fut}} = H_{GCM_k^{fut}} \cdot R_k \quad (3)$$

where  $H\_GCM_{k,QM}^{fut}$  is the downscaled data by multiplicative quantile mapping. This method can help to find the CDF of future data by multiplying each future datum of

$$F_{H\_GCM_k}^{-1} [F_{H\_GCM_k^{fut}} (H_{GCM_k^{fut}})] \text{ to the corresponding } R_k \left[ F_{H\_GCM_k^{fut}} (H_{GCM_k^{fut}}) \right].$$

### 3.3.2.2. Additive quantile mapping

It is necessary to define a ratio which is different by the multiplication quantile mapping ratio which can be obtained from the cumulative distribution function of the observation and baseline data to be able to downscale the future data by adding this ratio to GCM future data. This ratio can be defined as below:

$$R_k \left[ F_{H\_GCM_k^{fut}} (H_{GCM_k^{fut}}) \right] = F_{H\_OBS_k}^{-1} \left[ F_{H\_GCM_k^{fut}} (H_{GCM_k^{fut}}) \right] - F_{H\_GCM_k}^{-1} \left[ F_{H\_GCM_k^{fut}} (H_{GCM_k^{fut}}) \right] \quad (4)$$

$k = 1, \dots, \dots, 12$

where  $F_{H\_GCM_k^{fut}}$  is the cumulative distribution function of GCM future data.  $R_k$  can be found for the past, baseline period and can be used to downscale the future data.

$$H\_GCM_{k,QM}^{fut} = H_{GCM_k^{fut}} + R_k \quad (5)$$

where  $H\_GCM_{k,QM}^{fut}$  is the downscaled data by additive quantile mapping. Hence, this method can help to find the CDF of future data by adding each future data of

$$F_{H\_GCM_k}^{-1} [F_{H\_GCM_k^{fut}} (H_{GCM_k^{fut}})] \text{ to the corresponding } R_k \left[ F_{H\_GCM_k^{fut}} (H_{GCM_k^{fut}}) \right].$$

This method of downscaling uses historical data for generating the future data. It uses a ratio which shows the statistical features of a data and its alteration between the historical GCM and observation data of the past. It is possible to map the GCM future data at station scale level by the equations mentioned earlier. First, it is appropriate to categorize the data on month by month basis in different matrices, and after that, apply the bias correction method for each matrix separately. At the end, it is important to order the data in their correct time slots. The different steps for spatial downscaling with bias correction are shown in Figure 9. Moreover, **Error!**

**Reference source not found.** shows the bias correction downscaling method could remove all the existed bias between the GCM and observational data.

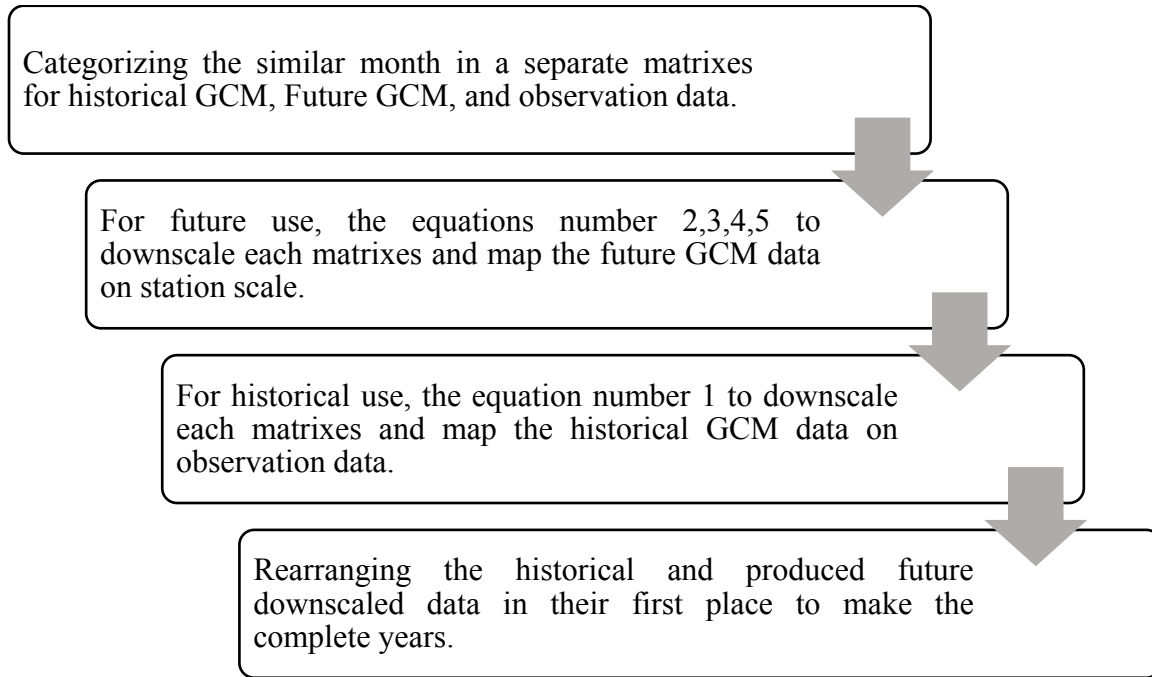


Figure 9: Methodology showing the bias correction (quantile mapping) downscaling process

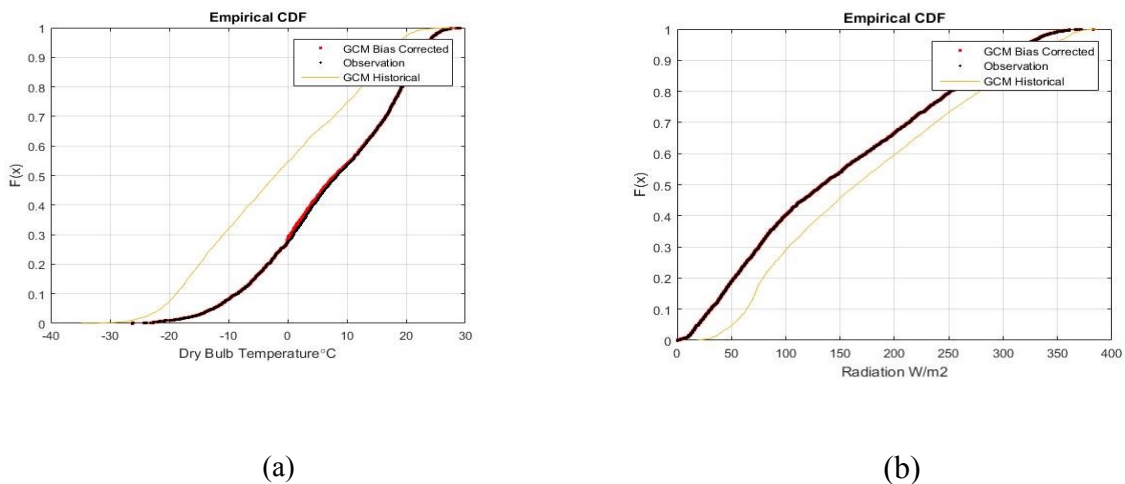


Figure 10: Cumulative distribution function of GCM bias corrected, observation, and GCM historical data compared for three weather parameters; a) Daily dry bulb temperature, and b) Daily radiation

### 3.3.3. Disaggregation

The Bias Correction method generates data in the daily format. Hence, prior to using them as an input into the TRNSYS software, the data must be downscaled from daily to hourly. It is possible to use hourly data as a contribution of the weather file, which is based on hourly data. In previous studies, the K-nearest neighbour (KNN) method has been applied for temporal downscaling methods which is based on finding the closest Euclidean distance between the daily GCM and observational data. Integration of the KNN method with the quantile mapping bias correction spatial downscaling has been found to undesirably dissemble the relations between the made quintiles by quantile mapping. This also reduces the compatibility and practicality of spatial and temporal downscaling.

For solving this problem, a modified disaggregation method has been proposed in Figure 11. This method uses the patterns of historical hourly observation data in such a way that for each future datum for a specific month, a day can be related to past observational data. Next, this data with its corresponding relation to that specific month and having a similar statistical feature; the datum is converted into its hourly pattern for that future day in that particular month.

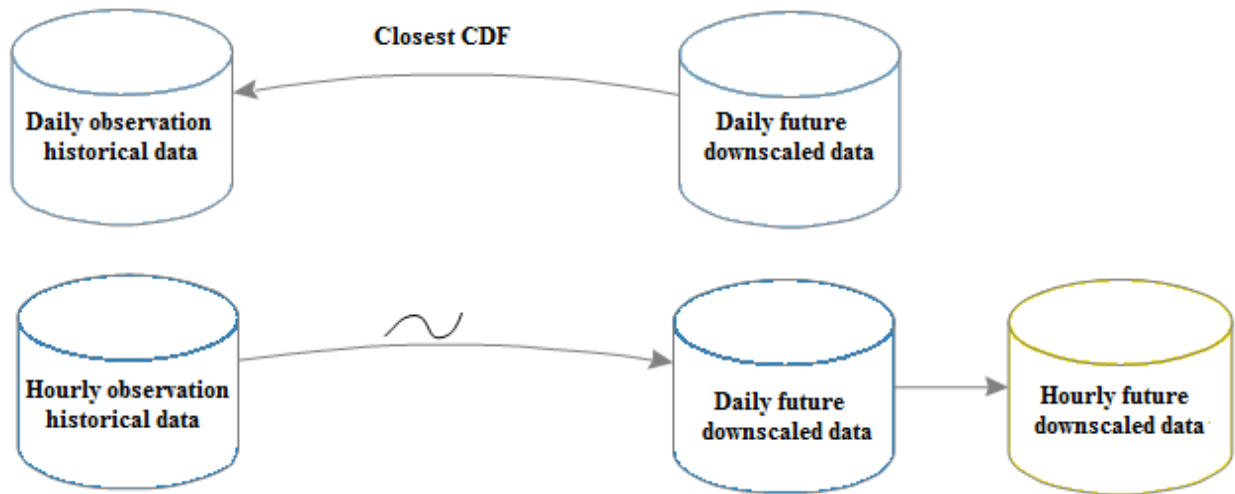


Figure 11: The procedure of disaggregation method for temporal downscaling

This method of disaggregation is adapted from the KNN method [93] which is one of the most fundamental and simple classification methods in statistics. Similar to the bias correction method, future and historical data are categorized on a month by month basis in separate matrices,

after which, the CDF of all data in each matrix is calculated for each month separately. For each datum in one particular future month, the closest CDF in the daily downscaled GCM data is matched to the identical observational data of the same month, which is as follow.

This mathematical calculation has been done for daily data for all months in the future. The next step is to find the mathematical patterns of hourly changes of the observational data for each day. For the radiation and humidity parameters, the average of hourly data for each day are considered, and each of the hourly datum is divided by the mean of that day. Therefore, the results are one ratio for each hour in historical data. For temperature, the average of hourly observational data for each day is calculated and the amount of each hour in one day is subtracted from the average of each day; therefore, this mathematical method can produce one ratio for each hour. The humidity and radiation can be multiplied to the corresponding day in the future; however, for temperature, this ratio should be added to the corresponding day in the future.

The bias correction method can be multiplicative or additive; similarly, this modified quantile based k-nearest method for humidity and radiation can be multiplicative, and for temperature can be additive. Moreover, both the bias correction and disaggregation methods are following the quantile role. This shows the importance of consistency and compatibility in such mathematical calculation. Figure 12 shows the steps for performing this modified temporal downscaling.

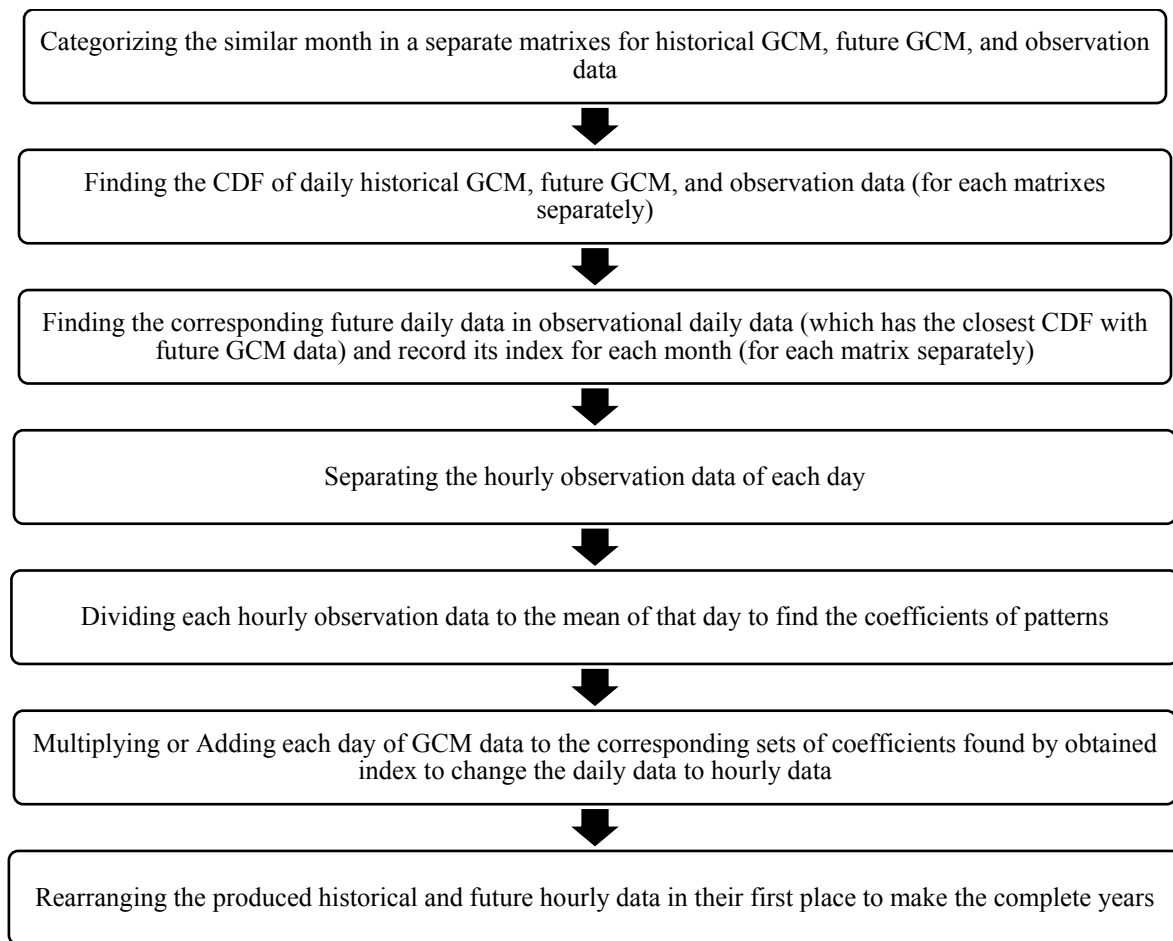


Figure 12: Methodology showing the temporal downscaling (disaggregation) process

The advantage of this method is the high processing speed for performing the temporal downscaling calculations by omitting the extra steps of assigning the weight and doing heavy computational and calculation for classification. Moreover, this method has more compatibility with the quantile mapping bias correction which makes it more practical for the impact assessment project on thermal performance of buildings. After performing temporal disaggregation, it is important to arrange the data in their time order for the building energy software to be functional.

### **3.4.Using generated future weather data as an input of building energy simulation software**

The direct normal radiation and diffuse horizontal radiation can be generated from global horizontal radiation by using the Type 16 (mode 2) in TRNSYS. The mode 2 is based on the

fundamental developed by [94]; this mode can estimate the diffuse component of the total horizontal radiation which is ( $I_d/I$ ).

Mode 2 is a function of clearness index, solar altitude angle, ambient temperature, and relative humidity. Hence, it gives more accurate results than the other modes which is as follows [94]:

Interval:  $0 \leq K_T \leq 0.3$ ; Constraint:  $\frac{I_d}{I} \leq 1.0$

$$\frac{I_d}{I} = 1.000 - 0.232 K_T + 0.0239 \sin(\alpha) - 0.000682 T_a + 0.0195 \left(\frac{rh}{100}\right) \quad (13)$$

Interval:  $0.3 < K_T < 0.78$ ; Constraint:  $0.1 \leq \frac{I_d}{I} \leq 0.97$

$$\frac{I_d}{I} = 1.329 - 1.716 K_T + 0.267 \sin(\alpha) - 0.00357 T_a + 0.106 \left(\frac{rh}{100}\right) \quad (14)$$

Interval:  $0.78 < K_T$ ; Constraint:  $0.1 \leq \frac{I_d}{I}$

$$\frac{I_d}{I} = 0.426 K_T - 0.256 \sin(\alpha) + 0.00349 T_a + 0.0734 \left(\frac{rh}{100}\right) \quad (15)$$

For calculating the beam, radiation on a horizontal surface the diffuse horizontal radiation is subtracted from the global horizontal radiation.

$$I_b = I - I_d \quad (16)$$

Based on the different available inputs, the missing ones can be easily determined to generate all of the radiation types, which are important to complete the EPW file that is used as input for performing the simulation exercise.

In the current project the only generated weather parameters are global horizontal radiation, and surface temperature; hence, the best mode for separating the diffuse horizontal radiation and direct normal radiation is mode 2. The Type 16 in TRNSYS has been used as follows:

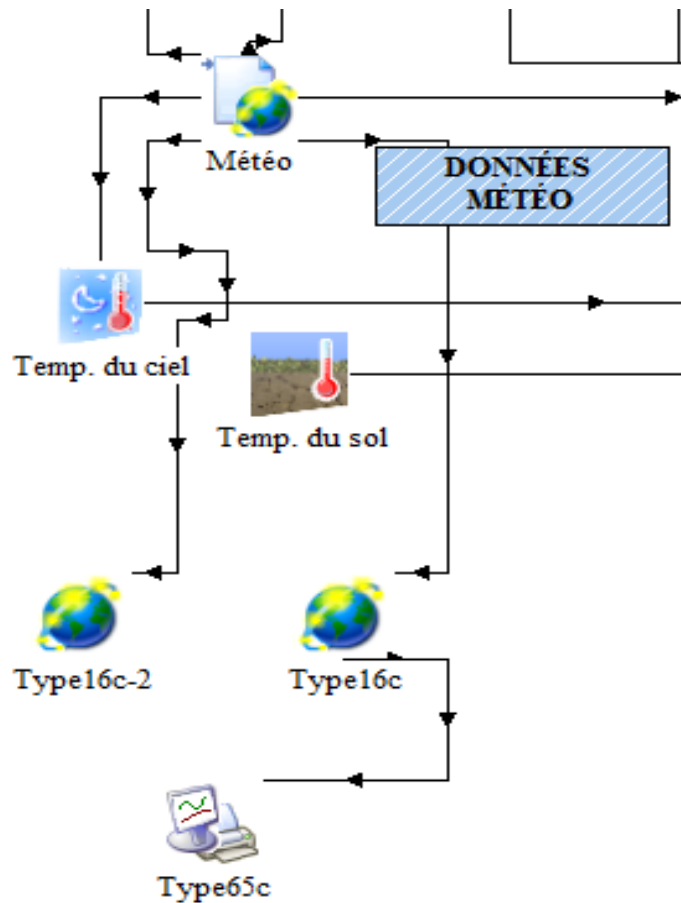


Figure 13: Connection between the TMY file and type 16 mode 2 in TRNSYS model.

Figure 13 shows the prediction of the diffuse and direct normal radiations which can be easily connected to the TMY file with the Type 16, mode 2. The only changing parameters over the time in the TMY file are global horizontal radiation, and dry bulb temperature. The output is the diffuse horizontal radiation and direct normal radiation. The diffuse horizontal radiation and direct normal radiation during climate change can be directly connected and used as an input for building design. At the end, the parameters dry bulb temperature, global horizontal radiation, direct normal radiation, and diffuse horizontal radiation, which are subject to change as a result of climate change, have been predicted and used as an input.

This methodology attempts to compensate for the shortcomings mentioned in the literature review by introducing a practical and compatible spatial and temporal downscaling. Moreover, the following results and discussion tends to eliminate the lack of detailed study on the heating and cooling load.

# Chapter 4

## 4. Results and discussion

In this chapter, results obtained from the future weather data (on hourly basis) and the impact of climate change on heating, cooling and also on the peak load are presented. Moreover, the way of impact assessment is arranged based on the impact assessment procedure commonly used in climate change science and hydrology, which contains ensemble, comparison (between different RCPs), and variability (comparison between different global circulation models). Therefore, this chapter is divided into two subsections, weather data and load calculation, each part including the aforementioned impact assessment analysis.

### 4.1. Weather data

#### 4.1.1. RCP4.5

##### 4.1.1.1. Ensemble analysis results

The first thing to be analyzed in a good impact assessment of climate change on the thermal performance of the building is the general behavior of the load. As shown in Figure 14, the temperature is increasing over time. Figure 14 shows that the temperature in the third period is very close to the temperature in the second period, which is attributable to the RCPs behavior in RCP4.5, then the temperature increases before leveling off after 2100.

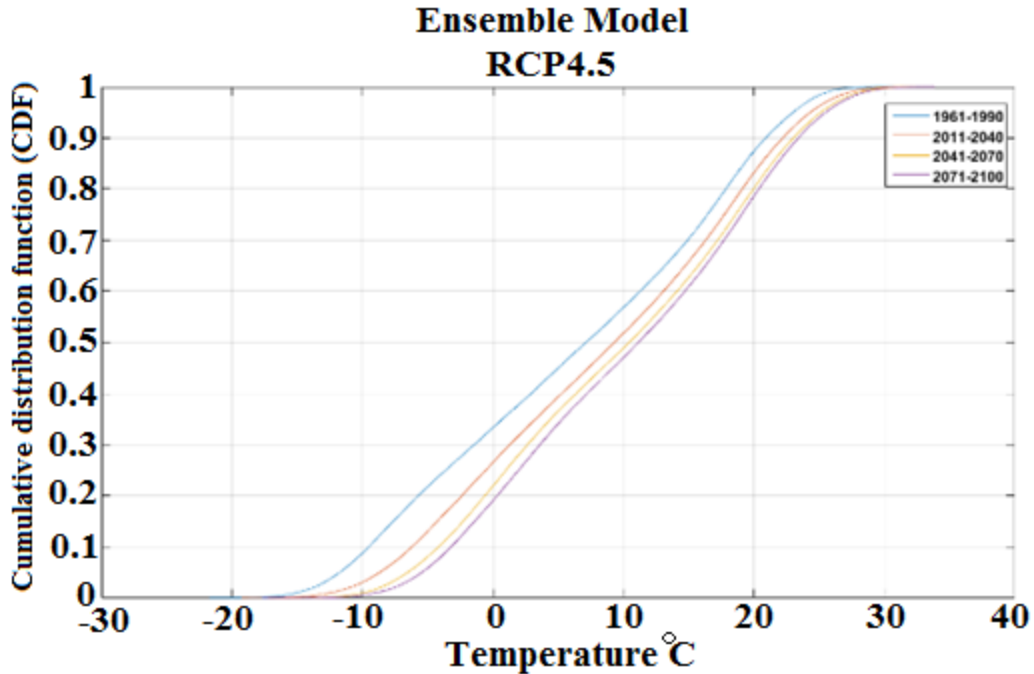


Figure 14: Cumulating distribution function of hourly temperature based on RCP4.5 in four periods of historical, 2011-2040, 2041-2070, and 2071-2100 and ensemble GCM model

Table 12 can support Figure 14, which shows the statistical values of the temperature and radiation affected by the climate change. The inference from the table is that the average temperature will rise by 25.6%, 35.7% and 40% in the first, second and the third period respectively, when compared, to the historical period. The median increases for the temperature which is affected by the climate change. It is also seen from the table that standard deviation is decreasing over the time, which illustrate the amount of variation and dispersion are declining and also the data tends to be closer to the mean. The average radiation in the first period will increase by 3.37% and in the second period will again rise by 4.08%, and also in the third period, it will grow by 4.9% comparing to the historical period. In addition, the standard deviation of radiation is rising over time which shows the data is likely to be far from the average value. Moreover, the median will increase.

Table 12: Statistical values of ensemble model of hourly temperature and radiation based on RCP4.5 in four periods of 1961-1990, 2011-2040, 2041-2070, 2071-2100.

<i>Period of analysis</i>	<i>RCP4.5 (Ensemble)</i>	<i>Average</i>	<i>Standard deviation</i>	<i>Median</i>
<i>1961-1990</i>	<b>Temperature (°C)</b>	6.36	11.38	7.12
	<b>Radiation (W/m<sup>2</sup>)</b>	157.44	216.53	6.75
<i>2011-2040</i>	<b>Temperature (°C)</b>	8.55	10.68	9.30
	<b>Radiation (W/m<sup>2</sup>)</b>	162.92	223.83	6.88
<i>2041-2070</i>	<b>Temperature (°C)</b>	9.80	10.25	10.43
	<b>Radiation (W/m<sup>2</sup>)</b>	164.11	225.32	6.98
<i>2071-2100</i>	<b>Temperature (°C)</b>	10.51	10.02	11.14
	<b>Radiation (W/m<sup>2</sup>)</b>	165.61	227.14	7.11

#### 4.1.2. RCP8.5

##### 4.1.2.1. Ensemble analysis results

It is inferred from Figure 15 that similar to RCP4.5, the temperature is increasing over the time, but the distance between the periods are almost the same. Table 13 can support Figure 15, which shows the average temperature will increase in the first, second, and third period by 25.8%, 40.5%, and 50.7%, respectively, in comparison to the historical period. This increase in temperature shows that over time the rise in temperature will be more noticeable based on RCP8.5. The median temperature based on RCP8.5 is increasing as well, but the standard deviation is dropping over time, which shows the data tends to be closer to the average value.

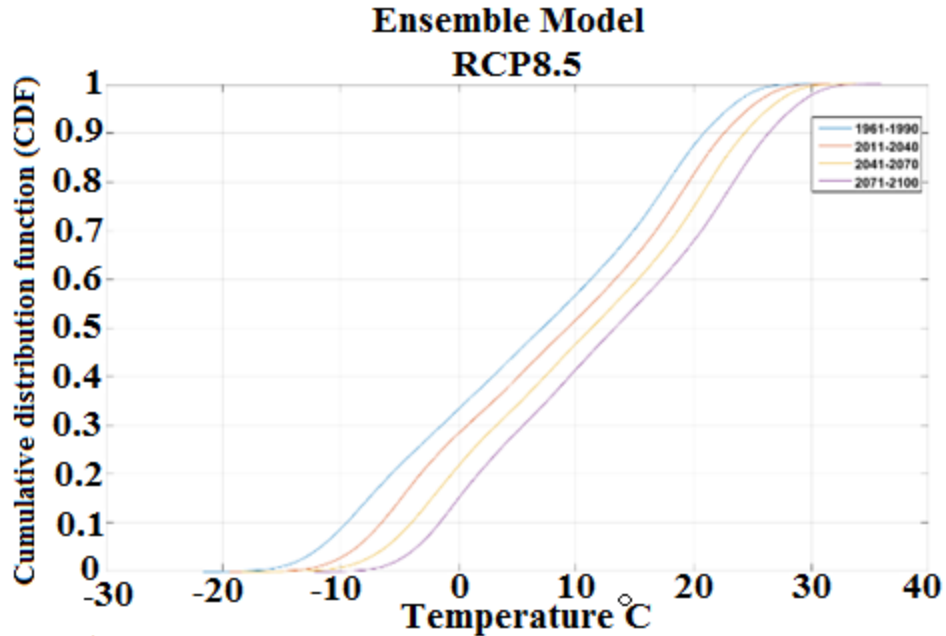


Figure 15: Cumulating distribution function of hourly temperature based on RCP8.5 in four periods of 1961-1990, 2011-2040, 2041-2070, and 2071-2100 and ensemble GCM model

The average radiation based on RCP8.5 will rise in the first, second, and third period by 3.7%, 4.8%, and 4.43% respectively, in comparison to historical period although it will decrease in the third period by 0.4% in comparison to the second period. Moreover, the standard deviation will be high in the first and second period by 3.2% and 4.2% respectively, and then will fall in the third period by 0.6% in comparison to the second period, whereas it is 3.6% more than the historical period. In addition, the median of global horizontal radiation is increasing over time.

Table 13: Statistical values of ensemble model of hourly temperature and radiation based on RCP8.5 in four periods of 1961-1990, 2011-2040, 2041-2070, 2071-2100

<i>Period of analysis</i>	<i>RCP8.5 (Ensemble)</i>	<i>Average</i>	<i>Standard deviation</i>	<i>Median</i>
<i>1961-1990</i>	<b>Temperature (°C)</b>	6.36	11.38	7.12
	<b>Radiation (W/m<sup>2</sup>)</b>	157.44	216.53	6.75
<i>2011-2040</i>	<b>Temperature (°C)</b>	8.55	10.99	9.27
	<b>Radiation (W/m<sup>2</sup>)</b>	163.67	223.87	7.05
<i>2041-2070</i>	<b>Temperature (°C)</b>	10.67	10.68	11.32
	<b>Radiation (W/m<sup>2</sup>)</b>	165.49	226.17	7.09
<i>2071-2100</i>	<b>Temperature (°C)</b>	12.84	10.50	13.30
	<b>Radiation (W/m<sup>2</sup>)</b>	164.70	224.64	7.09

### **4.1.3. Comparison (RCP4.5 and RCP8.5)**

The comparison of results obtained from RCP4.5 (Table 12) and RCP8.5 (Table 13) is construed that the average temperature in the historical and the first period are the same, but in the second and the third period, the temperature predicted based on RCP8.5, is 8.15% and 18.22% higher than RCP4.5. Moreover, the standard deviation of temperature based on RCP8.5 except for historical period, which is almost the same, is higher than RCP4.5 by 2.8%, 4.02%, and 4.5%, respectively, which shows the temperature data based on RCP8.5 tends to be closer to the mean comparing to the temperature data based on RCP4.5.

The average radiation in a historical period is the same based on either RCP8.5 or RCP4.5, but in the first and second period in RCP8.5, it is 0.42% and 0.78% more than RCP4.5. Moreover, in the third period this trend will change and in RCP4.5 it will be 0.54% more than in RCP8.5. Furthermore, the standard deviation of radiation based on RCP4.5 and RCP8.5 in historical and first period is the same, but in the second period based on RCP8.5, it is 0.3% more than RCP4.5 and in the third period based on RCP4.5 is 1.1% more than RCP8.5. Therefore, the results of standard deviation show that in the second period, the data based on RCP8.5 is likely to be closer to the mean in comparison to RCP4.5. Conversely, in the third period, the data based on RCP4.5 tends to be closer to the mean in comparison to RCP8.5.

In conclusion, based on the obtained results it can be deduced that the temperature and radiation in RCP4.5 and RCP8.5 are getting further from each other over time, and this difference will reach its maximum in the third period.

## **4.2. Load calculation**

Having analyzed the changes that climate change makes on the weather parameters, the impact of these changes on heating and cooling load can be evaluated. As seen from Table 14 which shows the statistical values of heating and cooling load based on RCP4.5, the average heating load might get decreased in Montreal in the first, second, and third period in comparison to historical period by 14.7%, 22.9%, and 27.5 %, respectively. Moreover, the maximum heating load is going to decline in the first, second, and third period by 8.69%, 8.9%, and 13.3% in

comparison to a historical period which shows that the decreases in the average load are much more than the reductions in the maximum load.

The standard deviation in the first, second, and third period will decrease by 11.08%, 17.07%, and 20.7%, respectively, in comparison to the historical period. The standard deviation results for heating load show that the data in the first, second, and third periods tend to be far from the mean value. The obtained results demonstrate that heating load will decrease by 27.5% in the third period on average due to the climate change. On the other hand, based on RCP4.5, the average cooling load will increase by 11.1%, 17.2%, and 22.5% in the first, second, and third period respectively in comparison to the historical period. Moreover, the maximum cooling load will rise in the first, second, and third period in comparison to historical period by 4.26%, 9.74%, and 10.5%, respectively. Likewise, the results show that climate change affects the average load more considerably than the maximum load. In addition, the standard deviation is going to grow by 8.1%, 11.7%, and 15% in the first, second, and third period respectively, in comparison to the historical period. The increase in the standard deviation illustrates the cooling load data is going to be farther from mean values. In conclusion, the cooling load will increase because of the impact of climate change, which shows the significance of impact analysis on the thermal performance of buildings and investigating a solution compatible with the case study in order to mitigate the impact of climate change on these changes in the energy demand.

Table 14: Statistical values of ensemble model of hourly heating and cooling load based on RCP4.5 in four periods of 1961-1990, 2011-2040, 2041-2070, and 2071-2100.

<i>Period of analysis</i>	<i>RCP4.5 (Ensemble)</i>	<i>Maximum</i>	<i>Average</i>	<i>Standard deviation</i>	<i>Median</i>
<i>1961-1990</i>	<b>Heating Load (kWh)</b>	34.54	8.32	8.29	6.01
	<b>Cooling Load (kWh)</b>	21.30	2.41	4.53	0.01
<i>2011-2040</i>	<b>Heating Load (kWh)</b>	31.57	7.09	7.40	4.79
	<b>Cooling Load (kWh)</b>	22.25	2.75	4.92	0.04
<i>2041-2070</i>	<b>Heating Load (kWh)</b>	31.44	6.41	6.84	4.14
	<b>Cooling Load (kWh)</b>	23.61	2.97	5.17	0.07
<i>2071-2100</i>	<b>Heating Load (kWh)</b>	29.95	6.03	6.56	3.72
	<b>Cooling Load (kWh)</b>	23.82	3.10	5.30	0.09

The statistical features of heating and cooling load calculated based on RCP8.5 are shown in Table 15. The results show that the average heating load will drop by 10.8%, 22.8%, and 34.9%

in the first, second, and third period, respectively, in comparison to the historical period. Moreover, the maximum heating load will decrease in the first, second, and third period by 3.7%, 7.8%, and 22.02% in comparison to the historical period. As can be seen, the effect of climate change on the average thermal load obtained based on RCP8.5 is more substantial than on maximum values.

The obtained results convey that the standard deviation will diminish by 4.8%, 13.4%, and 21.9% in the first, second, and third period, respectively, in comparison to the historical period. This decrease in standard deviation for the heating load results reveals that there is a tendency for the heating load to be closer to the mean values. Finally, the median of the heating load from historical period to the third period will be dropping continuously.

By analyzing the cooling load (calculated based on RCP8.5), increasing in the trend is observed. The average cooling load based on RCP8.5 will increase by 14.2%, 25%, and 36.8% in the first, second, and third period, respectively, compared to the historical period. By comparing the heating and cooling load results, it can be inferred that the effect of climate change is more on the cooling load than the heating load. Therefore, changes in the cooling load are more considerable than changes in the heating load in each period based on RCP8.5. Conversely, the effect of climate change based on RCP4.5 is more noticeable on heating load than on cooling load. Hence, changes in the cooling load are less than the heating load based on RCP4.5. By analyzing the maximum cooling load which is calculated based on RCP8.5, increasing the maximum cooling load by 1.3%, 10.1%, and 15.4% in the first, second, and third period, respectively is observed, compared to the historical period. Similarly, the increase in the average cooling load are more than the increase in the maximum cooling load.

The standard deviation of the cooling load based on RCP8.5 will increase over the time by 11.7%, 19.6%, and 27.4% in the first, second, and third period, respectively, compared to the historical period. The rises in the standard deviation show the cooling load data tends to be farther from the mean values over time. Finally, similar to the Avg (average), max (maximum), and STD (standard deviation), the median of the cooling load based on RCP8.5 will go up.

Table 15: Statistical values of ensemble model of hourly heating and cooling load based on RCP8.5 in four periods of 1961-1990, 2011-2040, 2041-2070, 2071-2100.

<i>Period of analysis</i>	<i>RCP8.5 (Ensemble)</i>	<i>Maximum</i>	<i>Average</i>	<i>Standard deviation</i>	<i>Median</i>
<b>1961-1990</b>	<b>Heating Load (kWh)</b>	34.54	8.32	8.29	6.01
	<b>Cooling Load (kWh)</b>	21.30	2.41	4.53	0.01
<b>2011-2040</b>	<b>Heating Load (kWh)</b>	33.29	7.48	7.80	5.04
	<b>Cooling Load (kWh)</b>	21.61	2.84	5.12	0.05
<b>2041-2070</b>	<b>Heating Load (kWh)</b>	31.80	6.42	7.12	3.72
	<b>Cooling Load (kWh)</b>	23.72	3.29	5.64	0.12
<b>2071-2100</b>	<b>Heating Load (kWh)</b>	26.93	5.46	6.40	2.43
	<b>Cooling Load (kWh)</b>	25.28	3.82	6.25	0.28

By comparing the results achieved from RCP4.5 and RCP8.5, it is understood that the average heating load in the first and second period will decrease more based on RCP4.5 and in the third period, it will decline substantially based on RCP8.5. The maximum value of the heating load in the first and second period will drop more based on RCP4.5, but in the third period, it will decrease much more based on RCP8.5.

By comparing the average cooling load estimated it is inferred that in the first, second, and third period it will increase more noticeably based on RCP8.5 compared to RCP4.5. Furthermore, the maximum cooling load in the first period will experience more enhancement based on RCP4.5, while based on RCP8.5 it will be more in the second, and third periods.

After analyzing the statistical features of heating and cooling load, it is important to investigate the impact of climate change on total heating and cooling load as well as the total load see Table 16 and Table 17. Based on the results, the total heating load will decrease in the first, second, and third period by 14.7%, 22.9%, and 27.5% respectively, compared to the historical period. As can be seen, reductions in the total heating load are considerable, especially in the third period.

The total cooling load based on RCP4.5 will climb by 12.3%, 18.7%, and 22.1% in the first, second, and third period, respectively, compared to the historical period. As can be seen, the rises in the total cooling load are marked, especially in the third period.

By comparing the total heating load and the total cooling load based on RCP4.5, one can understand that the decreases in the total heating load are more significant than the increases in the total cooling load. Therefore, the total load will diminish by 8.2%, 12.5%, and 14.9% in the first, second, and third period respectively, compared to the historical period.

Analyzing the total heating load based on RCP8.5 shows it will decrease by 10.13%, 22.8%, and 34.4% in the first, second, and third period respectively. Moreover, the total cooling load will go up by 15.19%, 26.7%, and 36.9% in the first, second, and third period respectively, compared to the historical period. By comparing the heating and the cooling load in RCP8.5 it can be said that increase in the cooling load are still less than decrease in the heating load. Therefore, the total load in Montreal based on RCP8.5 will decline by 3.8%, 9.4%, and 13.5% in the first, second, and third period, respectively.

It is also inferred that the total heating load in the first and second period will decrease more markedly based on RCP4.5, while in the third period it is more based on RCP8.5. Furthermore, by drawing a comparison of total cooling load between RCP4.5 and RCP8.5, it can be seen that it will increase more based on RCP8.5 than based on RCP4.5 in all the periods.

The total load (estimated based on RCP4.5) will decrease more considerably compared to RCP8.5 in all the periods. Therefore, one can see the advantages of the impact of climate change in a cold climate, especially based on RCP4.5.

In conclusion, the total load will decline due to the impact of climate change in Montreal city, which is located in a cold climate region. Analyzing the heating load and cooling load behavior shows the importance is focusing on installing appropriate cooling devices or changing the insulation or building envelopes. The mitigation strategies for reducing the impact of climate change will be defined region by region according to the number of changes in the total load and heating and cooling load in detail.

Table 16: Total heating and cooling load, and total load per year based on RCP4.5 in four different periods of 1961-1990, and 2011-2040, 2041-2070, and 2071-2100.

<i>RCP4.5</i>	<i>1961-1990</i>	<i>2011-2040</i>	<i>2041-2070</i>	<i>2071-2100</i>
<b>Total Heating Load (kWh/year)</b>	72944.63	62163.3	56203.93	52882.93
<b>Total Cooling Load (kWh/year)</b>	21165.17	24152.69	26061.9	27177.26
<b>Total Load (kWh/year)</b>	94109.81	86315.9	82265.84	80060.19

Table 17: Total heating and cooling load, and total load per year based on RCP8.5 in four different periods of 1961-1990, and 2011-2040, 2041-2070, and 2071-2100.

<i>RCP8.5</i>	<i>1961-1990</i>	<i>2011-2040</i>	<i>2041-2070</i>	<i>2071-2100</i>
<b>Total Heating Load (kWh/year)</b>	72944.63	65550.86	56284.73	47847
<b>Total Cooling Load (kWh/year)</b>	21165.17	24957.23	28899.44	33547
<b>Total Load (kWh/year)</b>	94109.81	90508.09	85184.17	81394

#### 4.2.1. Heating load RCP4.5

##### 4.2.1.1. Ensemble analysis results

In order to have an appropriate impact assessment on thermal performance of buildings, it is important to conduct ensemble analysis. Figure 16 shows the cumulative distribution function of the heating load based on RCP4.5 in different periods from historical to the third period. The inference from the figure is that the heating load is dropping over time because of the effect of climate change.

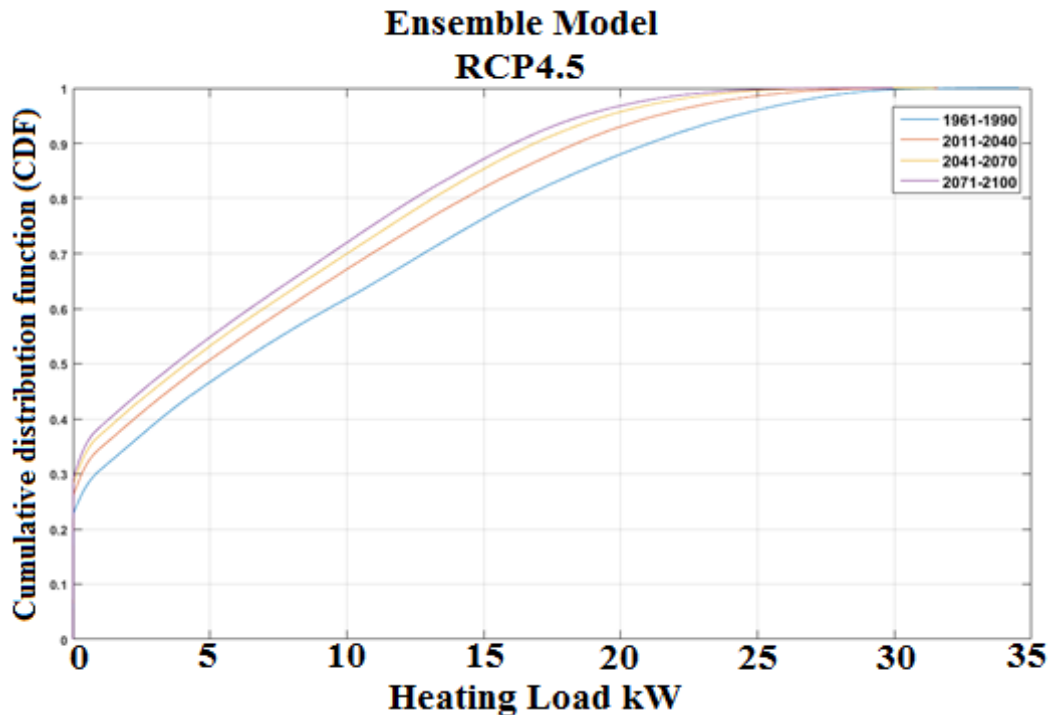


Figure 16: Cumulating distribution function of the hourly heating load based on RCP4.5 in four periods of 1961-1990, 2011-2040, 2041-2070, and 2071-2100 and ensemble GCM model

The other point that can be summarised from this figure is that in the second and third period the heating loads are very close to each other. This trend seems justifiable by RCP4.5 trend

regarding radiative forcing. Based on the aforementioned definition of radiative forcing of RCP4.5, it will increase to a certain level and then will level out. This stabilization is going to start in the third period while the acceleration of changes will start to diminish in the second period.

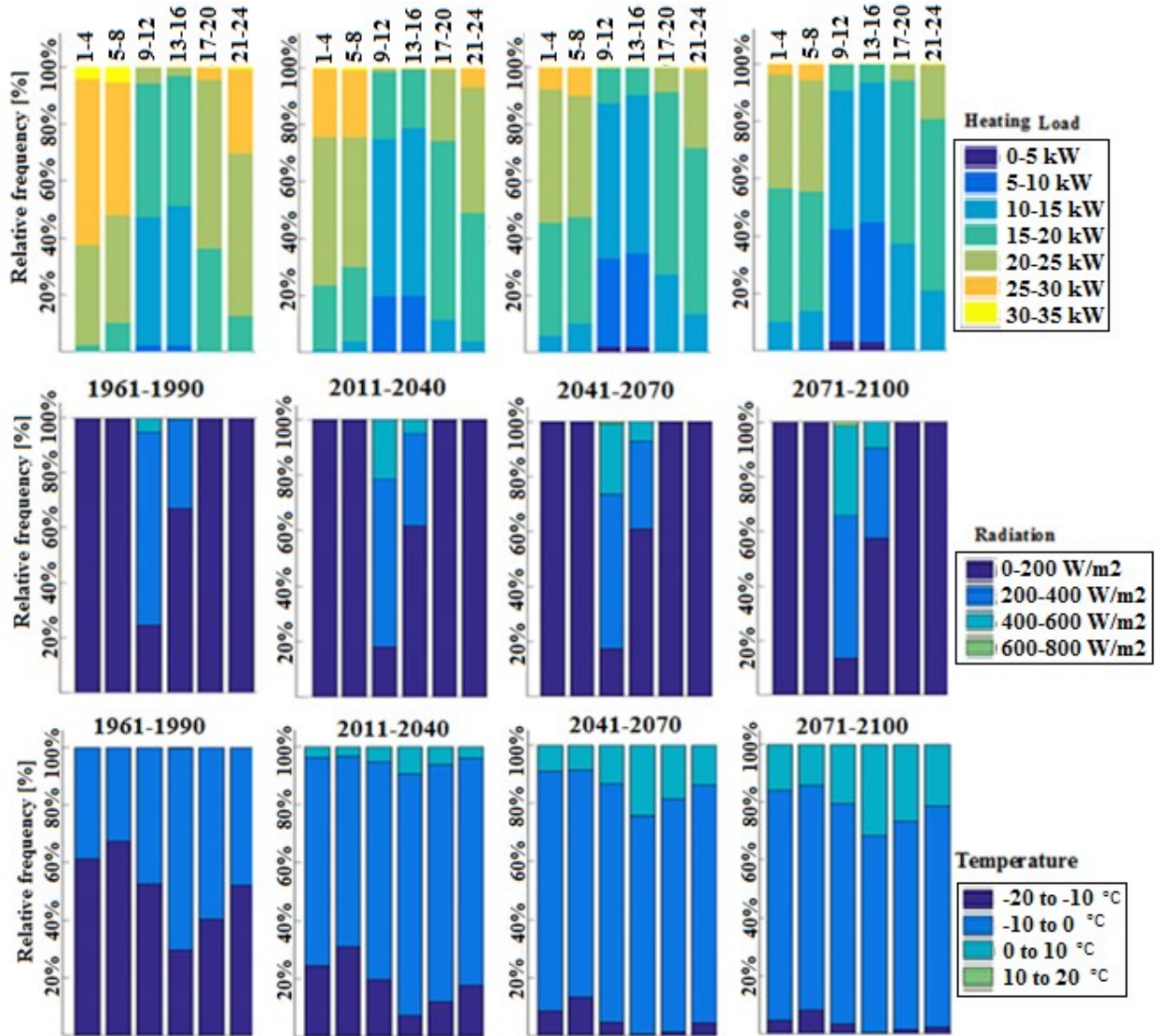


Figure 17: Hourly relative frequency of heating load based on RCP4.5 on January in four periods of 1961-1990, 2011-2040, 2041-2070, and 2071-2100 and ensemble GCM model.

Figure 17 shows the ensemble hourly behavior of the load based on RCP4.5 in January, due to the impact of climate change on the hourly heating load, as it is decreasing over time. As can be seen, some parts of the heating peak load will disappear because of the effect of climate change. For instance, the peak load of 30-35 kW will disappear from the second period. Moreover, the load of 25-30 kW will disappear at 17:00 h-20:00 h from the second period. Furthermore, by

analyzing the hourly radiation and temperature profile, the reason for the reduction in the hourly heating load in every 4 hours is revealed. As the radiation profile depicts, it is rising over time and in the hours that there is more radiation like 9:00 h-12:00 h and 13:00 h-16:00 h, the heating load has its lowest amount. In addition, the hourly temperature is increasing over time and therefore it is the main reason for the decrease in the heating load and also in the hours that the radiation is maximum, this reduction will exacerbate. For example, at 9:00 h-12:00 h and 13:00 h-16:00 h some parts of the load like 30-35 kW and 25-30 kW will disappear. Moreover, the heating load of 20-25 kW will start to disappear at 13:00 h-16:00 h in the first period and at 9:00 h – 12:00 h in the second period. According to the results, in January in the hour that radiation is the highest while is increasing because of the effect of climate change, the heating load is the lowest. Therefore, one can generate more energy from harnessing solar energy when one needs less energy, consequently, should develop thermal storage technologies.

Table 18: Relative frequency of different parts of the hourly heating load on December, January, and February based on RCP4.5 in four different periods of 1961-1990, 2011-2040, 2041-2070, and 2071-2100

Load (kW)	<b><u>Heating Load [Relative frequency] – Ensemble RCP4.5 Scenario</u></b>											
	1961-1990			2011-2040			2041-2070			2071-2100		
Month	Dec	Jan	Feb	Dec	Jan	Feb	Dec	Jan	Feb	Dec	Jan	Feb
30-35	0.3%	1.6%	1.08%	0.1%	0.1%	0.07%	0.02%	0.004%	0	0	0	0
25-30	9%	23.1%	12.9%	4.3%	9.09%	2.8%	1.6%	3.08%	0.9%	1.03%	1.6%	0.2%
20-25	29.2%	<u>33%</u>	<u>29.9%</u>	21.3%	28.1%	16.5%	15.3%	20.8%	9.03%	13.1%	17.1%	4.6%
15-20	<u>34.1%</u>	25.6%	27.6%	<u>36.4%</u>	<u>33.4%</u>	<u>36.9%</u>	<u>37.04%</u>	<u>36.9%</u>	<u>35.06%</u>	<u>36.8%</u>	<u>36.7%</u>	30.4%
10-15	21.7%	15.7%	21.1%	27.1%	22.4%	24.4%	31.1%	27.6%	29.7%	32.8%	29.7%	<u>34.8%</u>
5-10	5.4%	0.8%	7.02%	10%	6.5%	16.4%	13.9%	10.7%	19.4%	14.9%	13.6%	21.4%
0-5	0.02%	0	0.2%	0.5%	0.08%	2.5%	0.8%	0.7%	5.8%	1.1%	1.1%	8.4%
Period	1961-1990			2011-2040			2041-2070			2071-2100		

By analyzing the frequency of the heating load based on RCP4.5 according to Table 18, one can understand that lower tail of the heating load will rise, while the upper tail of the load will drop. Moreover, the maximum value of the heating load will happen in the middle, which will increase in December from historical to the second period while in the third period will decrease slightly. Furthermore, for January in the historical period, it represents the load of 20-25 kW,

whose frequency will increase, and it will shift to the load of 15-20 kW. In the second period, its frequency only will go up while it will not shift to other loads. The maximum load in the third period will not shift to the other loads, but its frequency will fall slightly. Finally, in February in the historical period the maximum load occurred for the load of 20-25 kW, while in the first period its frequency will rise, it will subsequently shift to the lower load of 15-20 kW. Moreover, in the second period its frequency will decrease while it will not shift to another load and in the third period its frequency will again dip and shift to the lower load of 10-15 kW.

The other fundamental behavior that can be observed from the aforementioned tables is that by decreasing the frequency of heating load from the top parts of the heating load, it will be distributed amongst other parts of the loads and all parts will receive a portion of it.

In conclusion, the heating load is declining on average, while the upper tail will go down which some parts of that will disappear and some other parts will be added to the middle and lower tail of the heating load. Therefore, in the future because of the effect of climate change on heating load, the intensive load of 30-35 kW will not be any more the critical load that is necessary to be supplied, and also the maximum heating load frequency will happen in lower loads.

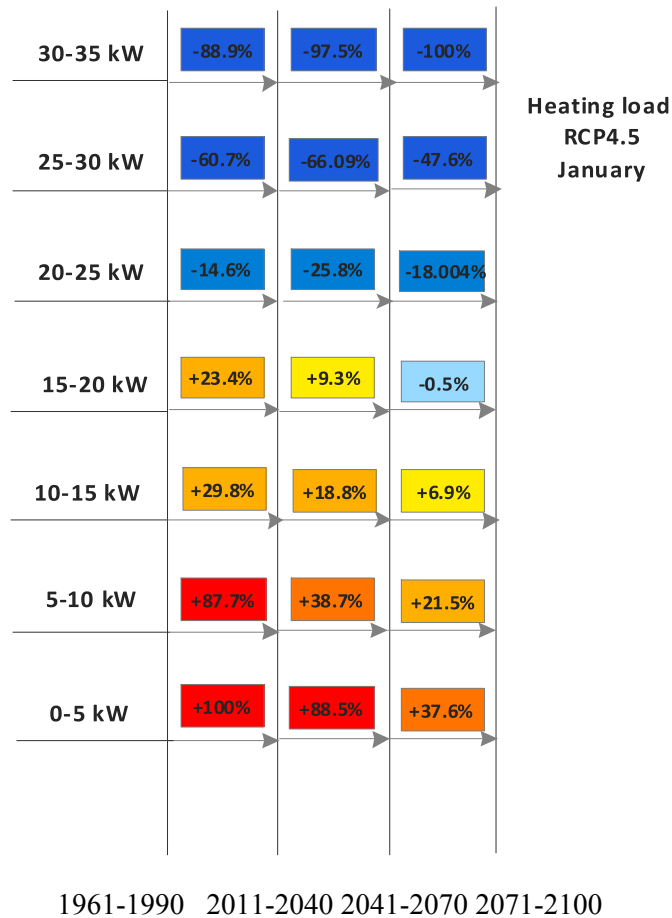


Figure 18: Percentage of climate change effect on different parts of the hourly heating load based on RCP4.5 in January in four different periods of 1961-1990, 2011-2040, 2041-2070, and 2071-2100.

Figure 18 shows the impact of climate change on the heating load in January. As this figure indicates, the climate change has the most effect on the upper and lower tail of the load, whereas, its effect decreases from the upper tail to the middle and from the lower to the middle. The climate change has the least effect on the load of 15-20 kW in January. Moreover, the climate change has a dropping effect on the loads more than 15-20 kW and an additive effect on the loads less than the transient load of 15-20 kW.

#### **4.2.1.2. Uncertainty assessment**

Table 19 shows the variability of different global circulation models for heating load based on RCP4.5. In the first period, the max, Avg, and STD are minimum in Ensemble, MIROC\_ESM, and Ensemble, respectively, and CNRM\_CM5 has the highest values for all of these statistical parameters.

In the second period, the max, Avg, and STD in Ensemble, MIROC\_ESM, and CanESM2 have the least amount, respectively, and in MIROC5, CNRM\_CM5, and IPSL\_CM5A\_LR have the highest values, respectively. Therefore, the other GCM models are between the maximum and minimum values.

In the third period, for the max, Avg, and STD statistical values, MIROC\_ESM, MIROC\_ESM, and CanESM2 have the lowest values, respectively, and IPSL\_CM5A\_LR has the highest values for all three aforementioned statistical parameters. Other GCM models' results are between maximum and minimum values for each statistical parameter.

Table 19: Statistical values of different GCM models of the hourly heating load based on RCP4.5 in four periods of 1961-1990, 2011-2040, 2041-2070, 2071-2100.

<i>Models RCP4.5 Heating Load kWh</i>	<i>1961-1990</i>				<i>2011-2040</i>				<i>2041-2070</i>				<i>2071-2100</i>			
	<i>Max</i>	<i>AVE</i>	<i>STD</i>	<i>Median</i>												
<i>CanESM2</i>	37.03	8.40	8.70	6.005	32.20	7.10	7.50	4.80	33.70	6.20	6.80	4.20	29.40	5.80	6.40	3.80
<i>CNRM_CM5</i>	36.80	8.40	8.70	6.005	39.30	7.80	8.30	5.20	34.10	7.10	7.80	4.50	34.90	6.70	7.50	4.02
<i>MIROC_ESM</i>	36.60	8.40	8.70	6.005	35.06	6.60	7.60	3.90	36.60	6.00	7.00	3.10	28.20	5.60	6.80	2.60
<i>IPSL_CM5A_LR</i>	36.40	8.40	8.70	6.005	34.40	7.40	8.20	4.50	34.70	7.10	8.10	4.10	35.90	6.80	8.04	3.60
<i>MIROC5</i>	36.70	8.40	8.70	6.005	32.10	7.50	8.30	4.60	37.40	6.70	7.70	3.70	32.70	6.40	7.50	3.40
<i>Ensemble</i>	34.50	8.40	8.70	6.005	31.50	7.10	7.40	4.70	31.40	6.40	6.80	4.10	29.90	6.03	6.50	3.70

## 4.2.2. Heating load RCP8.5

### 4.2.2.1. Ensemble analysis results

Figure 19 shows the cumulative distribution function of the heating load based on RCP8.5, which depicts that the heating load will increase over the time. The main inference from the figure is that almost equal distance between the probability values of each period was not observed in heating load based on RCP4.5.

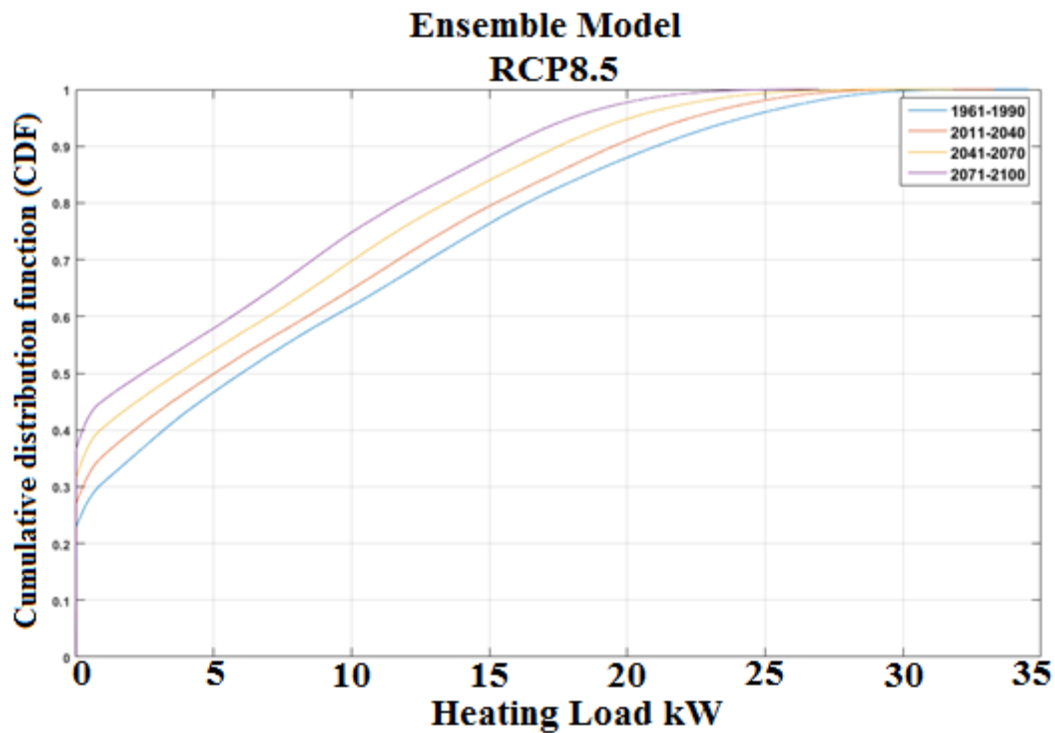


Figure 19: Cumulating distribution function of the hourly heating load based on RCP8.5 in four periods of 1961-1990, 2011-2040, 2041-2070, and 2071-2100 and ensemble GCM model.

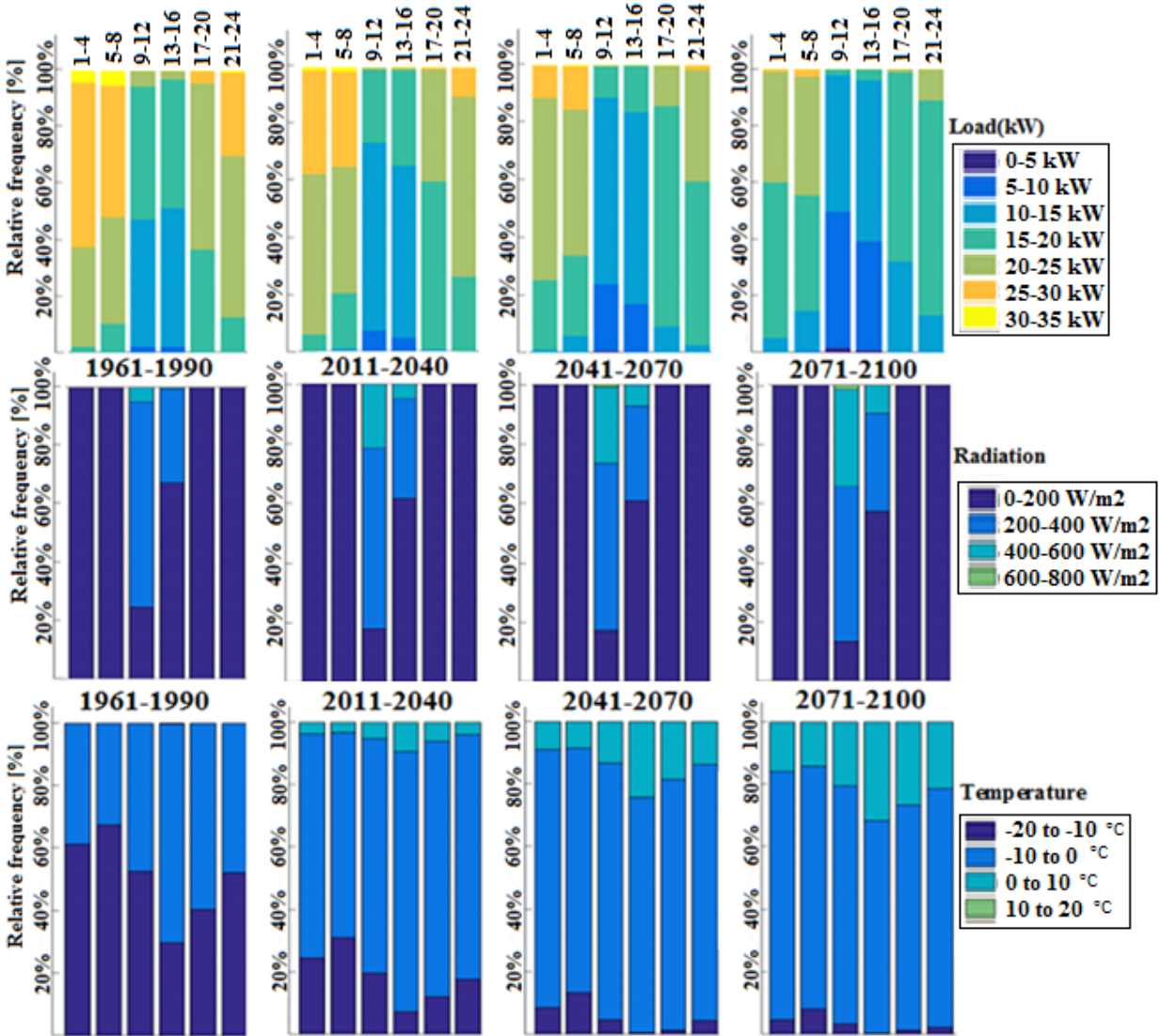


Figure 20: Hourly relative frequency of heating load based on RCP8.5 in January in four periods of 1961-1990, 2011-2040, 2041-2070, and 2071-2100 and ensemble GCM model.

Figure 20 shows the hourly ensemble of the heating load based on RCP8.5 in January which indicates that the heating load will drop over the time. Moreover, the climate change effect on the hourly behavior of the heating peak load shows that some peak loads will disappear in the future in this month. For example, the peak load of 30-35 kW for the hour 21:00 h-24:00 h will start to disappear from the first period. Furthermore, at 1:00 h-4:00 h and 5:00 h-8:00 h, it will start to disappear in the third period. In addition, the load of 25-30 kW at 17:00 h-20:00 h will start to disappear in the second period and this peak load will disappear at 21:00 h-24:00 h in the third period.

By analyzing the hourly radiation and temperature profile one can explain the reason for this reduction. As can be seen, the hourly radiation at the hours that radiation exists such as 9:00 h – 12:00 h and 13:00 h-16:00 h will increase from historical to the third period. At 9:00 h – 12:00 h and 13:00 h-16:00 h that due to radiation, the heating load is the lowest, especially in the future that as the radiation increases, the heating load at 9:00 h-12:00 h and 13:00 h-16:00 h will decrease. Furthermore, at 9:00 h-12:00 h and 13:00 h-16:00 h that one has the maximum radiation the load of 20-25 kW will start to disappear in the first period and the load of 15-10 kW will fall dramatically to the third period. Moreover, by analyzing the hourly temperature profile, which is increasing over time, one can see that this weather parameter is the chief factor for the decrease in the heating load after the radiation.

Table 20: Relative frequency of different parts of the hourly heating load in December, January, and February based on RCP8.5 in four different periods of 1961-1990, 2011-2040, 2041-2070, and 2071-2100.

Load (kW)	<b><u>Heating Load [Relative frequency] – Ensemble RCP8.5 Scenario</u></b>											
	1961-1990			2011-2040			2041-2070			2071-2100		
Month	Dec	Jan	Feb	Dec	Jan	Feb	Dec	Jan	Feb	Dec	Jan	Feb
30-35	0.37%	1.6%	1.08%	0	0.4%	0.03%	0	0.05%	0.03%	0	0	0
25-30	9%	23.16%	12.92%	3.69%	13.44%	5.33%	1.28%	4.64%	1.57%	0.03%	0.61%	0.01%
20-25	29.23%	33%	29.95%	25.58%	34.16%	23.33%	14.77%	27.88%	12.3%	7.32%	15.42%	3.75%
15-20	34.18%	25.61%	27.66%	38.02%	28.36%	35.53%	41.39%	35.47%	38.72%	36.36%	40.77%	31.68%
10-15	21.71%	15.74%	21.1%	25.65%	21.55%	21.3%	29.21%	25.12%	24.66%	36.21%	28.22%	34.08%
5-10	5.45%	0.8%	7.02%	6.99%	2.06%	13.92%	13.16%	6.71%	19.04%	18.83%	14.52%	21.95%
0-5	0.026%	0	0.24%	0.04%	0	0.53%	0.16%	0.11%	3.64%	1.22%	0.43%	8.49%
Period	1961-1990			2011-2040			2041-2070			2071-2100		

The frequencies and their percentages of the heating load based on RCP8.5 are shown in Table 20. As can be noted, the upper tail of the heating load is dropping over time, while the lower tail of the load is rising and the middle part of the load is fluctuating. Like RCP4.5, some parts of the falling frequencies from the upper tails of the load will remove and some other parts will be added to the lower tail or middle part of the load. This is the reason why the lower tail of the heating load always increases while the middle part sometimes increases and sometimes decreases.

The other point that can be perceived from these tables is that the climate change targets, mainly the upper tail of load and lowers some frequencies on that parts in the future. This behavior of the load explains the importance of supplying the peak load in the future.

The interesting result from these tables is the behavior of the maximum frequency of heating load, which usually occurs in the middle of the load. For example, the maximum frequency in December will always happen in the load of 15-20 kW, but because of the impact of climate change will increase to the second period, while in the third period it will decline slightly. Moreover, in January, the maximum frequency occurs in the load of 20-25 kW and then in the first period again will happen in the load of 20-25 kW, while its frequency will increase. In the second period, it will shift to the load of 15-20 kW, while its frequency will go up again, and in the third period, it will also happen in the load of 15-20 kW, while its frequency will increase. Therefore, it is understood that the maximum load frequency in January will rise continuously from historical to the third period and it will shift to the lower loads. Finally, the maximum load frequency in February occurred in the load of 20-25 kW in the historical period, and in the first period, it will shift to the lower load of 15-20 kW, while its frequency will increase. Moreover, in the second period it will happen again in the load of 15-20 kW, while its frequency will rise, and in the third period, it will shift to the lower load of 10-15 kW, whereas its frequency will decrease in this period.

As the results show, the maximum frequency of heating load in the future due to the impact of climate change tends to shift to the lower loads, while its frequency tends to increase and sometimes it will decrease slightly in the third period.

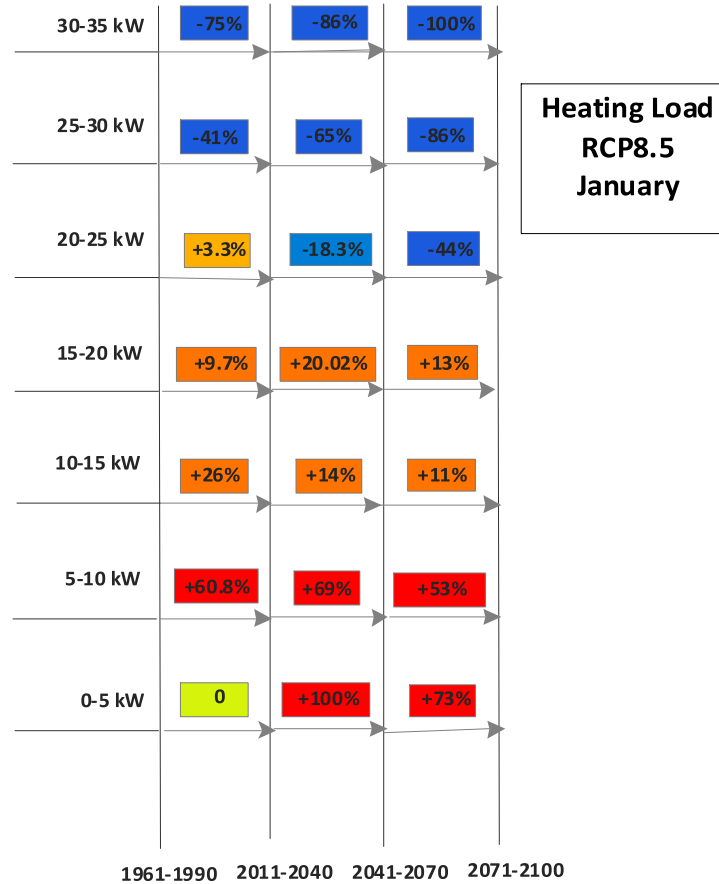


Figure 21: Percentage of climate change effect on different parts of the hourly heating load based on RCP8.5 in January in four different periods of 1961-1990, 2011-2040, 2041-2070, and 2071-2100.

Figure 21 shows the impact of climate change on each part of the heating load based on RCP8.5 in January. As it illustrates, the climate change has the most effect on the upper and lower tail of the load and with moving toward the middle from both upper tail and lower tail, this effect will fall. The load of 20-25 kW shows a transient behavior which the climate change has a dropping effect on the loads more than this amount and an additive effect on the loads less this value. It is worth mentioning that the climate change does not have any effect on the load of 0-5 kW from historical to the first period and also the peak load in the third period will be twice as high as the peak load in the second period.

#### 4.2.2.2. Uncertainty assessment

Table 21 shows the variability of different GCM models in comparison to Ensemble model based on RCP8.5 for the heating load. In the first period, MIROC5, MIROC\_ESM, and CanESM2 have the lowest amounts of the max, Ave, and STD, respectively, and IPSL\_CM5A\_LR, CNRM\_CM5, and IPSL\_CM5A\_LR have the most values, respectively. Therefore, the other GCM models are among these models.

In the second period, MIROC5, MIROC\_ESM, and MIROC\_ESM have the lowest values of max, Ave, and STD, respectively, and the GCM model of IPSL\_CM5A\_LR has the highest values for all the aforementioned statistical parameters.

In the third period, the statistical parameters of max, Ave, and STD, have the lowest values in the GCM models of MIROC5, MIROC\_ESM, and CanESM2, respectively, which is similar to the first period. Moreover, the GCM models of IPSL\_CM5A\_LR, CNRM\_CM5, and IPSL\_CM5A\_LR have the highest values respectively for the aforementioned statistical parameters.

The results indicate that most of the time heating load in Ensemble model in the historical period is less than in the other GCM models, but in the future, it will be placed in the middle of chosen GCM models.

Table 21: Statistical values of different GCM models of the hourly heating load based on RCP8.5 in four periods of 1961-1990, 2011-2040, 2041-2070, 2071-2100.

<b>Models RCP8.5 Heating Load kWh</b>	<i>1961-1990</i>				<i>2011-2040</i>				<i>2041-2070</i>				<i>2071-2100</i>			
	<i>Max</i>	<i>AVE</i>	<i>STD</i>	<i>Median</i>												
<b><i>CanESM2</i></b>	37.03	8.4	8.7	6.005	33.03	7.2	7.7	5.04	28.9	6.3	7.07	3.9	28.5	5.2	6.1	2.5
<b><i>CNRM_CM5</i></b>	36.8	8.4	8.7	6.005	35.8	7.6	8.1	5.1	32.5	6.7	7.5	4.03	29.06	5.9	7.02	2.9
<b><i>MIROC_ESM</i></b>	36.6	8.4	8.7	6.005	34.2	6.9	7.8	4.2	30.2	5.8	7.02	2.9	27.5	4.8	6.2	1.3
<b><i>IPSL_CM5A_LR</i></b>	36.4	8.4	8.7	6.005	39.4	7.5	8.4	4.5	33.6	6.7	7.9	3.4	33.1	5.9	7.3	2.2
<b><i>MIROC5</i></b>	36.7	8.4	8.7	6.005	29.9	7.4	8.1	4.6	27.1	6.02	7.2	2.9	25.2	5.1	6.6	1.6
<b><i>Ensemble</i></b>	34.5	8.4	8.7	6.005	33.2	7.4	7.8	5.04	31.8	6.4	7.1	3.7	26.9	5.4	6.4	2.4

### 4.2.3. Comparison (RCP4.5 and 8.5)

By comparing the obtained results of RCP4.5 and RCP8.5, it can be inferred that because of the effect climate change on hourly heating load it will drop more based on RCP8.5 than RCP4.5, especially in the third period. As can be seen, some peak loads in December will disappear in the second and third period based on RCP8.5, while based on RCP4.5 they will still remain in the second and third period. For example, the peak load of 25-30 kW at 17:00 h-20:00 h and 21:00 h-24:00 h based on RCP8.5 will disappear in the second period, whereas they will happen in the second period based on RCP4.5. Moreover, the peak load of 25-30 kW will disappear from all the hours in the third period of RCP8.5, while it will occur at 1:00 h-4:00 h and 5:00 h-8:00 h based on RCP4.5 in the third period. In addition, the peak load of 20-25 kW will disappear at 17:00 h-20:00 h in the third period of RCP8.5, while it will happen in the third period of RCP4.5 at 17:00 h-20:00 h. Moreover, at 9:00 h-12:00 h in the third period, the radiation is at its maximum state, which causes the heating load to be at its minimum, as can be seen; the load of 15-20 kW will disappear based on RCP8.5, while it will still exist based on RCP4.5.

By analyzing the months of January and February, it can be figured out that the only difference between the obtained results from RCP4.5 and RCP8.5 is the hourly heating load in the future based on RCP8.5 is less than RCP4.5, especially the peak loads.

Finally, by analyzing the obtained results from the month February, one can see that the load of 25-30 kW will disappear at 1:00 h-4:00 h in the third period based on RCP8.5, while it will happen in the future based on RCP4.5.

The other difference between the obtained results from RCP4.5 and RCP8.5 is associated with the maximum frequency, which in January based on RCP8.5, will happen in the load of 20-25 kW, while based on RCP4.5 it will occur in the load of 15-20 kW, and the last discrepancy is the amount of frequency in each period and month, which is sometimes more based on RCP4.5 and at other times is more based on RCP8.5.

The main differences of the impact of climate change on each part of the heating load between RCP4.5 and RCP8.5 are as follows:

- In December from first to second and second to the third period, the climate change effect on peak load of 30-35 kW is zero based on RCP8.5 but in the maximum state based on RCP4.5.
- In January, first, the transient load based on RCP8.5 is 20-25 kW, while based on RCP4.5, it is 15-20 kW. Second, the percentage of the impact of climate change on the load of 0-5 kW from historical to the first period based on RCP8.5 is zero, while based on RCP4.5 is additive and very high.
- In February the peak load of 30-35 kW from the first period to the second period based on RCP8.5 is zero, while based on RCP4.5, it is dropping and very high. Moreover, from the second period to the third period it is zero based on RCP4.5, but dropping and intensive based on RCP8.5.

#### **4.2.4. Cooling load RCP4.5**

##### **4.2.4.1. Ensemble analysis results**

Based on Figure 22 which shows the cumulative distribution function of cooling load over time based on RCP4.5, the cooling load is increasing over time. As this figure depicts, like heating load, the behavior of cooling load in the second and third period based on RCP4.5 is almost the same. This phenomenon is justifiable by RCP4.5 radiative forcing behavior, which in the middle of the second period its acceleration will decline to be stabilized at the end of the third period.

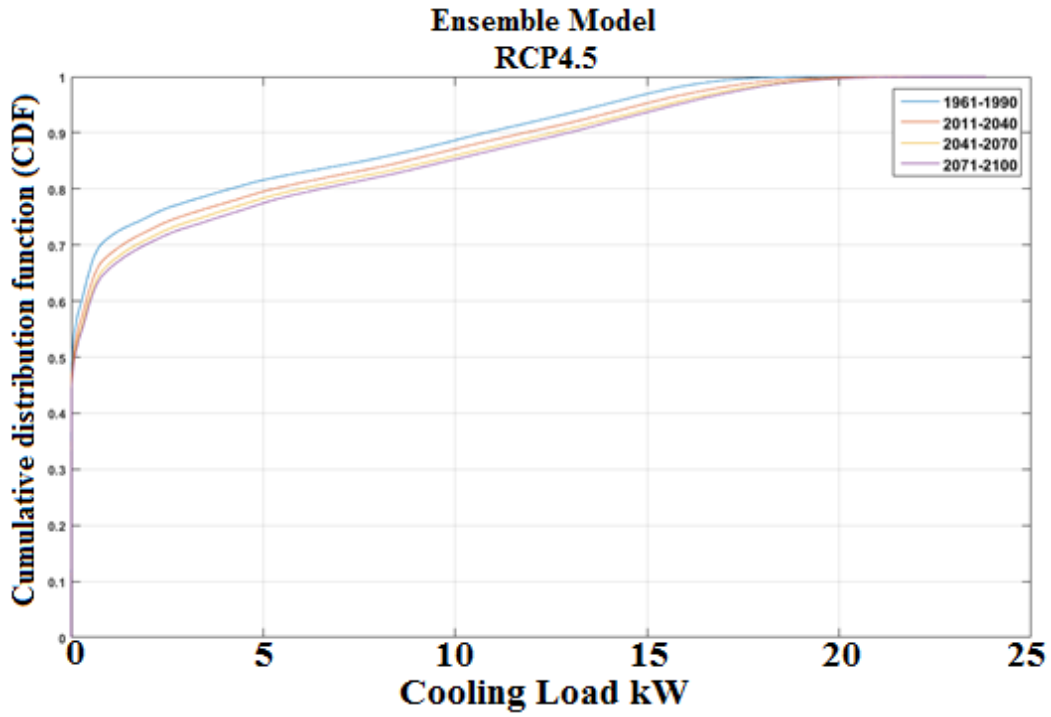


Figure 22: Cumulating distribution function of the hourly cooling load based on RCP4.5 in four periods of 1961-1990, 2011-2040, 2041-2070, and 2071-2100 and ensemble GCM models.

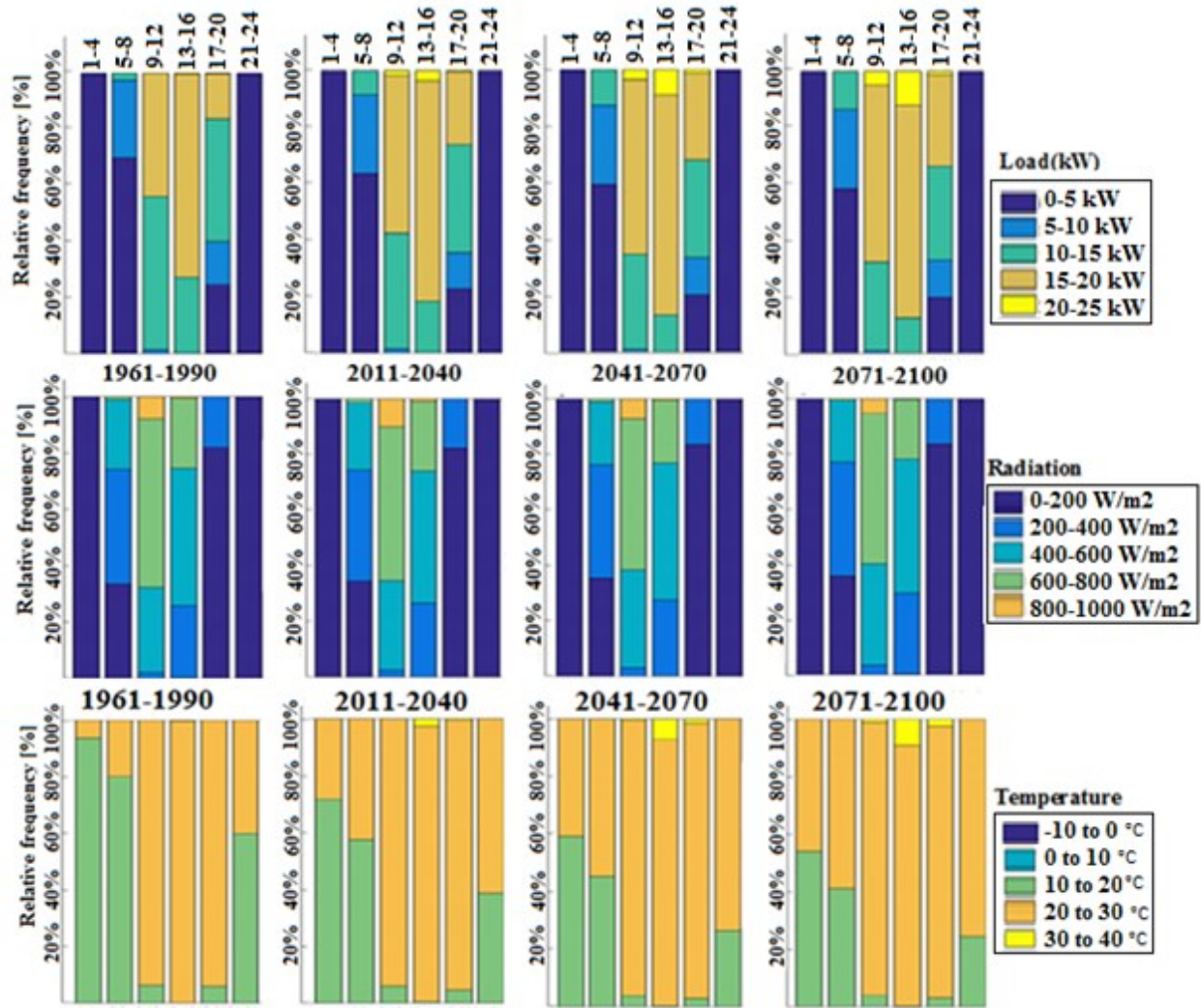


Figure 23: Hourly relative frequency of cooling load based on RCP4.5 in July in four periods of 1961-1990, 2011-2040, 2041-2070, and 2071-2100 and ensemble GCM model

Figure 23 Shows the ensemble hourly cooling load based on RCP4.5 in July. As this figure shows, the hourly cooling load in this month based on RCP4.5 will go up. Impact of climate change results in appearing high peak loads in the future like in the load of 20-25 kW which will start to appear at 9:00 h-12:00 h and 13:00 h-16:00 h in the first period and also at 17:00 h-20:00 h which will start to appear in the second period.

Evaluating the hourly radiation and temperature in the future, which will increase in the first period and then will decrease in the second and third period reveals that radiation has the most impact on cooling load in the hours that there is the most radiation such as 9:00 h-12:00 h and 13:00 h-16:00 h. As can be seen, at 9:00 h-12:00 h and 13:00 h-16:00 h that the radiation is in its

maximum state, the cooling load has its maximum value. Therefore, it can be a sign for doing an adequate and accurate mitigation of the impact of climate change, since whenever the cooling load is the max, the radiation is max and therefore this advantage can be applied in order to supply required energy for the cooling load in future.

By analyzing the hourly temperature, it can be declared that the temperature in this month has the most impact on cooling load after radiation. As these results reveal, the function of temperature is mostly to increase the average load, whereas the function of radiation is mainly to increase the peak loads. For instance, the temperature at 13:00 h-16:00 h in the third period is the highest, and as the radiation figure shows it is very high in this hour. Therefore, the temperature increases the cooling load and radiation exacerbate this trend, which affects the peak load more considerably, and sometimes creates higher peak loads. The frequencies and relative frequencies of the cooling load based on RCP4.5 are gathered in Table 22. As shown in these figures, both of the loads of 30-35 kW and 25-30 kW will not exist in the future; and the peak load will start from the load of 20-25 kW. According to the results, the lower tail of the cooling load is decreasing while the upper tail of the load is increasing. Considering the impact of climate change, the behavior of the cooling load shows that climate change in cooling load targets the lower tail of the cooling load and reduces it, while these moved frequencies will be transferred to the middle and upper tail of the cooling load. As can be seen, the increase in the upper tail of the cooling load is significant, which can lead to serious problems in the future. One point that is evident from the hourly cooling load is that the maximum cooling load occurs only in the lower tail of the load, which here is the load of 0-5 kW. For example, the maximum cooling load in June happened in the load of 0-5 kW, which will diminish in the first, second, and third period, respectively. The months of July and August follow the same trend in the future. The next maximum cooling load will happen almost in the middle of the load. For example, in June the second maximum cooling load in historical period happened in the load of 10-15 kW and will decrease in the first period, but still occurs in the load of 10-15 kW, but in the second period the second maximum frequency will shift to upper load of 15-20 kW, while slightly decreasing. Moreover, in the third period, the second frequency will remain in the load of 15-20 kW but will rise slightly. Therefore, when the shift happens, the frequency will drop, and if there were not a shift in the load, the frequency of cooling load would rise most of the time. The second maximum frequency tends to shift up in general, and the frequencies that become separated from the lower tail of the load are likely to

move upward. In the month July, the second maximum frequency will remain just in the load of 15-20 kW, but its frequency will rise to the second period and then in the third period will fall minimally. Moreover, in August, the second maximum load will happen and remain in the load of 10-15 kW, but its frequency will decrease in the first period and will grow in the second period and then will decrease in the third period.

Table 22: Relative frequency of different parts of the hourly cooling load in Jun, July, and August based on RCP4.5 in four different periods of 1961-1990, 2011-2040, 2041-2070, and 2071-2100

Load (kW)	<b>Cooling Load [Relative frequency] – Ensemble RCP4.5 Scenario</b>											
	1961-1990			2011-2040			2041-2070			2071-2100		
<b>30-35</b>	0	0	0	0	0	0	0	0	0	0	0	0
<b>25-30</b>	0	0	0	0	0	0	0	0	0	0	0	0
<b>20-25</b>	0.009%	0.08%	0	0.1%	0.9%	0.08%	0.6%	2.2%	0.02%	0.7%	3.06%	0.03%
<b>15-20</b>	5.9%	<u>22%</u>	7.5%	15.6%	<u>26.6%</u>	9.9%	<u>22.2%</u>	<u>28.4%</u>	10.8%	<u>25.1%</u>	<u>28.4%</u>	10.5%
<b>10-15</b>	<u>31.7%</u>	21.3%	<u>29.4%</u>	<u>26.9%</u>	17.6%	<u>24.8%</u>	21.7%	15.6%	<u>25.4%</u>	19.5%	15.1%	<u>24.8%</u>
<b>5-10</b>	10.5%	7.4%	9.2%	8.05%	7.03%	11.4%	7.5%	7.07%	10.3%	7.3%	7.1%	11%
<b>0-5</b>	<u>51.6%</u>	<u>49.1%</u>	53.7%	<u>49.2%</u>	<u>47.6%</u>	<u>53.5%</u>	<u>47.7%</u>	<u>46.6%</u>	<u>53.3%</u>	<u>47.1%</u>	<u>46.2%</u>	<u>53.4%</u>
<b>Month</b>	<b>Jun</b>	<b>July</b>	<b>Aug</b>	<b>Jun</b>	<b>July</b>	<b>Aug</b>	<b>Jun</b>	<b>July</b>	<b>Aug</b>	<b>Jun</b>	<b>July</b>	<b>Aug</b>
<b>Period</b>	<b>1961-1990</b>			<b>2011-2040</b>			<b>2041-2070</b>			<b>2071-2100</b>		

Figure 24 shows the percentage of the impact of climate change on the cooling load based on RCP4.5 in July. As can be seen, the climate change does not have any effect on loads of 25-30 and 30-35 kW, because there is not any cooling load frequency after the load of 20-25 kW. The most impact of climate change on the cooling load in July is in the cooling peak load of 20-25 kW, which will decrease to reach its least impact, which is happening in the lower tail of the cooling load in the load of 0-5 kW. It is possible to consider the load of 15-20 kW as a transient load which the climate change has an additive effect on the loads higher than this load and a dropping effect on the loads lower than this load.

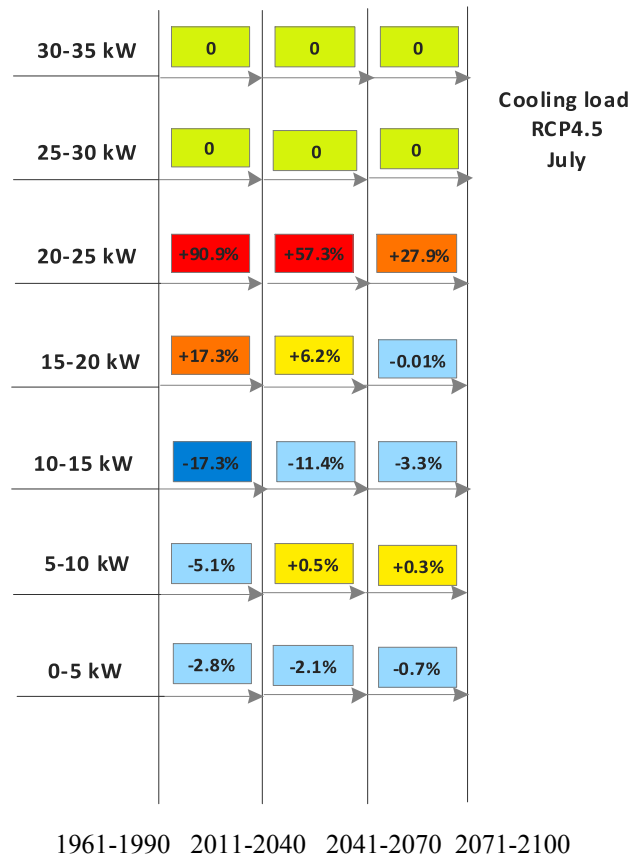


Figure 24: Percentage of climate change effect on different parts of the hourly cooling load based on RCP4.5 in July in four different periods of 1961-1990, 2011-2040, 2041-2070, and 2071-2100.

The amount of climate change effect on the peak load of 20-25 kW is not comparable with the other parts of the load, which shows the climate change will target the cooling load and will increase it more than the other parts. One interesting point in the analysis of the degree of impact of climate change on the cooling load is having an additive effect among dropping effects in the load of 5-10 kW from historical to the first period and first period to the third period.

#### 4.2.4.2. Uncertainty assessment

Table 23 demonstrates the variability of different global circulation models for the cooling load obtained based on RCP4.5. In the first period, the max, Ave, and STD of the MIROC5, CNRM\_CM5, and Ensemble have the least values respectively, while MIROC\_ESM has the most value of all of the aforesaid statistical parameters.

Moreover, in the second period, the least values of the max, Ave, and STD will happen in the GCM models of MIROC5, CNRM\_CM5, and CanESM2 respectively, while the most value of all three aforementioned statistical parameters will occur in MIROC\_ESM.

Finally, in the third period, the least values of the max, Ave, and STD will happen in Ensemble, CanESM2, and CanESM2 models respectively, while the most values of all three aforementioned statistical parameters will happen in MIROC\_ESM. The other models are among the maximum and minimum models in each period. As the results reveal, MIROC\_ESM in the future have the most statistical values.

Table 23: Statistical values of different GCM models of the hourly cooling load based on RCP4.5 in four periods of 1961-1990, 2011-2040, 2041-2070, and 2071-2100.

<i>Models RCP4.5 Cooling Load kWh</i>	<i>1961-1990</i>				<i>2011-2040</i>				<i>2041-2070</i>				<i>2071-2100</i>			
	<i>Max</i>	<i>AVE</i>	<i>STD</i>	<i>Median</i>												
<i>CanESM2</i>	23.2	2.4	4.6	0.005	23.9	2.7	5.03	0.03	23.6	2.9	5.1	0.05	26.1	2.9	5.1	0.06
<i>CNRM_CM5</i>	21.2	2.4	4.6	0.007	22.8	2.6	4.9	0.02	23.1	2.8	5.2	0.04	24.9	3.04	5.4	0.06
<i>MIROC_ESM</i>	23.3	2.4	4.6	0.006	30.2	3.1	5.6	0.04	26.3	3.3	5.8	0.08	30.9	3.5	6.05	0.1
<i>IPSL_CM5A_LR</i>	23.3	2.4	4.6	0.007	22.6	2.8	5.1	0.04	24.3	3.09	5.5	0.06	27.5	3.3	5.7	0.09
<i>MIROC5</i>	23.5	2.4	4.6	0.006	22.07	2.8	5.1	0.04	22.7	3.1	5.5	0.08	24.8	3.2	5.6	0.1
<i>Ensemble</i>	21.3	2.4	4.6	0.008	22.2	2.7	4.9	0.04	23.6	2.9	5.1	0.07	23.8	3.1	5.3	0.09

## 4.2.5. Cooling load RCP8.5

### 4.2.5.1. Ensemble analysis results

The ensemble cumulative function of the cooling load based on RCP8.5 has been shown in Figure 25. As can be seen, the cooling load will grow over time due to the effect of climate change. One point that can be understood from this figure is almost equal distances between the periods from historical to the third period, which is in contrast to RCP4.5.

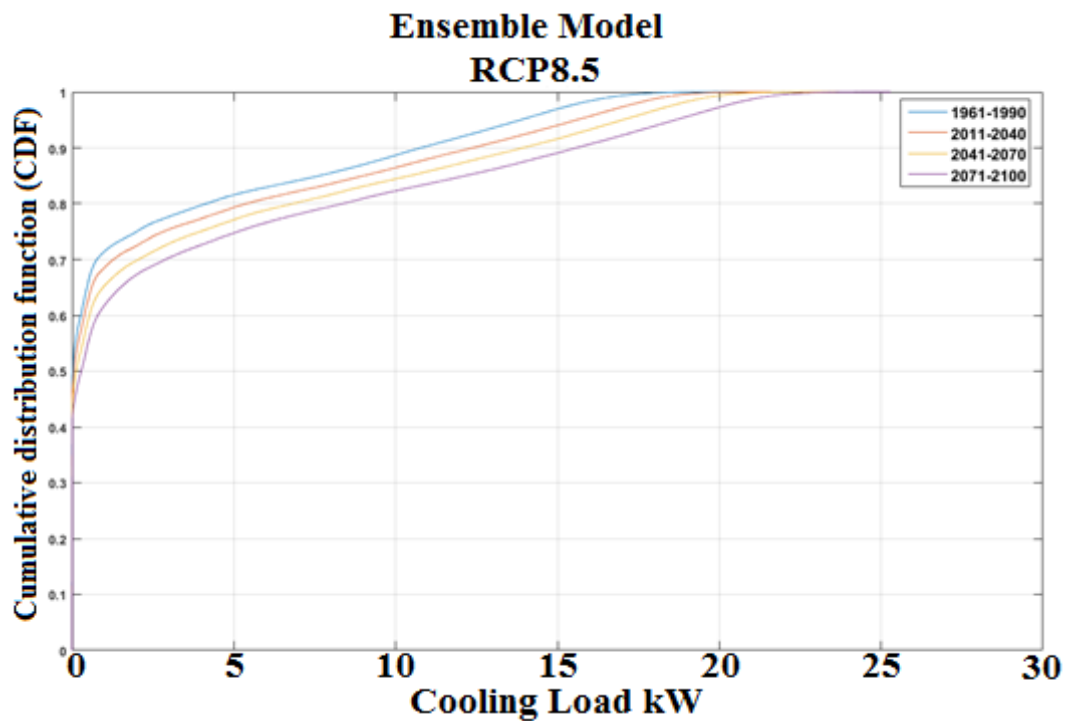


Figure 25: Cumulating distribution function of the hourly cooling load based on RCP8.5 in four periods of 1961-1990, 2011-2040, 2041-2070, and 2071-2100 and ensemble GCM model.

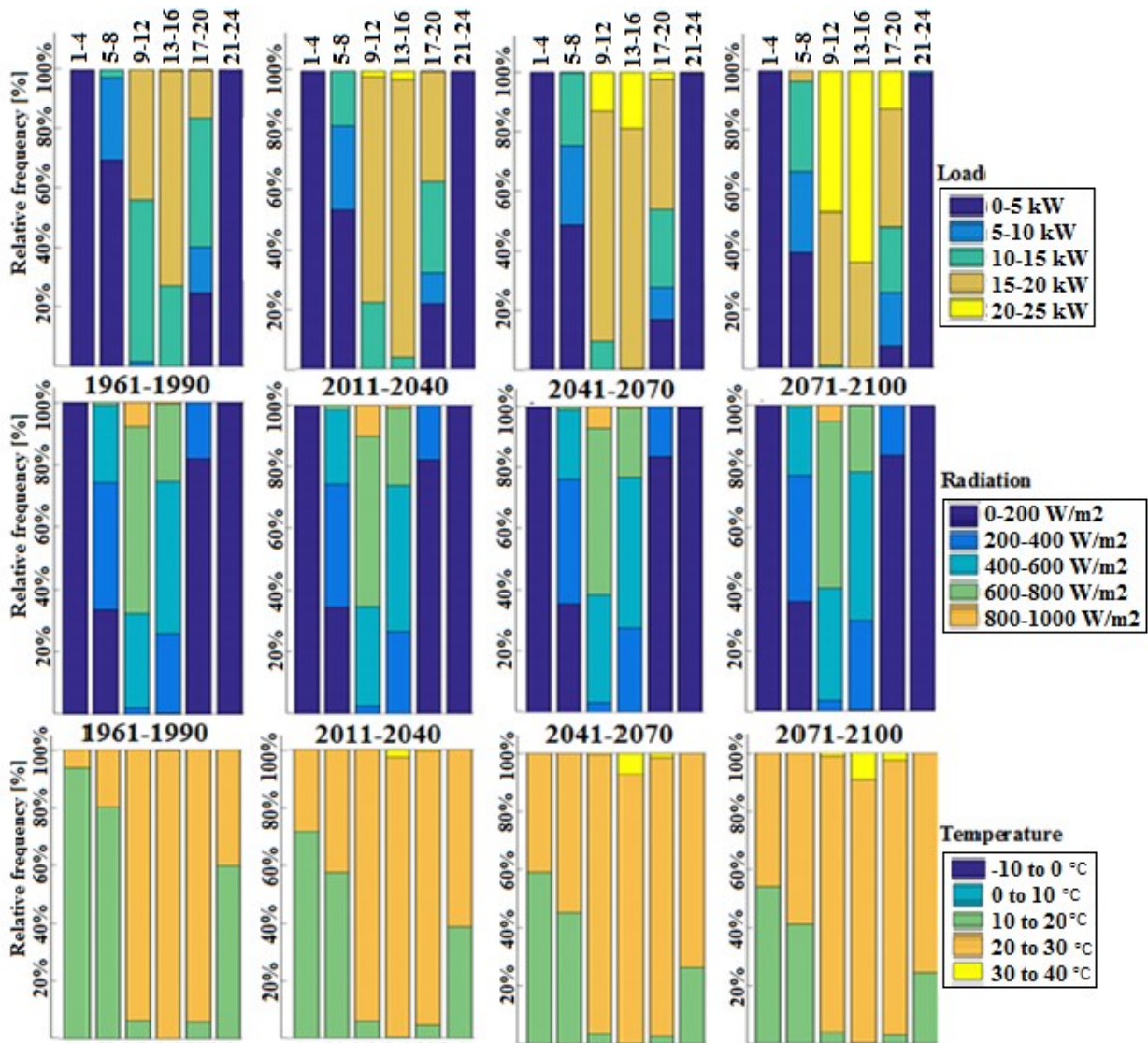


Figure 26: Hourly relative frequency of cooling load based on RCP8.5 in July in four periods of 1961-1990, 2011-2040, 2041-2070, and 2071-2100 and ensemble GCM model

The ensemble hourly cooling load based on RCP8.5 in July has been shown in Figure 26. As this figure displays, the hourly cooling load will rise because of the effect of climate change. The load of 20-25 kW will start to appear at 9.00 h -12.00 h and 13.00 h -16.00 h in the first period and at 17:00 h-20:00 h in the second period. Moreover, the load of 15-20 kW at 5:00 h-8:00 h will appear for the first time in the third period.

In July, the increase in the peak load of 20-25 kW shows a significant enhancement which will be the main concern for supplying this amount of energy in the future in summer in Montreal, Canada.

Studying the hourly behavior of the radiation and temperature shows the reason for the rise in the cooling load based on RCP8.5 in the future. As can be seen, the radiation will climb in the first period and then will go down to the third period. The effect of radiation is more considerable in the hours that it is in its maximum, including 9:00 h-12:00 h and 13:00 h-16:00 h, which leads to the most cooling load in that hours in the future in July.

By analyzing the hourly temperature profile, one can realize the significance of the effect of temperature in this month, which is the second main reason for the increase in the cooling load in this month in the future. The temperature based on RCP8.5 will have a marked enhancement in the third period, which reveals its effect on dramatic enhancement of cooling load in the third period.

The ensemble cooling load frequency and relative frequency based on RCP8.5 are gathered in Table 24. As these tables show, the load of 30-35 kW and 25-30 kW will not occur in the future. The peak load in the cooling load based on RCP8.5 starts from the load of 20-25 kW. The maximum load will happen only in the lower tail of the load and by considering the effect of climate change it will push some frequencies from the lower tail of the cooling load to the upper parts of the load, especially the peak load. As can be seen, the peak cooling load is going to go up significantly in the future, especially in the third period that will be one of the main concerns for supplying this amount of energy.

The second maximum cooling load frequency in June happens in the load of 10-15 kW; in the first period its frequency will decrease, and in the second period it will shift to the upper load of 15-20 kW, while its frequency will rise. Moreover, in the third period, the second frequency in June will remain in the load of 15-20 kW, while its frequency will rise more considerably.

In July the second maximum load will occur in the load of 15-20 kW, which will grow in the first period and then will drop in the second period and then will decrease more in the third period while remaining in the load of 15-20 kW.

Finally, in August the maximum load frequency will happen in the load of 10-15 kW which will remain in this load in the first period while its frequency will decrease. Moreover, the second maximum load in August in the second period will shift to the load of 15-20 kW while its frequency

will go up. At the end, this second maximum frequency of the cooling load in the third period will remain in the load of 15-20 kW whereas its frequency will increase.

Table 24: Relative frequency of different parts of the hourly cooling load in Jun, July, and August based on RCP8.5 in four different periods of 1961-1990, 2011-2040, 2041-2070, and 2071-2100.

Load (kW)	<b>Cooling Load [Relative frequency] – Ensemble RCP8.5 Scenario</b>											
	1961-1990			2011-2040			2041-2070			2071-2100		
Month	Jun	July	Aug	Jun	July	Aug	Jun	July	Aug	Jun	July	Aug
<b>30-35</b>	0	0	0	0	0	0	0	0	0	0	0	0
<b>25-30</b>	0	0	0	0	0	0	0	0	0	0	0.01%	0
<b>20-25</b>	0.009%	0.08%	0	0.01%	0.7%	0.04%	1.2%	5.6%	0.7%	6.1%	20.7%	5.4%
<b>15-20</b>	5.9%	<u>22.%</u>	7.5%	17%	<u>34.3%</u>	17.5%	<u>28.2%</u>	<u>33.7%</u>	<u>24.4%</u>	<u>32.2%</u>	<u>21.7%</u>	<u>26.9%</u>
<b>10-15</b>	<u>31.7%</u>	21.3%	<u>29.4%</u>	<u>26.3%</u>	12.5%	<u>22.9%</u>	17.1%	10.1%	18.09%	10.8%	8.8%	12.7%
<b>5-10</b>	10.5%	7.4%	9.2%	7.7%	6.4%	8.6%	7.4%	6.2%	7.9%	7.2%	7.7%	8.07%
<b>0-5</b>	<u>51.6%</u>	<u>49.1%</u>	<u>53.7%</u>	<u>48.8%</u>	<u>45.8%</u>	<u>50.8%</u>	<u>45.9%</u>	<u>44.2%</u>	<u>48.7%</u>	<u>43.5%</u>	<u>40.9%</u>	<u>46.8%</u>
<b>Period</b>	<b>1961-1990</b>			<b>2011-2040</b>			<b>2041-2070</b>			<b>2071-2100</b>		

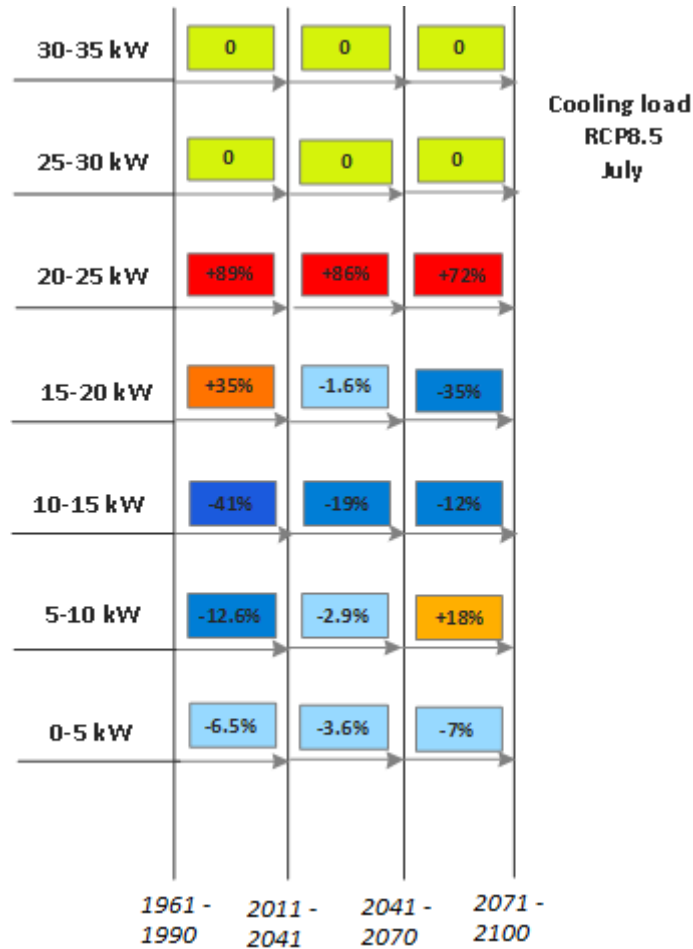


Figure 27: Percentage of climate change effect on different parts of the hourly cooling load based on RCP8.5 in July in four different periods of 1961-1990, 2011-2040, 2041-2070, and 2071-2100.

Figure 27 shows the climate change impact on the load based on RCP8.5 in July. Based on the obtained results, the climate change does not have any effect on loads of 25-30 and 30-35 kW. Moreover, the climate change has the most effect on the peak load of 20-25 kW and with moving toward the lower tail of the load this effect decreases.

The load of 15-20 kW functions as a transient load and the climate change has to drop effect on the loads lower than this load. This rule does not apply to the load of 5-10 kW from second to the third period in which climate change shows an additive effect on the load that is between the dropping parts.

#### **4.2.5.2. Uncertainty assessment**

Based on Table 25 in the first period the max, Ave, and STD will occur in the Ensemble, CNRM\_CM5, and CNRM\_CM5 respectively, while the maximum of all three statistical parameters will happen in MIROC\_ESM model. In addition, in the second period, the minimum values of all three aforementioned statistical parameters will occur in CNRM\_CM5, while the maximum amounts will happen in IPSL\_CM5A\_LR, MIROC\_ESM, and IPSL\_CM5A-LR respectively.

In the third period, the Ave, and STD will occur in CNRM\_CM5, and CNRM\_CM5 models, whereas the maximum will happen in IPSL\_CM5A\_LR, MIROC\_ESM, and MIROC\_ESM respectively. The results indicate that usually, CNRM\_CM5 has the minimum cooling load amongst the other GCM models and also MIROC\_ESM has the minimum cooling load based on RCP8.5 amongst the other GCM models.

Table 25: Statistical values of different GCM models of the hourly cooling load based on RCP8.5 in four periods of 1961-1990, 2011-2040, 2041-2070, 2071-2100.

<b>Models RCP8.5 Cooling Load kWh</b>	<i>1961-1990</i>				<i>2011-2040</i>				<i>2041-2070</i>				<i>2071-2100</i>			
	<i>Max</i>	<i>AVE</i>	<i>STD</i>	<i>Median</i>												
<i>CanESM2</i>	23.2	2.4	4.6	0.005	23.4	2.8	5.2	0.03	25.07	3.2	5.6	0.07	24.3	3.7	6.2	0.1
<i>CNRM_CM5</i>	21.2	2.4	4.6	0.007	22.9	2.6	4.9	0.02	22.6	3.07	5.4	0.07	24.4	3.4	5.9	0.1
<i>MIROC_ESM</i>	23.3	2.4	4.6	0.006	24.2	2.9	5.3	0.06	25.8	3.4	5.8	0.1	26.9	4.1	6.5	0.3
<i>IPSL_CM5A_LR</i>	23.3	2.4	4.6	0.007	23.2	2.8	5.2	0.04	27.09	3.3	5.9	0.1	28.5	3.9	6.5	0.2
<i>MIROC5</i>	23.5	2.4	4.6	0.006	24.03	2.8	5.2	0.04	24.05	3.4	5.7	0.1	26.9	3.9	6.3	0.3
<i>Ensemble</i>	21.3	2.4	4.5	0.01	21.6	2.8	5.1	0.05	23.7	3.2	5.6	0.1	25.2	3.8	6.2	0.2

#### 4.2.6. Comparison (RCP4.5 and 8.5)

By comparing the hourly cooling load obtained, based on RCP4.5 and RCP8.5, can see that the cooling load based on RCP8.5 will increase more than RCP4.5, especially in the third period. The rise in the cooling load in the third period, based on RCP8.5, is due to the radiative forcing trend, based on RCP8.5, will go up continuously, while in the third period, based on RCP4.5, its increase will be reduced. By comparing the hourly results of RCP4.5 and RCP8.5 in June, one can see that at 9:00 h-12:00 h in the second period the load of 20-25 kW will happen just based on RCP8.5 and also in the third period this load will happen at 9:00 h-12:00 h, 13:00 h-16:00 h, and 17:00 h-20:00 h based on RCP8.5 while based on RCP4.5 it will only happen at 13:00 h-16:00 h. Moreover, in July the load of 20-25 kW based on RCP8.5 will happen at 9:00 h-12:00 h and 13:00 h-16:00 h in the second and third period, while based on RCP4.5 it will not happen at all.

By comparing the monthly behavior of the cooling load, it can be figured out that the load of 20-25 kW will occur more frequently based on RCP8.5 in comparison to RCP4.5, especially in July, which will turn this month into a critical month in the future.

The main differences of the impact of climate change on each part of the cooling load between RCP4.5 and RCP8.5 are as follows:

- In August from first to the second period and second to the third period, the effect of climate change will drop considerably in RCP4.5. This decline is the most in the load of 20-25 kW from first to the second period, which in RCP4.5 is a dropping effect while in RCP8.5 is an additive effect. In June from historical to the first period, the effect of climate change based on RCP8.5 is less than RCP4.5, especially in the load of 20-25 kW, which is zero based on RCP8.5 but +93.7% based on RCP4.5. In July from second to the third period, the effect of climate change will have a considerable drop. Moreover, the distribution of the additive effect of climate change is different, which in the loads less than 15-20 kW based on RCP4.5, it happens in 2 points, but based on RCP8.5, it occurs in one point in the load of 5-10 kW.

# Chapter 5

## 5. Conclusion, limitation, and future work

### 5.1. Concluding remarks on the present work

Previous spatiotemporal downscaling methods being applied in impact assessment on thermal performance of buildings suffer from the consistency between the downscaling and disaggregation methods. They are also so complicated or too simple which creates some difficulties for engineers to apply these approaches in real day-to-day projects. In the present work, a spatiotemporal downscaling method using quantile mapping bias correction method combined with a modified quantile-based k-nearest neighbor method for disaggregation in conjunction with TRNSYS has been introduced.

The reason for using quantile mapping bias correction in this project is mainly due to its ability to correct the existed bias of all statistical properties such as mean, standard deviation, quantile, and etc. Moreover, as quantile mapping deals with the entire empirical distribution it is better for correcting variables that deviate from normal distribution. Furthermore, this is one of the simplest and the most straightforward methodology to match the statistical properties. The disaggregation method has been inspired from the k -nearest neighbor method. Quantile k-nearest neighbor method has been used and modified to be compatible with the quantile mapping bias correction. In this method, matching with Euclidean distance has been substituted with the CDF matching which can maintain the quantile relationships made by quantile mapping bias correction. Therefore, this disaggregation method is more compatible with the quantile mapping bias correction spatial downscaling.

Finally, by combining two quantile mapping bias correction and modified quantile k-nearest neighbor downscaling, a simple but fully quantile-based approach to continuous downscaling of climate variables, which can be used readily by specialists is proposed. This similarity between the spatial and temporal downscaling (both follow the quantile role) can lead to having more compatibility and consistency in our cascade downscaling approach.

In this project five Global Circulation Models of CanESM2, MIROC\_ESM, CNRM\_CM5, MIROC5, and IPSL\_CM5A\_LR have been used to analyze the heating and cooling load in the historical period and future periods of 2011-2040, 2041-2070, and 2071-2100. The results of these five GCM models have been assessed and compared in two states of general behavior and detailed behavior (hourly analysis of the load) of the heating and cooling load. Additionally, the peak heating and cooling load have been analyzed. Therefore, as well as investigating the impact of climate change on general behavior of the load, this project went more into detail to see what would be the effect of climate change on each part of the load, especially the peak load. The impact assessment procedure in this project comprises Ensemble analysis, comparison (comparison of different RCPs), and variability (comparison of different GCM models). The detailed analysis of the load has been separated into three parts:

- 1- Hourly analysis of each part of the load separately which are affected by the climate change.
- 2- Analyzing the frequency of each part of the load separately which are affected by the climate change.
- 3- Analyzing the amount of climate change effect (the rate of climate change impact in percentage) on each part of the load.

The main results (all obtained from hourly data) are as follows:

Frequency analysis:

Heating load:

- The frequency of heating load will decrease from the top parts of the heating load and will be distributed amongst the other parts of the loads and all parts will receive some especially the lower tail of the load. Therefore, in the future due to the effect of climate change on heating load, an intensive load of 30-35 kW will not be critical load anymore that is necessary to be supplied.
- As the obtained results demonstrate, the maximum frequency of heating load in the future because of the impact of climate change tends to shift to the lower loads and while its frequency tends to increase, sometimes it will decrease slightly in the third period.

Cooling Load:

- Neither the load of 30-35 kW nor the load of 25-30 kW will exist in the future and the peak load will start from the load of 20-25 kW.
- The lower tail of the cooling load is declining while the upper tail of the load is increasing. Basically, the climate change will push some frequencies from the lower tail of the cooling load to the upper parts of the load, especially the peak load
- The rise in the upper tail of the cooling load (the peak cooling load) is significant which can lead to a serious problem in the future.
- The maximum cooling load will only occur in the lower tail of the load which here is the load of 0-5 kW. Also, the maximum cooling load in June will happen in the load of 0-5 kW, which will decrease in the first, second, and third period, respectively. The months of July and August have the same trend in the future.
- The second maximum cooling load will happen almost in the middle of the load. Moreover, it tends to shift up most of the time.

Climate change effect:

Heating load:

- The climate change has more effect on the upper and lower tail of the heating load and by going toward the middle, its effect decreases. In the heating load, there is always a transient load which the climate change has an additive effect on the loads lower than it and a dropping effect on the loads higher than it.

Cooling load:

- The climate change does not have any effect on loads of 25-30 and 30-35 kW because there is not any cooling load frequency more than 20-25 kW, which shows the maximum cooling load is around 20-25 kW.
- The impact of climate change is the most on the upper tail of the cooling load which is 20-25 kW in here and with moving toward the lower tail of the cooling load, the effect of climate change will declines which is the least in the lower tail of the cooling load. Moreover, the amount of climate change effect on the peak load of 20-25 kW is not comparable to the other parts of the load, which indicates the climate change will target the

cooling peak load and will increase it more than the other parts. The most impact of the climate change on cooling load is on the load of 20-25 kW from historical to the first period.

- Most of the time, there is not any transient load in the cooling load and the additive effect of the climate change on the cooling load will suddenly change into the dropping effect. This dropping effect will decrease until it reaches the lower tail of the load.

In conclusion, this thesis proposed a practical and systematic package of generating the weather data for impact assessment on thermal performance of building which is proper for analyzing the heating and cooling load in details. Moreover, based on the obtained results, analyzing the general and detailed behavior of the load are both crucial. In order to do an accurate mitigation on the impact of climate change on buildings, should classify the impact of climate change on each part of the load, especially on the peak load, which varies more than the other parts. Having analyzed hourly behavior of the load, frequency, and the rate of climate change effect on the heating and cooling load in the future work, one should find practical solutions for cooling peak shaving with fewer money investments.

## **5.2.Future work**

The future work is as follows:

- Adding wind speed, and atmospheric pressure to previous weather parameters because of the indirect impact that have on heating and cooling load.
- Analyzing the impact of climate change on the other regions and different weather conditions especially in hot climates that the total energy consumption increases.
- Analyzing the impact of climate change in high rise buildings and offices because of different energy consumption pattern that they have in comparison to residential buildings.
- Mitigating the impact of climate change on thermal performance of the building with considering the monthly and hourly behavior of the heating and cooling load.
- Using renewable energies and passive cooling methods for mitigating the impact of climate change on hourly and monthly cooling load.

- Investigating the new control strategies or optimization technics with considering the climate change and its effect on the load.
- Revising the terms and conditions in building engineering to be compatible with the climate change effects and also changing the calculation methods, and building science equations especially the National code of Canada and ASHRAE books

## References

- [1] Beer J, Mende W, Stellmacher R. The role of the sun in climate forcing 2000;19:403–15.
- [2] Cubasch U, Wuebbles D, Chen D, Facchini MC, Frame D, Mahowald N, et al. Introduction in Climate Change 2013. Intergov Panel Clim Chang 2013 Phys Sci Basis Contrib Work Gr I to Fifth Assess Rep Intergov Panel Clim Chang 2013:119–58. doi:10.1017/CBO9781107415324.007.
- [3] NASA. Earth Observatory 2018. <https://earthobservatory.nasa.gov/Features/EnergyBalance/page4.php>.
- [4] Lowe DC, Zealand N. Changes in Atmospheric Constituents and in Radiative Forcing (IPCC 2007). *Change* 2007;30:129–234. doi:10.1103/PhysRevB.77.220407.
- [5] Pachauri, Rajendra K. et al. Climate Change 2014 Synthesis Report Summary Chapter for Policymakers. *Ipcc* 2014:31. doi:10.1017/CBO9781107415324.
- [6] University of East Anglia. 2017 likely to be third warmest year on record 2017. <https://phys.org/news/2017-11-warmest-year.html>.
- [7] Flato, G., Marotzke, J., Abiodun, B., Braconnot, P., Chou, S.C., Collins, W.J., Cox, P., Driouech, F., Emori, S., Eyring, V. and Forest C. *Climate Change 2013 The Physical Science Basis* 2013;5:741–866.
- [8] Boorman, P., McDonald, R. and Hill S. Climate change scenarios for the United Kingdom: the UKCIP02 scientific report. *Tyndall Centre for Climate Mental Sciences University* 2002;96:218224.
- [9] Ierley GR. General circulation models. *Earth Syst Environmetal Sci* 2001:20–4.
- [10] Wilby RL, Troni J, Biot Y, Tedd L, Hewitson BC, Smith DM, et al. A review of climate risk information for adaptation and development planning. *Int J Climatol* 2009;29:1193–215.
- [11] Taylor KE, Stouffer RJ, Meehl GA. An Overview of CMIP5 and the Experiment Design. *Bull Am Meteorol Soc* 2011;93:485–98. doi:10.1175/BAMS-D-11-00094.1.
- [12] Obasi GOP, Töpfer K. Emissions Scenarios: Summary for Policymakers; a Special Report of IPCC Working Group III. *Intergovernmental Panel on Climate Change*; 2000.
- [13] Moss RH, Edmonds JA, Hibbard KA, Manning MR, Rose SK, Vuuren DP Van, et al. The next generation of scenarios for climate change research and assessment. *Nature* 2010;463:747–56. doi:10.1038/nature08823.
- [14] Society A, Law I. The Kyoto Protocol to the United Nations Framework Convention on Climate Change. *Am Soc Int Law ; Cambridge Univ Press Stable URL* 2017;92:315–31.
- [15] Nakicenovic N, Alcamo J, Davis G, de Vries B, Fenhann J, Gaffin S, et al. Special report on emissions scenarios: a special report of Working Group III of the Intergovernmental Panel on Climate Change. 2000.
- [16] Jentsch MF, James PAB, Bourikas L, Bahaj AS. Transforming existing weather data for worldwide locations to enable energy and building performance simulation under future climates. *Renew Energy* 2013;55:514–24. doi:10.1016/j.renene.2012.12.049.
- [17] Alley RB, Berntsen T. Summary for Policymakers Summary for Policymakers. A Rep Work Gr I Intergov Panel Clim Chang 2000.
- [18] Vuuren DP Van, Edmonds J, Kainuma M, Riahi K, Nakicenovic N, Smith SJ, et al. The representative concentration pathways : an overview. *Clim Chang* 2011:5–31. doi:10.1007/s10584-011-0148-z.

- [19] Belcher SE, Hacker JN, Powell DS. Constructing design weather data for future climates. *Build Serv Eng Res Technol* 2005;26:49–61.
- [20] Jee J, Kim S. Sensitivity Study on High-Resolution WRF Precipitation Forecast for a Heavy Rainfall Event. *Atmosphere (Basel)* 2017. doi:10.3390/atmos8060096.
- [21] Brown C, Greene A, Block P, Giannini A. Review of downscaling methodologies for Africa climate applications. *Int Res Inst Clim Soc Columbia Univ* 2008;15:5–8.
- [22] Trzaska S, Schnarr E. A review of downscaling methods for climate change projections. United States Agency Int Dev by Tetra Tech ARD 2014:1–42.
- [23] Goodess CM, Anagnostopoulou C, Bárdossy A, Frei C, Harpham C, Haylock MR, et al. An intercomparison of statistical downscaling methods for Europe and European regions – assessing their performance with respect to extreme temperature and precipitation events 2005 ( published as CRU RP11 in 2012 ) Climatic Research Unit School of Environmental Sciences University of East Anglia About the Climatic Research Unit CRU Research Publications series 2012;2005.
- [24] Chen J, Brissette FP, Chaumont D, Braun M. Performance and uncertainty evaluation of empirical downscaling methods in quantifying the climate change impacts on hydrology over two North American river basins. *J Hydrol* 2013;479:200–14. doi:10.1016/j.jhydrol.2012.11.062.
- [25] Sunyer MA, Madsen H, Ang PH. A comparison of different regional climate models and statistical downscaling methods for extreme rainfall estimation under climate change. *Atmos Res* 2012;103:119–28. doi:10.1016/j.atmosres.2011.06.011.
- [26] Zorita E, Von Storch H. The analog method as a simple statistical downscaling technique: comparison with more complicated methods. *J Clim* 1999;12:2474–89.
- [27] Shen P. Impacts of climate change on U . S . building energy use by using downscaled hourly future weather data. *Energy Build* 2017;134:61–70. doi:10.1016/j.enbuild.2016.09.028.
- [28] Wang L, Liu X, Brown H. Prediction of the impacts of climate change on energy consumption for a medium-size office building with two climate models. *Energy Build* 2017;157:218–26. doi:10.1016/j.enbuild.2017.01.007.
- [29] Huang K, Hwang R. Future trends of residential building cooling energy and passive adaptation measures to counteract climate change: The case of Taiwan. *Appl Energy* 2016;184:1230–40. doi:10.1016/j.apenergy.2015.11.008.
- [30] Wang H, Chen Q. Impact of climate change heating and cooling energy use in buildings in the United States. *Energy Build* 2014;82:428–36. doi:10.1016/j.enbuild.2014.07.034.
- [31] Hamlet AF, Salathé EP, Carrasco P. *Statistical Downscaling Techniques for Global Climate Model Simulations of Temperature and Precipitation with Application to Water Resources Planning Studies* 2010.
- [32] Wood AW, Leung LR, Sridhar V, Lettenmaier DP. Hydrologic implications of dynamical and statistical approaches to downscaling climate model output. *Clim Chang* 2004:189–216.
- [33] Livneh, Ben, Eric A. Rosenberg, Chiyu Lin, Bart Nijssen, Vimal Mishra, Kostas M. Andreadis, Edwin P. Maurer and DPL. A long-term hydrologically based dataset of land surface fluxes and states for the

- conterminous United States: Update and extensions. *J Clim* 2002;26:9384–92. doi:10.1175/JCLI-D-12-00508.1.
- [34] Gudmundsson L, Bremnes JB, Haugen JE. Technical Note : Downscaling RCM precipitation to the station scale using statistical transformations – a comparison of methods. *Hydrol Earth Syst Sci* 2012;3383–90. doi:10.5194/hess-16-3383-2012.
- [35] Piani C, Haerter JO, Coppola E. Statistical bias correction for daily precipitation in regional climate models over Europe. *Theor Appl Climatol* 2010;187–92. doi:10.1007/s00704-009-0134-9.
- [36] Teutschbein C, Seibert J. Bias correction of regional climate model simulations for hydrological climate-change impact studies : Review and evaluation of different methods. *J Hydrol* 2012;456–457:12–29. doi:10.1016/j.jhydrol.2012.05.052.
- [37] Leander R, Buishand et al. Estimated changes in flood quantiles of the river Meuse from resampling of regional climate model output 2008:331–43. doi:10.1016/j.jhydrol.2007.12.020.
- [38] Teutschbein C, Seibert J. Is bias correction of regional climate model (RCM) simulations possible for non-stationary conditions ? 2013:5061–77. doi:10.5194/hess-17-5061-2013.
- [39] Christensen JH, Boberg F, Christensen OB, Lucas-picher P. On the need for bias correction of regional climate change projections of temperature and precipitation. *Geophys Res Lett* 2008;35. doi:10.1029/2008GL035694.
- [40] Maraun D. Nonstationarities of regional climate model biases in European seasonal mean temperature and precipitation sums. *Geophys Res Lett* 2012;39:1–5. doi:10.1029/2012GL051210.
- [41] Camici S, Brocca L, Melone F, Moramarco T. Impact of Climate Change on Flood Frequency Using Different Climate Models and Downscaling Approaches. *J Hydrol Eng* 2014;19:4014002. doi:10.1061/(ASCE)HE.1943-5584.0000959.
- [42] Piani C, Haerter JO. Two dimensional bias correction of temperature and precipitation copulas in climate models. *Geophys Res Lett* 2012;39:1–6. doi:10.1029/2012GL053839.
- [43] Michelangeli P, Vrac M, Loukos H. Probabilistic downscaling approaches : Application to wind cumulative distribution functions. *Geophys Res Lett* 2009;36:2–7. doi:10.1029/2009GL038401.
- [44] Willems P, Vrac M. Statistical precipitation downscaling for small-scale hydrological impact investigations of climate change. *J Hydrol* 2011;402:193–205. doi:10.1016/j.jhydrol.2011.02.030.
- [45] Sunyer MA, Madsen H, Rosbjerg D, Arnbjerg-Nielsen K. A Bayesian Approach for Uncertainty Quantification of Extreme Precipitation Projections Including Climate Model Interdependency and Nonstationary Bias. *J Clim* 2014:7113–32. doi:10.1175/JCLI-D-13-00589.1.
- [46] G. Bürger, S. R. Sobie, A. J. Cannon, A. T. Werner and TQM. Downscaling Extremes — An Intercomparison of Multiple Statistical Methods for Present Climate. *J Clim* 2013:4366–88. doi:10.1175/JCLI-D-11-00408.1.
- [47] Alex J. Cannon, Stephen R. Sobie and TQM. Bias Correction of GCM Precipitation by Quantile Mapping : How Well Do Methods Preserve Changes in Quantiles and Extremes? *J Clim* 2015:6938–59. doi:10.1175/JCLI-D-14-00754.1.
- [48] Li H, Sheffield J, Wood EF. Bias correction of monthly precipitation and temperature fields from Intergovernmental Panel on Climate Change AR4 models using equidistant quantile matching. *Atmospheres*

- 2010;115. doi:10.1029/2009JD012882.
- [49] Urg J, Frei C, Vidale PL. Downscaling from GCM precipitation: A benchmark. *J Climatol* 2006;689:679–89. doi:10.1002/joc.1287.
- [50] Bo J, Terray L, Habets F, Martin E. Statistical and dynamical downscaling of the Seine basin climate for hydro-meteorological studies. *Int J Climatol* 2007;1655:1643–55. doi:10.1002/joc.
- [51] Chen J, Brissette P, Chaumont D, Braun M. Finding appropriate bias correction methods in downscaling precipitation for hydrologic impact studies over North America. *Water Resour Res* 2013;49:4187–205. doi:10.1002/wrcr.20331.
- [52] Pierce DW, Das T, Cayan DR, Maurer EP, Snyder MA, Sloan LC, et al. Probabilistic estimates of future changes in California temperature and precipitation using statistical and dynamical downscaling. *Clim Dyn* 2013;839–56. doi:10.1007/s00382-012-1337-9.
- [53] Hayhoe K, Cayan D, Field CB, Frumhoff PC, Maurer EP, Miller NL, et al. Emissions pathways , climate change , and impacts on California. *Proc Natl Acad Sci U S A* 2004;101.
- [54] Maurer EP, Hidalgo HG. Utility of daily vs . monthly large-scale climate data : an intercomparison of two statistical downscaling methods 2010:1125–38. doi:10.5194/hess-14-1125-2010.
- [55] Themeßl MJ, Gobiet A, Leuprecht A. Empirical-statistical downscaling and error correction of daily precipitation from regional climate models. *Int J Climatol* 2011;1544:1530–44. doi:10.1002/joc.2168.
- [56] Miao C, Su L, Sun Q, Duan Q. A nonstationary bias-correction technique to remove bias in GCM simulations. *J Geophys Res Atmos* 2015:5718–35. doi:10.1002/2015JD024159.
- [57] CICS. Downscaling background. Frequently Asked Questions. Accessed 6/5/2013 2006. [http://www.ipcc-data.org/ddc/ddc\\_faq.html](http://www.ipcc-data.org/ddc/ddc_faq.html).
- [58] Dickinson R, Rm Enico. A regional climate model for the western US. *Clim Chang* 1989. doi:10.1016/S0360-3199(01)00119-7.
- [59] Ahmed KF. Bias Correction and Downscaling of Climate Model Outputs Required for Impact Assessments of Climate Change in the U . S . Northeast Bias Correction and Downscaling of Climate Model Master of Science 2011.
- [60] The world bank group. Climate Change Knowledge Portal 2015. <http://sdwebx.worldbank.org/climateportal/>.
- [61] Crawley DB, Shirey DB, Cornick SM, Jarrett PL, Lott JN, Morris RJ, et al. Climatic Data for Building Design Standards 2013. <https://www.ashrae.org/technical-resources/bookstore/ashrae-climate-data-center>.
- [62] Jentsch MF, Bahaj AS, James PAB. Climate change future proofing of buildings—Generation and assessment of building simulation weather files. *Energy Build* 2008;40:2148–68.
- [63] Wang X, Chen D, Ren Z. Assessment of climate change impact on residential building heating and cooling energy requirement in Australia. *Build Environ* 2010;45:1663–82. doi:10.1016/j.buildenv.2010.01.022.
- [64] Chan ALS. Developing future hourly weather files for studying the impact of climate change on building energy performance in Hong Kong. *Energy Build* 2011;43:2860–8. doi:10.1016/j.enbuild.2011.07.003.
- [65] Roshan GR, Orosa JA, Nasrabadi T. Simulation of climate change impact on energy consumption in buildings , case study of Iran. *Energy Policy* 2012;49:731–9. doi:10.1016/j.enpol.2012.07.020.

- [66] Wan KKW, Li DHW, Pan W, Lam JC. Impact of climate change on building energy use in different climate zones and mitigation and adaptation implications. *Appl Energy* 2012;97:274–82. doi:10.1016/j.apenergy.2011.11.048.
- [67] Dodoo A, Gustavsson L. Energy use and overheating risk of Swedish multi-storey residential buildings under different climate scenarios. *Energy* 2016;97:534–48. doi:10.1016/j.energy.2015.12.086.
- [68] Invidiata A, Ghisi E. Impact of climate change on heating and cooling energy demand in houses in Brazil. *Energy Build* 2016;130:20–32. doi:10.1016/j.enbuild.2016.07.067.
- [69] Sabunas A, Kanapickas A. Estimation of climate change impact on energy consumption in a residential building in Kaunas, Lithuania, using HEED Software. *Energy Procedia* 2017;128:92–9. doi:10.1016/j.egypro.2017.09.020.
- [70] Du H, Edge J, Underwood C. Modelling the impacts of new UK future weather data on a school building. *Proc Build Simul* 2011.
- [71] Shibuya T, Croxford B. The effect of climate change on office building energy consumption in Japan. *Energy Build* 2016;117:149–59. doi:10.1016/j.enbuild.2016.02.023.
- [72] Robert A, Kummert M. Designing net-zero energy buildings for the future climate , not for the past. *Build Environ* 2012;55:150–8. doi:10.1016/j.buildenv.2011.12.014.
- [73] Nik VM, Kalagasidis AS. Impact study of the climate change on the energy performance of the building stock in Stockholm considering four climate uncertainties. *Build Environ* 2013;60:291–304. doi:10.1016/j.buildenv.2012.11.005.
- [74] Alves CA, Duarte DHS, Gonc FLT. Residential buildings ’ thermal performance and comfort for the elderly under climate changes context in the city of São Paulo , Brazil. *Energy Build* 2016;114:62–71. doi:10.1016/j.enbuild.2015.06.044.
- [75] Taylor ZT. Climate Change Impacts on Residential and Commercial Loads in the Western U . S . Grid. *IEEE Trans Power Syst* 2008;25:6547.
- [76] Gomes N, Pina A, Ferrão P, Fournier J, Lacarrière B, Corre O Le. Modeling the long-term effect of climate change on building heat demand: Case study on a district level. *Energy Build* 2016;126:77–93. doi:10.1016/j.enbuild.2016.04.082.
- [77] Olonscheck M, Holsten A, Kropp JP. Heating and cooling energy demand and related emissions of the German residential building stock under climate change. *Energy Policy* 2011;39:4795–806. doi:10.1016/j.enpol.2011.06.041.
- [78] Filippín C, Ricard F, Flores Larsen S, Santamouris M. Retrospective analysis of the energy consumption of single-family dwellings in central Argentina. Retrofitting and adaptation to the climate change. *Renew Energy* 2017;101:1226–41. doi:10.1016/j.renene.2016.09.064.
- [79] Karimpour M, Belusko M, Xing K, Boland J, Bruno F. Impact of climate change on the design of energy efficient residential building envelopes. *Energy Build* 2015;87:142–54. doi:10.1016/j.enbuild.2014.10.064.
- [80] Wong SL, Wan KKW, Li DHW, Lam JC. Impact of climate change on residential building envelope cooling loads in subtropical climates. *Energy Build* 2010;42:2098–103. doi:10.1016/j.enbuild.2010.06.021.

- [81] Dirks JA, Gorrissen WJ, Hathaway JH, Skorski DC, Scott MJ, Pulsipher TC, et al. Impacts of climate change on energy consumption and peak demand in buildings: A detailed regional approach. *Energy* 2015;79:20–32. doi:10.1016/j.energy.2014.08.081.
- [82] CelinaFilippin, FlorenciaRicard, Larsen S, MattheosSantamouris. Retrospective analysis of the energy consumption of single-family dwellings in central Argentina. Retrofitting and adaptation to the climate change. *Renew Energy* 2017;101:1226–41.
- [83] National snow and ice data centre. Quick Facts on Arctic Sea Ice 2018. <https://nsidc.org/cryosphere/quickfacts/seaice.html>.
- [84] Bastani A, Haghghat F, Jalon C. Investigating the effect of control strategy on the shift of energy consumption in a building integrated with PCM wallboard. *Energy Procedia* 2015;78:2280–5. doi:10.1016/j.egypro.2015.11.365.
- [85] Sumaila P. Contrôle du chauffage pour la gestion de la demande résidentielle Rapport technique sur la création d ' un modèle résidentiel fonctionnel 2010.
- [86] Yao W, Li Z, Lu Y, Jiang F, Li C. Proceedings of the 8th International Symposium on Heating, Ventilation and Air Conditioning. Springer 2014;261:653–63. doi:10.1007/978-3-642-39584-0.
- [87] Liu BY, Richard C. Jordan. The interrelationship and characteristic distribution of direct, diffuse and total solar radiation. *Sol Energy* 1960;4.3:1–19.
- [88] Paliaga G, Schoen LJ, Alspach PF, Arens EA, Aynsley RM, Bean R, et al. Thermal Environmental Conditions for Human Occupancy. ASHRAE Stand 2014;8400.
- [89] Kattsov V, Federation R, Reason C, Africa S et al. Evaluation of Climate Models 9. Ipc 2013.
- [90] WCRP. CMIP5 - Coupled Model Intercomparison Project Phase 5 - Overview 2008. <https://cmip.llnl.gov/cmip5/>.
- [91] Environment Canada. Engineering Climate Datasets 2017. [http://climate.weather.gc.ca/prods\\_servs/engineering\\_e.html](http://climate.weather.gc.ca/prods_servs/engineering_e.html).
- [92] Bennett JC, Grose MR, Corney SP, White CJ, Holz GK, Katzfey JJ, et al. Performance of an empirical bias-correction of a high-resolution climate dataset. *Int J Climatol* 2014;34:2189–204. doi:10.1002/joc.3830.
- [93] Leif E. Peterson. K-nearest\_neighbor. Scholarpedia 2009;4:1883.
- [94] D.T.Reindl, W.A.Beckman, J.A.Duffie. Diffuse fraction correlations. *Sol Energy* 1990;45:1–7.